# ผลของการฉายรังสีแกมมาต่อสมบัติพื้นฐานของฟิล์มบางแบบเพอรอฟสไกต์เตรียมโดยเทคนิคโซล-เจล

นางสาวอรณิชา คงวุฒิ



วิทยานิพนธ์นี้เป็นส่วนหนึ่งของการศึกษาตามหลักสูตรปริญญาวิทยาศาสตรมหาบัณฑิต
สาขาวิชาฟิสิกส์ ภาควิชาฟิสิกส์
คณะวิทยาศาสตร์ จุฬาลงกรณ์มหาวิทยาลัย
ปีการศึกษา 2553

# EFFECTS OF GAMMA RAY IRRADIATION ON FUNDAMENTAL PROPERTIES OF PEROVSKITE THIN FILMS PREPARED BY A SOL-GEL TECHNIQUE

Miss Ornnicha Kongwut



A Thesis Submitted in Partial Fulfillment of the Requirements
for the Degree of Master of Science Program in Physics
Department of Physics
Faculty of Science
Chulalongkorn University
Academic Year 2010

| | |
|---|---|
| Thesis Title | EFFECTS OF GAMMA RAY IRRADIATION ON FUNDAMENTAL PROPERTIES OF PEROVSKITE THIN FILMS PREPARED BY A SOL-GEL TECHNIQUE |
| By | Miss Ornnicha Kongwut |
| Field of Study | Physics |
| Thesis Advisor | Assistant Professor Satreerat K. Hodak, Ph.D. |

---

Accepted by the Faculty of Science, Chulalongkorn University in Partial Fulfillment of the Requirements for the Master's Degree

.....Vimolvan Pimpan..... Deputy Dean for Administrative Affairs, Acting Dean, The Faculty of Science

(Associate Professor Vimolvan Pimpan, Ph.D.)

THESIS COMMITTEE

.....Chaisingh Poo-Rakkiat..... Chairman

(Assistant Professor Chaisingh Poo-Rakkiat, Ph.D.)

.....Satreerat K. Hodak..... Thesis Advisor

(Assistant Professor Satreerat K. Hodak, Ph.D.)

.....Montian T.....Examiner

( Montian Tianprateep, Ph.D.)

.....S. Dangtip.....External Examiner

( Somsak Dangtip, Ph.D.)

อรณิชา คงวุฒิ : ผลของการฉายรังสีแกมมาต่อสมบัติพื้นฐานของฟิล์มบางแบบเพอรอฟสไกต์เตรียมโดยเทคนิคโซล-เจล. (EFFECTS OF GAMMA RAY IRRADIATION ON FUNDAMENTAL PROPERTIES OF PEROVSKITE THIN FILMS PREPARED BY A SOL-GEL TECHNIQUE) อ.ที่ปรึกษาวิทยานิพนธ์หลัก : ผู้ช่วยศาสตราจารย์ ดร. สตรีรัตน์ โฮคัด, 113 หน้า.

พหุผลึกฟิล์มบางแบเรียมไททาเนตเจือด้วยเหล็กและฟิล์มบางแคลเซียมคอปเปอร์ไททาเนตเจือด้วยเหล็กถูกปลูกบนแผ่นรองรับควอตซ์ที่อุณหภูมิ 800 องศาเซลเซียสโดยวิธีโซล-เจล ฟิล์มบางจะถูกฉายรังสีแกมมาจากเครื่อง Gammacel 220 Excell โดยมีธาตุ $^{60}Co$ เป็นแหล่งกำเนิดรังสีซึ่งมีอัตราการฉายรังสี 10 กิโลเกรย์ต่อชั่วโมงเพื่อตรวจสอบสมบัติทางแสงและสมบัติทางไฟฟ้าของฟิล์มบางที่เปลี่ยนแปลง ค่าการส่งผ่านแสงของฟิล์มบางแบเรียมไททาเนตเจือด้วยเหล็กลดลง 11% หลังจากฉายรังสีแกมมา 15 กิโลเกรย์ ขณะที่ฟิล์มบางแคลเซียมคอปเปอร์ไททาเนตเจือด้วยเหล็กลดลง 4.8% หลังจากฉายแกมมา 3 กิโลเกรย์ ตามลำดับ ค่าดัชนีหักเหของฟิล์มบางถูกวัดในช่วงความยาวคลื่น 350 - 750 นาโนเมตร ฟิล์มบางแบเรียมไททาเนตเจือด้วยเหล็กเพิ่มขึ้นจาก 2.17 - 1.88 เป็น 2.34 - 1.95 หลังจากฉายรังสีแกมมาที่ 15 กิโลเกรย์ และฟิล์มบางแคลเซียมคอปเปอร์ไททาเนตเพิ่มขึ้นจาก 1.76 - 1.99 เป็น 1.91 - 2.08 หลังจากฉายรังสีแกมมา 3 กิโลเกรย์ ตามลำดับ ค่าสัมประสิทธิ์การดูดกลืนของฟิล์มทั้งสองอยู่ในอันดับ $10^{-2}$ และเพิ่มขึ้นหลังจากการฉายรังสีแกมมา ค่าความจุของของฟิล์มแคลเซียมคอปเปอร์ไททาเนตเจือด้วยเหล็กเพิ่มขึ้นจาก 1.36 - 1.22 พิโคฟารัด เป็น 1.62 - 1.36 พิโคฟารัด ค่าคงที่ไดอิเล็กทริกของฟิล์มบางแคลเซียมคอปเปอร์ไททาเนตเพิ่มขึ้นจาก 314 - 280 เป็น 552 - 308 และค่าความสูญเสียไดอิเล็กทริกเพิ่มขึ้นจาก 0.020 - 0.013 เป็น 0.138 - 0.030หลังจากฉายรังสีแกมมา 5 กิโลเกรย์



ภาควิชา ฟิสิกส์ ลายมือชื่อนิสิต Ornnicha Kongwut

สาขาวิชา ฟิสิกส์ ลายมือชื่ออ.ที่ปรึกษาวิทยานิพนธ์หลัก Satreerat K. Hodak

ปีการศึกษา 2553

## 5072558123 : MAJOR PHYSICS
KEYWORDS : GAMMA IRRADIATION / PEROVSKITE THIN FILM / SOL-GEL TECHNIQUE

ORNNICHA KONGWUT : EFFECTS OF GAMMA RAY IRRADIATION ON FUNDAMENTAL PROPERTIES OF PEROVSKITE THIN FILMS PREPARED BY A SOL-GEL TECHNIQUE. THESIS ADVISOR : ASST. PROF. SATREERAT K. HODAK, Ph.D., 113 pp.

Polycrystalline Fe-doped barium titanate (Fe-doped $BaTiO_3$) and Fe-doped calcium copper titanate (Fe-doped $CaCu_3Ti_4O_{12}$) thin films were deposited on quartz substrates with the annealing temperature of 800$^oC$ by a sol-gel spin coating technique. The $^{60}Co$ source (Gammacel 220 Excell) with the exposure rate of 10 kGy/hr was used to irradiate our film in order to investigate the changes of their optical and electrical properties. The transmittance of Fe-doped $BaTiO_3$ film decreased by 11% after 15 kGy irradiation, while that of Fe-doped $CaCu_3Ti_4O_{12}$ film decreased by 4.8% after 3 kGy irradiation respectively. The refractive index of the films, as measured in the 350 - 750 nm wavelength range was in the 2.17 - 1.88 range and increased to 2.34 - 1.95 after gamma irradiation at 15 kGy for Fe-doped $BaTiO_3$ and increased from 2.24 - 2.00 range to 2.30 - 2.00 range for Fe-doped $CaCu_3Ti_4O_{12}$ upon the gamma irradiation with a 3 kGy dose, respectively. The extinction coefficient of both types of the films was in the order of $10^{-2}$ and increased after gamma irradiation. The capacitance of the $CaCu_3Ti_4O_{12}$ film before gamma ray irradiation which increases from 1.36 - 1.22 pF to 1.62 - 1.36 pF after gamma ray irradiation with 5 kGy doses. The dielectric constant of the $CaCu_3Ti_4O_{12}$ film increased from 314 - 280 to 552 - 308 and loss tangent of $CaCu_3Ti_4O_{12}$ film increased from 0.020 - 0.013 to 0.138 - 0.030.

Department : ..... Physics ..... Student's Signature Ornnicha Kongwut

Field of Study : ..... Physics ..... Advisor's Signature Satreerat K. Hodak

Academic Year : ..... 2010 .....

# Acknowledgements

First of all, I would like to express my sincere gratitude to Assistant Professor Dr. Satreerat K. Hodak my advisor, who introduced valuable advice, understanding and encouragement throughout this research as well as helpful comments and correction of this thesis.

My appreciation also extended to Associate Professor Dr. Chaisingh Poo-Rakkiat, Dr. Montian Tianprateep and Dr. Somsak Dangtip for serving as chairman and committee, respectively.

I am thankful to the financial supports from Department of Physics, Faculty of Science, Chulalongkorn University, Graduate Thesis Grant and National Research Council of Thailand (NRCT) for paying fund to attend conferences.

Especially, I would like to thank Mr. Areerat Kornduangkeaw and Miss Nungnut Jangsawang of the Thailand Institute of Nuclear Technology (TINT) for their kind to use Gammacel 220 Excell.

Thank to all my friends (Thidarat Supasai, Yumairoh Kasa, Pavarit promsena etc.) at the Department of Physics for their fun, help and suggestion when I have any problems throughout my study.

Finally, I would like to express my deepest gratitude to my parents and brother (Wuttirong Kongwut) for all their love, encouragements and understanding during my study at Chulalongkorn University.

# Contents

**Chapter** **Page**

**Chapter** **Page**

**Chapter** **Page**

# List of Tables

**Table** **Page**

# List of Figures

**Figure** **Page**

**Figure** **Page**

**Figure** **Page**

**Figure** **Page**

# CHAPTER I

# INTRODUCTION

## 1.1 Motivation

The innovative development at present has been used to improve and change properties of materials which are suitable to any desired applications. The effects of the inclusion of different transition metals on the structural, optical, electrical and magnetic properties of perovskite ($ABO_3$) thin films have been investigated. Various types of dopants and cations of different sizes can be accommodated in the $ABO_3$ sites [1, 2, 3, 4, 5, 6]. Barium titanate ($BaTiO_3$) is a well known perovskite material due to its high dielectric constant and its electric field tuning property. In addition, doping Fe ions into the $BaTiO_3$ lattice leads to the acquisition of both ferromagnetic and ferroelectric properties [7]. The ferromagnetism of Fe-doped $BaTiO_3$ ceramics was reported to be dependent upon the annealing atmosphere and Fe doping concentration, with the substitution by $Fe^{3+}$ occurring in Ti sites being confirmed by Mössbauer measurements [8, 9]. Herner et al. showed that doping barium strontium titanate ($BaSrTiO_3$) with Fe could reduce the loss tangent [10], by means of improving the dielectric properties compared to pure $BaSrTiO_3$. Another way to change the fundamental properties of these materials is by exposure to high energy electromagnetic radiation or high energy particles, such as X-rays, gamma rays, electron or neutron bombardment. The retained polarization, dielectric constant and coercive field of lead titanate films decreased upon increasing gamma irradiation doses, but the material was less sensitive to neutron irradiation [11]. From the literature review, fundamental properties of

various materials could be changed by gamma ray irradiation. Arshak et al. observed that the energy gap of a bismuth germanate film decreased from 1.95 eV to 1.76 eV after exposure to gamma irradiation with a 0.228 mGy [12]. Arshak et al. also reported that the capacitance for ZnO thick film exhibited from 21.58 pF at a dose of 1 mGy to 28.33 pF at 2.3 mGy dose and thick films of $SnO_2$ also showed an increase in the capacitance from 5.05 pF before irradiation to 8.69 pF at a dose 0.46 mGy [13]. Ta et al. have found that the capacitance-voltage (C-V) of Al/$Y_2O_3$/n-Si/Al capacitors before and after irradiation with cumulative dose of 2.4, 4.8, and 8.4 kGy moved towards the positive voltage when the irradiation dose increases [14]. Fasasi et al. have reported the use of high dose gamma irradiation to study the thermoluminescence glow curve characteristic of $BaTiO_3$ ceramics and the dose dependence on the glow curve [15]. These radiation imparted changes in $BaTiO_3$ are extremely useful for the effective design of modern radiation dosimeters for their low-cost and simplicity.

Many dosimeters such as thermoluminescent dosimeters (TLDs), optically-stimulated- luminescence (OSL) dosimeters and polymethylmethacrylate (PMMA) sheets are normally used for radiation safety [16]. The TLD material, which is commonly used to make badges, absorbs and stores energy when exposed to radiation and after heating the TLD releases the light. PMMA sheets could be used to stick with the products which are exposed to radiation. The change in the optical properties of PMMA is the indirect way of measuring the level and duration of radiation exposure. However, PMMA has a low melting temperature at 160 $^oC$ and most of the time can be used only once due to the ease of scratching. Nowadays researchers have investigated the potential of several metal oxides including both single- (e.g., ZnO, $SnO_2$,$WO_3$,$TiO_2$ and $Fe_2O_3$) and multi-component oxides ($BiFeO_3$, $MgAl_2O_4$, $SrTiO_3$ and $Sr_{1-y}Ca_yFeO_{3-x}$) to be usable as dosimeters. Also, it is important to be able to enhance the performance of dosimeters through the material processing.

## 1.2 Objective

The objective of this thesis is to study the effects of gamma ray irradiation on fundamental properties of four perovskite materials. These thin films were deposited by a sol-gel spin coating technique on quartz substrates and $Al_2O_3$ in order to investigate the optical and electrical, respectively. The first of choices in this study are $BaTiO_3$ and Fe-doped $BaTiO_3$ thin films. We focus mostly on the optical properties (%transmission, optical energy gap and complex refractive index) of these two materials before and after gamma ray irradiation with difference doses. The further investigation is on the effects of gamma ray irradiation on the optical properties of a new discovered material, Fe-doped calcium copper titanate thin film. Finally, the calcium copper titanate thin films deposited on $Al2O_3$ substrate was fabricated as coplanar capacitor. The electrical properties of calcium copper titanate thin films was measured in the form of capacitance before and after gamma ray irradiation. X-ray diffraction and atomic force microscope techniques were used to study crystal structure and surface morphology of the films. The composition of elements in the films was calculated by wavelength dispersive X-ray data. This thesis work is basically for further development of dosimeter based on changing optical and electrical properties of the films after exposure with different doses of gamma ray.

## 1.3 Thesis outline

This thesis is divided into six chapters. In Chapter I, we introduce the motivation, the objective, barium titanate, Fe-doped barium titanate, calcium copper titanate and Fe-doped calcium copper titanate. The theory of a sol-gel process, gamma ray, interactions between gamma ray and barium titanate, Fe-doped barium titanate, calcium copper titanate and Fe-doped calcium copper titanate films and determination of film thickness from transmission data will be presented in Chapter II. Fundamental of X-ray diffraction, wavelength dispersive

X-ray, energy dispersive X-ray spectroscopy, atomic force microscope and optical transmission will be explained in Chapter III. Chapter IV focuses on the films preparation, gamma ray irradiation experiment and UV-VIS-NIR spectroscopy set up. Chapter V presents the results of the experiments (X-ray diffraction, atomic force microscope, optical properties, electric properties). The final chapter, Chapter VI, is the conclusion of the thesis.

# CHAPTER II

# THEORETICAL BACKGROUND

The theory related to the fundamental properties of the barium titanate, Fe-doped barium titanate, calcium copper titanate and Fe-doped calcium copper titanate films will be presented. The sol-gel processing used to prepare these films in this research is presented in this chapter. The gamma ray and interactions between gamma ray and the materials will be also presented in this chapter. The last of this, the formula for thickness determination from transmission data will be derived.

## 2.1 Barium titanate, Fe-doped barium titanate, calcium copper titanate and calcium copper titanate thin films

### 2.1.1 Barium titanate (BTO)

Barium titanate ($BaTiO_3$), which was discovered 60 years ago, is a ferroelectric material that has gained much interest due to its many potential applications, such as high dielectric constant capacitors, dynamic random access memories, and piezoelectric and optical wave guide devices [17, 18, 19]. BTO is a perovskite material which is a typical $ABO_3$ where as Ba ion ($Ba^{2+}$) is at the A-sites and Ti ion ($Ti^{4+}$ as B) is at the B-sites. In Fig. 2.1, barium atoms are occupied at the eight corners of the cube, oxygen atoms are occupied at the faces, titanium atom

is at the center of the cube. A crystal structure of barium titanate depends on the temperature range [20]. At room temperature a tetragonal BTO is the most stable phase [21, 22]. A Curie temperature ($T_c$) of BTO, which is a temperature at which a tetragonal phase transform into a cubic phase, is about 120 $^o$C [23]. The lattice parameters of bulk BTO are 3.994 Å and 4.038 Å for the a-axis and c-axis [24].

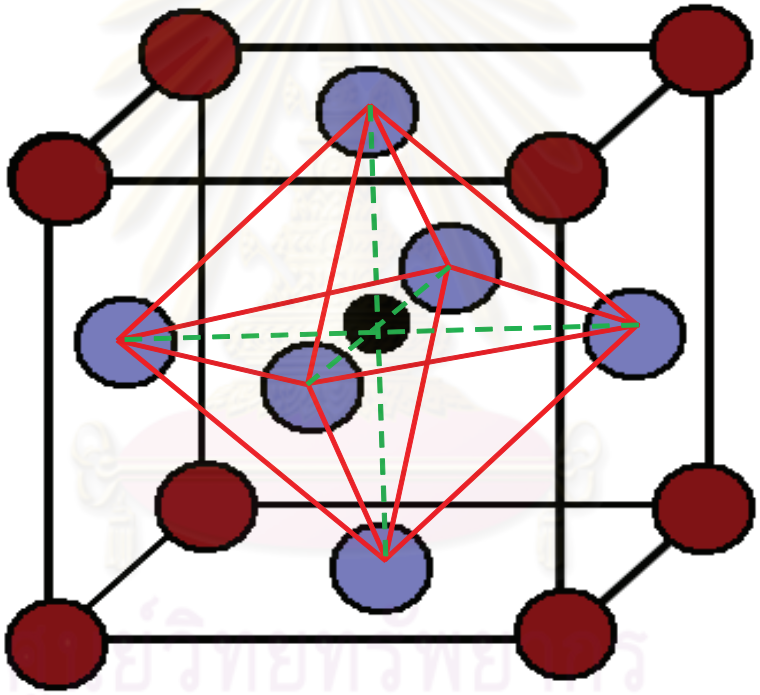

Figure 2.1: Unit cell structure of the BTO, with Ba atom in dark red, Ti atom in black and O atom in blue.

### 2.1.2 Fe-doped barium titanate (Fe-doped BTO)

Many research groups have been interested in optical properties of Fe-doped BTO. In 2002, Maier et al. studied structural and physical properties of ferroelectric and ferrimagnetic on $BaFe_xTi_{1-x}O_3$ (BFTO) thin film with $0.5 \leq x \leq 0.75$ and compared with those of BTO films under identical conditions [25]. They found that the replacement of 50% or more of Ti by Fe deteriorates the crystalline quality, leading to ferrimagnetic ordering well above room temperature, and BTO could be converted from an n-type to a p-type semiconductor. Stashans et al. investigated simulation of iron impurity in BTO crystals. They found that the equilibrium spatial configurations obtained for both cubic and tetragonal structures change in atomic interaction between the impurity atom and its surrounding O atoms. It is observed that the Fe atom has practically only covalent bonding with the four O atoms situated around it within the xy plane, while the interaction with the two oxygens along the z-axis is purely ionic [26].

### 2.1.3 Calcium copper titanate (CCTO)

Calcium copper titanate ($CaCu_3Ti_4O_{12}$) is a perovskite-like body centered cubic structure with a lattice parameter a = 7.391 Å [27]. Home et al. found that there were no any structural phase transition of CCTO from 100 K to 600 K [28]. Figure 2.2 shows the unit cell of CCTO, where Ca and Cu ions are occupied at A-sites and Ti cations reside at the B-site. CCTO has been studied in many research group due to its high dielectric constant about $10^4$ for polycrystal [29, 30, 31] and $10^5$ for single crystal [29] at room temperature. The high dielectric constant properties of CCTO are important in designing novel microelectronics such as microelectronic devices [30, 32, 33], memory devices [31], dynamic random access memories [31].

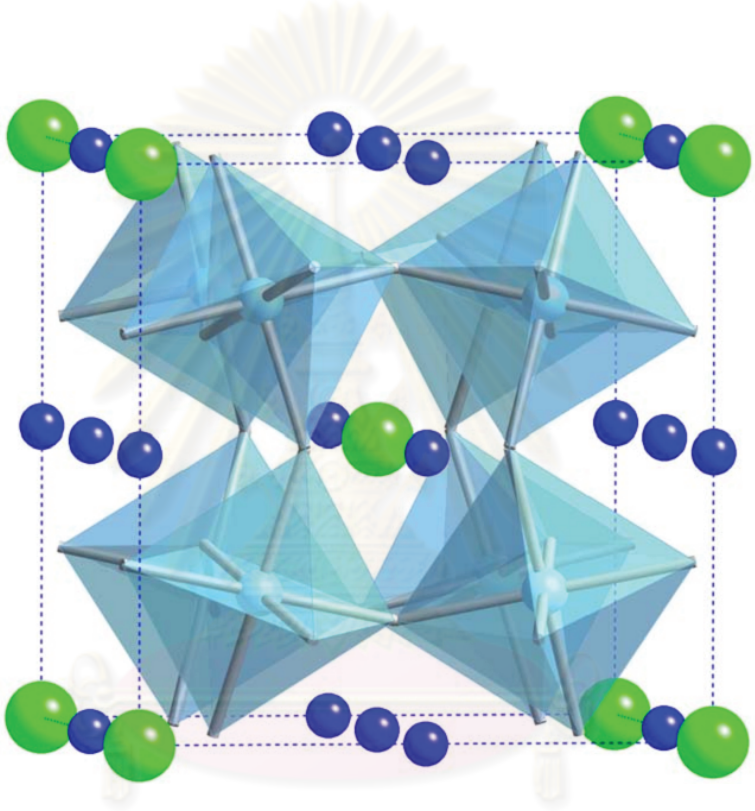

Figure 2.2: Unit cell structure of CCTO, with Ca atom in green, Cu atom in blue and $TiO_6$ octahedral in teal [27].

### 2.1.4 Fe-doped calcium copper titanate (Fe-doped CCTO)

In 2009, Krohns et al. showed correlations of structural, magnetic, and dielectric properties of undoped and doped CCTO [34]. They reported that dielectric constant of CCTO versus temperature increase after $CaCu_3Ti_{4-x}Fe_xO_{12}$ in the frequency range from 1 kHz to 1 MHz. The intrinsic relaxation showing up at higher temperatures in Fe-doped CCTO seems to correspond to the single intrinsic relaxation observed in the Mn-doped sample.

## 2.2 Sol-Gel processing

The definition of *sol* and *gel* will be mentioned before we described about sol-gel process. A *sol* is a colloidal suspension of solid particles in a liquid and *gel* is a substance that contains a continuous solid skeleton enclosing a continuous liquid phase. *Gel* can also be formed from particulate sols [35], when attractive dispersion forces cause them to stick together in such a way as to from a network polymers. A precursor (starting material) of the sol-gel process for preparation consist of a metal or metalloid element surrounded by various ligands (ligand is an ion or molecule that bond a central metal atom). Metal alkoxides are popular precursors because they react with water. The first step of a reaction is called hydrolysis as in the following reaction;



$$M(OR)_4 + H_2O \rightarrow HO - M(OR)_3 + ROH \tag{2.1}$$

where $R$ represents a ligand and $ROH$ is an alcohol; $M$ is metal;
the bar (-) indicates a chemical bond. Depending on the amount of water and catalyst are present, hydrolysis may go to completion (so that all of the $OR$ groups are replaced by $OH$)

$$M(OR)_4 + 4H_2O \rightarrow M(OH)_4 + 4ROH \tag{2.2}$$

and then two partially hydrolyzed molecules can link together in a condensation reaction;

$$(OR)_3M - OH + HO - M(OR)_3 \rightarrow (OR)_3M - O - M(OR)_3 + H_2O \quad (2.3)$$

or

$$(OR)_3M - OR + HO - M(OR)_3 \rightarrow (OR)_3M - O - M(OR)_3 + ROH \quad (2.4)$$

By definition, condensation creates a small molecule (such as water or alcohol). This reaction can continue to build larger and larger metal containing molecules by the process of polymerization. Followed by drying process, the water or alcohol form the condensation process is removed and then a volume reduction takes place. In this process the drying temperature should be high enough to remove the free alcohol, water, catalyst and other compound. The common temperature used in preheat process is about 100 $^{o}$C - 200 $^{o}$C [36, 37]. Most gels are amorphous (much noncrystalline), even after drying, but they could turn to be crystalline with heating at higher temperatures [36, 37]. It is necessary to heat or sinter the gel to a high enough temperature to produce crystalline material. Sintering is a process of collapse of pores driven by surface energy. Material moves by viscous flow or diffusion to eliminate porosity and reduce the solid-vapor interfacial. In amorphous materials, transport of atoms occurs by viscous flow; in crystalline materials sintering involves diffusion. For crystalline gels there are the further complications of grain growth and phase transformation.

## 2.3 Gamma ray

Gamma ray is an electromagnetic (EM) radiation as shown in Fig. 2.3. EM radiation differs in frequency and energy.

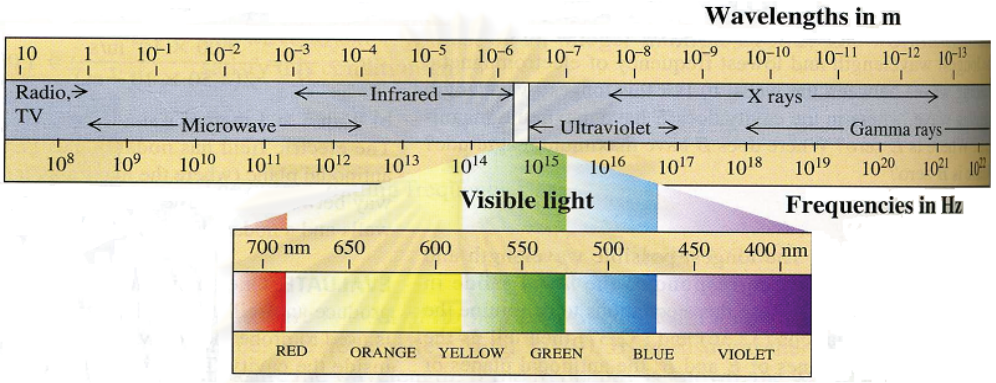


Figure 2.3: The electromagnetic spectrum.

From Fig. 2.3, gamma rays have the wavelength less than $10^{-10}$ nm and the frequency more than $10^{18}$ Hz, respectively. They have the energy more than 10 keV and therefore they can penetrate more than other radiations such as alpha and beta rays [38]. Gamma ray was produced when a nucleus is placed in an excited state, either by bombardment with high energy particles or by a radioactive transformation, it can decay to the ground state. This process is called gamma decay shown in equation 2.5 for $^{60}$Co.

$$^{60}Co^{*} \rightarrow ^{60}Co + \gamma \tag{2.5}$$

where $^{60}$Co$^{*}$ is an excited state; $^{60}$Co is a ground state and $\gamma$ represent gamma ray.

## 2.4 Interactions between gamma ray and materials

High energy electromagnetic radiation or high energy particles, such as X-rays, gamma rays, electron or neutron bombardment could change the physical properties of materials. Defects in material could be created when the high energy electromagnetic or particles have enough energy to overcome the Coulomb force between ions and break the chemical bond. A negative ion could be removed and this ion vacancy can subsequently trap an electron. This process is called oxygen vacancies (known as colour centers) or F centres (from Farbe, the German word for colour) presented in oxide material in form of Schottky or Frenkel defects. The colour centres are produced during high energy irradiation and they annihilated under the room temperature. Point equilibrium of colour centres for individual material depending on one particular dose rate and parameters of the material such as thickness [39] and dopant [39] can predict the behavior of those materials under different doses. There are two types of defects in barium titanate; the type that preserves the stoichiometry (Schottky) and the type that changes the stoichiometry that occurs at the dopant substituted cells. Oxygen vacancy defects are commonly found in $BaTiO_3$ due to an insufficient oxygen supply during the film processing [40]. Intrinsic Schottky defects in BTO are believed to form according to the following process: [15].

$$Ba_{Ba} + Ti_{Ti} + 3O_o \Rightarrow V''_{Ba} + V''''_{Ti} + 3V_o^{\bullet\bullet} + Ba_s + Ti_s + 3O_s \qquad (2.6)$$

where $Ba_{Ba}$, $Ti_{Ti}$, $3O_O$ are occupied $Ba$, $Ti$ and $O$ sites, respectively, $V''_{Ba}$, $V''''_{Ti}$ and $3V_o^{\bullet\bullet}$ are vacancies of $Ba$, $Ti$ and $O$ atoms, respectively, and $Ba_s$, $Ti_s$ and $3O_s$ are the Schottky defects, respectively.

For CCTO under gamma irradiation;

$$Ca_{Ca}+3Cu_{Cu}+4Ti_{Ti}+12O_O \Rightarrow V''_{Ca}+3V''_{Cu}+4V''''_{Ti}+12V_O^{\bullet\bullet}+Ca_s+3Cu_s+4Ti_s+12O_s \quad (2.7)$$

where $Ca_{Ca}$, $3Cu_{Cu}$, $4Ti_{Ti}$, $12O_O$ are occupied $Ca$, $Cu$, $Ti$ and $O$ sites, respectively, $V''_{Ca}$, $3V''_{Cu}$, $4V''''_{Ti}$ and $12V_o^{\bullet\bullet}$ are vacancies of $Ca$, $Cu$, $Ti$ and $O$ atoms, respectively, and $Ca_s$, $3Cu_s$, $4Ti_s$ and $12O_s$ are the Schottky defects, respectively.

Note that the notation from equation 2.6 and 2.7 is called Kröger-Vink notation, where $A_A$ indicates that A-atom on an A-site; $V_A$ denotes a vacancy on A-site; positive charge is marked by a point (e.g. $V^{\bullet}$), negative charge is marked by a hyphen or dash (e.g. $V'$) to distinguish this relative charge from the absolute charge.

## 2.5 Thickness determination from transmission data

A method proposed in this thesis is to determine the thickness from the interference fringes of the transmission spectra. The concept of this method is based on the interference between the light reflecting from the film surface (1) and from the film-substrate interface (2) as shown in Fig. 2.4. The simplest ideal case to obtain perfect transmission spectra is that the film is perfectly flat and has a uniform thickness. The transmission (T) of the system depends on the parameters such as the optical constants, the film thickness, the wavelength of the light and the indices of refraction ($n$) of substrate and the medium above the film. In this thesis, we used quartz which 1 mm thick as substrate at which $n$ is about 1.47 at 532 nm whereas that for Fe-doped BTO is about 1.85 and for Fe-doped CCTO is about 1.95 at the same wavelength used quartz as blank substrate in the

optical transmission experiment due to its high melting temperature point and transparency, respectively.

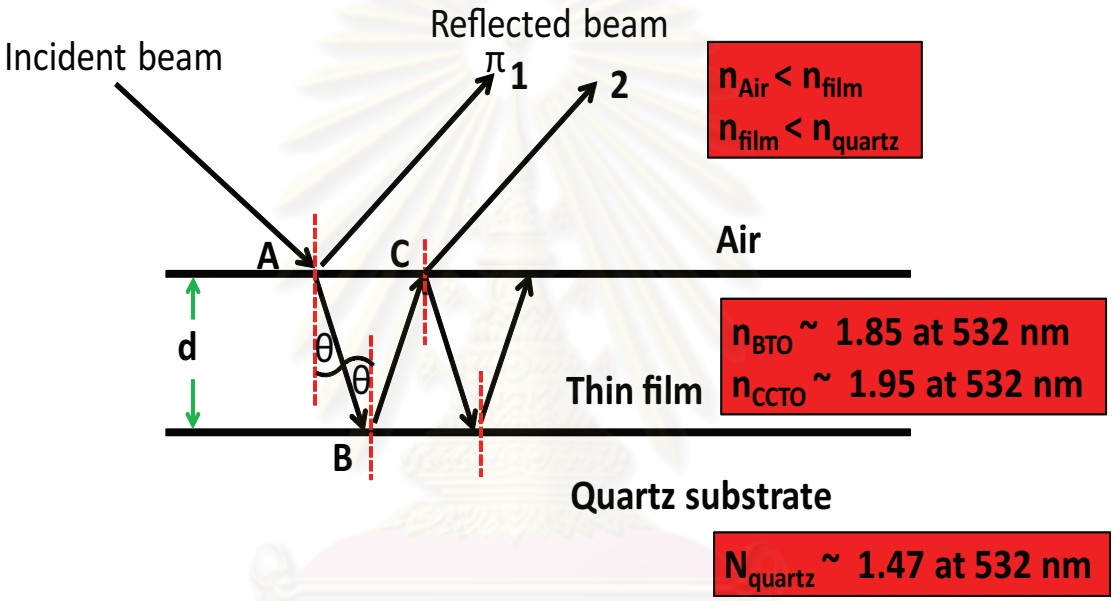


Figure 2.4: Interference between light reflecting from the film surface (1) and from the film-substrate (2) interface.

A wave traveling from a medium of refractive index $n_1$ toward a medium of refractive index $n_2$ undergoes a $180^o$ phase change upon reflection when $n_2 > n_1$ and no phase change if $n_2 < n_1$. The wavelength of light $\lambda_n$ in a medium whose refractive index $n$ is

$$\lambda_n = \frac{\lambda}{n} \tag{2.8}$$

where $\lambda$ is the wavelength of light in free space.

Since $n_{air} < n_{thinfilm}$, the reflected beam at the point A, which reflected from the upper film surface, has phase change $180^o$ or $\pi$. The beam 2, which is reflected from the lower surface film at the point B and then transmitted through the film at the point C, have no phase change because of $n_{thinfilm} > n_{quartz}$ at the point C. Therefore, the beam 1 has the phase change of $180^o$ relative to the beam 2. The path difference between beam 1 and beam 2 is equal to $2d\sin\theta$. When $\theta$ is small angle or the light perpendicular with the film surface, we get the condition for destructive interference

$$2n_{film}d = m\lambda \tag{2.9}$$

where m = 0, 1, 2, ....

The condition for constructive interference is

$$2n_{film}d = (m + \frac{1}{2})\lambda \tag{2.10}$$

where m = 0, 1, 2, ....

In Fig. 2.5, at long wavelengths (photon energies less than the band gap), the transmission (T) shows oscillations from interference effects in the transparent film. At short wavelength (photon energies greater than the band gap), the transmitted light intensity decreases to zero.

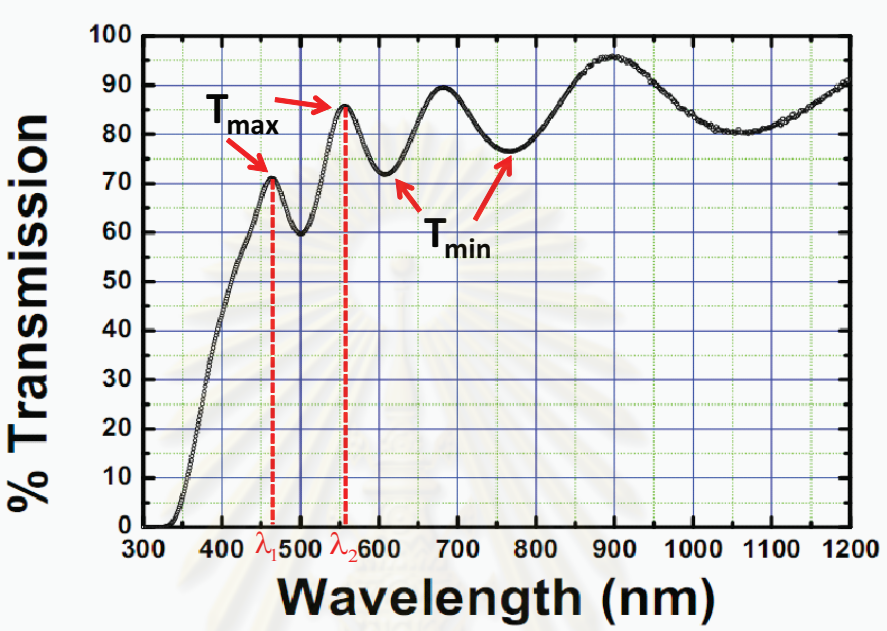


Figure 2.5: The transmission spectra of Fe-doped BTO films with 8 layers.

The notation of $T_{max}$ and $T_{min}$ refer to the value of the maximum and minimum in T. From equation 2.9, when we consider two maxima of the transmission patterns according to wavelengths $\lambda_1$ and $\lambda_2$, we can write

$$2n_{film}d = (m + \frac{1}{2})\lambda_1 \tag{2.11}$$

$$2n_{film}d = (m + \frac{1}{2})\lambda_2 \tag{2.12}$$

From equation 2.11 and 2.12, we can solve for the film thickness (d) as follows:

$$d = \frac{\lambda_1\lambda_2}{2[n(\lambda_1)\lambda_2 - n(\lambda_2)\lambda_1]} \tag{2.13}$$

## 2.6 Dielectric properties

In this section, we are interested in fundamentals of linear dielectric properties of matter. The relation between the dielectric constant and the dipole moment stating with the displacement field $\overrightarrow{D}$ is shown in equation 2.14

$$\overrightarrow{D} = \varepsilon_0 \overrightarrow{E} + \overrightarrow{P} \tag{2.14}$$

where $\overrightarrow{E}$ is macroscopic electric field, $\varepsilon_0$ is the vacuum permittivity and $\overrightarrow{P}$ is the macroscopic polarization. The polarization $\overrightarrow{P}$ and the electric field $\overrightarrow{E}$ are related to

$$\overrightarrow{P} = \varepsilon_0 \chi \overrightarrow{E}$$

where $\chi$ is the susceptibility. Substituting for $\overrightarrow{P}$ in equation 2.14

$$\overrightarrow{D} = \varepsilon_0 (1 + \chi) \overrightarrow{E}$$

This allows to define the material's permittivity, $\chi$, and dielectric constant, $\varepsilon'$:

$$\varepsilon = \varepsilon_0 (1 + \chi) \rightarrow \varepsilon' = \frac{\varepsilon}{\varepsilon_0} = (1 + \chi) \tag{2.15}$$

writing $\overrightarrow{D} = \varepsilon_{\ 0}\, \varepsilon' \overrightarrow{E}$ and substituting in equation 2.14, we get

$$\varepsilon' - 1 = \frac{P}{\varepsilon_0 E} = \frac{M}{\varepsilon_0 V E} \tag{2.16}$$

where the polarization has been replaced with the total dipole moment of the sample ($M$) divided by the volume ($V$).

# CHAPTER III

# CHARACTERIZATION TECHNIQUES

Our films were characterized using various techniques such as X-ray diffractometry, field emission scanning electron microscopy, atomic force microscopy and optical spectroscopy, respectively. X-ray diffraction technique were used to study crystal structure of the films including the contamination substances which could be found in the films during the film processing. The compositions of the films were obtained using a wavelength dispersive X-ray spectrometer (WDX) equipped with an electron probe microscopic spectrometer (EPMS) and energy dispersive X-ray spectrometer (EDX) equipped with field emission scanning electron microscopy (FSEM: HITASHI model S-4700) . The roughness of our films are determined by atomic force microscopy (AFM). The optical transmittance spectra of the films were measured using UV-VIS-NIR spectrometer. The refractive index and the extinction coefficient before and after gamma irradiation as a function of the gamma dose were extracted from the transmittance spectra using the envelope method [41]. The band gap was also calculated from the transmittance spectra using the Tauc relation [42].



## 3.1 X-ray diffraction

X-rays is the electromagnetic radiation with energies in the range of 100 eV - 100 keV. X-ray was discovered by Wilhelm Röntgen. X-ray techniques provide important tools for scientists and researchers and use in the field of material characterization. X-ray diffractometers are used for the study of mineral deposits, thin

films and phase transformations. The wavelength of X-rays suitable for measuring the crystal structure is in the range from 0.5 Å to 3 Å that is comparable to the size of atom. In general, the X-ray wavelength value depends on a type of the target used as the anode in a vacuum tube. For example, the X-ray which has a wavelength of 1.54 Å are produced by accelerated electron beam with high voltage collided with the Cu target. When the X-ray incident beam falls onto a crystal, the beam are diffracted. The angle of incidence formed by a ray incident on a surface and a perpendicular to the surface at the point of incident is equal to the reflection angle which is measured from the reflected ray to the surface normal.

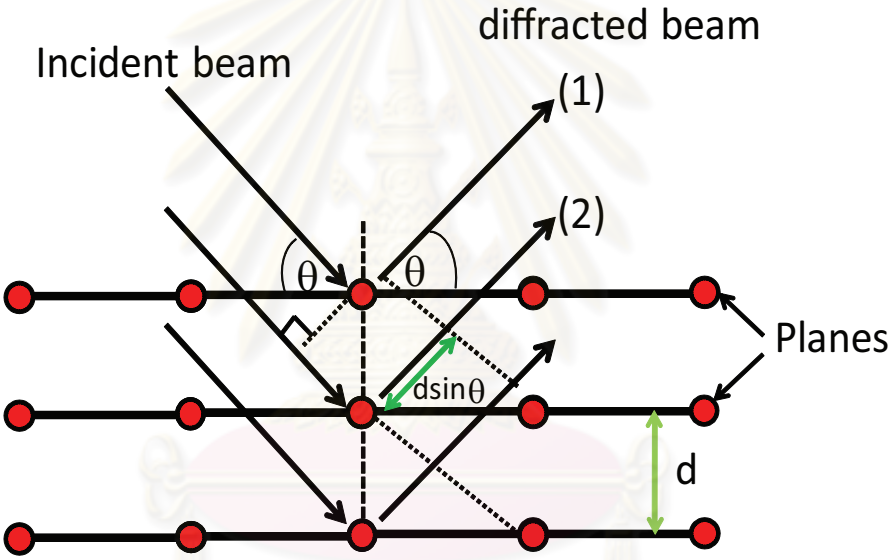


Figure 3.1: X-ray diffraction from crystal structure by Bragg'law.

From Fig. 3.1, when the path difference between path(1) and path(2) equals to an integer number, n times $\lambda$, constructive interference will occur

$$2d\sin\theta = n\lambda \tag{3.1}$$

where $d$ is a spacing between successive atomic planes in the crystal; $\theta$ is the incident angle between the lattice plane and the incident beam; $\lambda$ is wavelength of X- ray beam; n is an integer number.

Equation 3.1 is known as Bragg's law. The constructive interference signals can be detected by a detector in form of intensity at varied diffraction angles ($2\theta$). For the same element or material, the intensity of the constructive is the highest at the same diffraction angle. The interplanar spacing of ($hkl$) planes can be defined by d = $d_{hkl}$, where $h$, $k$ and $l$ are Miller indicies. The relationship between the Miller indicies, lattice constants (a,b,c) and interplanar spacing for BTO of tetragonal phase and CCTO of the cubic structure can be shown in equation (3.2) and equation (3.3), respectively.

$$\frac{1}{d^2} = \frac{h^2 + k^2}{a^2} + \frac{l^2}{c^2} \tag{3.2}$$

$$\frac{1}{d^2} = \frac{h^2 + k^2 + l^2}{a^2} \tag{3.3}$$

For standard BTO, the lattice constants equal to 0.3994 nm for a and b and 0.4038 nm for c [24], respectively. The lattice constants of standard cubic CCTO are a = b = c = 0.73798 nm [27].

## 3.2 Wavelength dispersive X-ray spectroscopy

A wavelength dispersive X-ray spectrometry (WDX) was the original microprobe spectroscopy technique developed to measure X-ray intensities and determine chemical compositions of sample. The main point of the electron microprobe is crystals with specific lattice spacing as shown in table 3.1.

X-rays are produced after an accelerated electron beam collides with the sample. All X-ray will emit at the angle ($\psi$) to enter the WDS spectrometer. X-ray of each element has a distinct wavelength, and by adjusting the angle of the crystal in the spectrometer, it will diffract the wavelength according to Bragg's law from equation 3.1. The diffraction of X-rays are directed into the detector (proprotional counter tube), which has a thin wire at a middle. The reflected X-rays

Table 3.1: Several crystals used in the wavelength dispersive spectrometer.

| Crystal | Plane of crystal | lattice spacing |
|---|---|---|
| LiF | (200) | 2d = 4.027Å |
| $SiO_2$ | (1011) | 2d = 6.686Å |
| PG (pyrolytic graphite) | (002) | 2d = 6.71Å |
| PET (pentaerythritol) | (002) | 2d = 8.742Å |
| ADP (ammonium dihydrogen phosphate) | (101) | 2d = 10.64Å |
| KAP (potassium hydrogen phthalate) | (1010) | 2d = 26Å |

to the detector are different by changing the position of crystals relative to the sample. The sample, crystals and detector are lied on a Rowland circle in order to focus X-ray efficiently. The X-rays are absorbed by gas molecules in the proportional counter tube, photoelectrons is emitted in this process. Photoelectrons are accelerated to a wire in order to add ionization. Two general types of detectors are used to seal and flow of gas to the counter. The seal of proportional counters have a thick window that protects leakage of gas in the detector. Another one is the gas flow proportional counter which have thin window. The X-ray intensities of each element of sample are counted in a detector at a specific beam current, the count rates are compared to those of standards containing known values of the elements of sample.

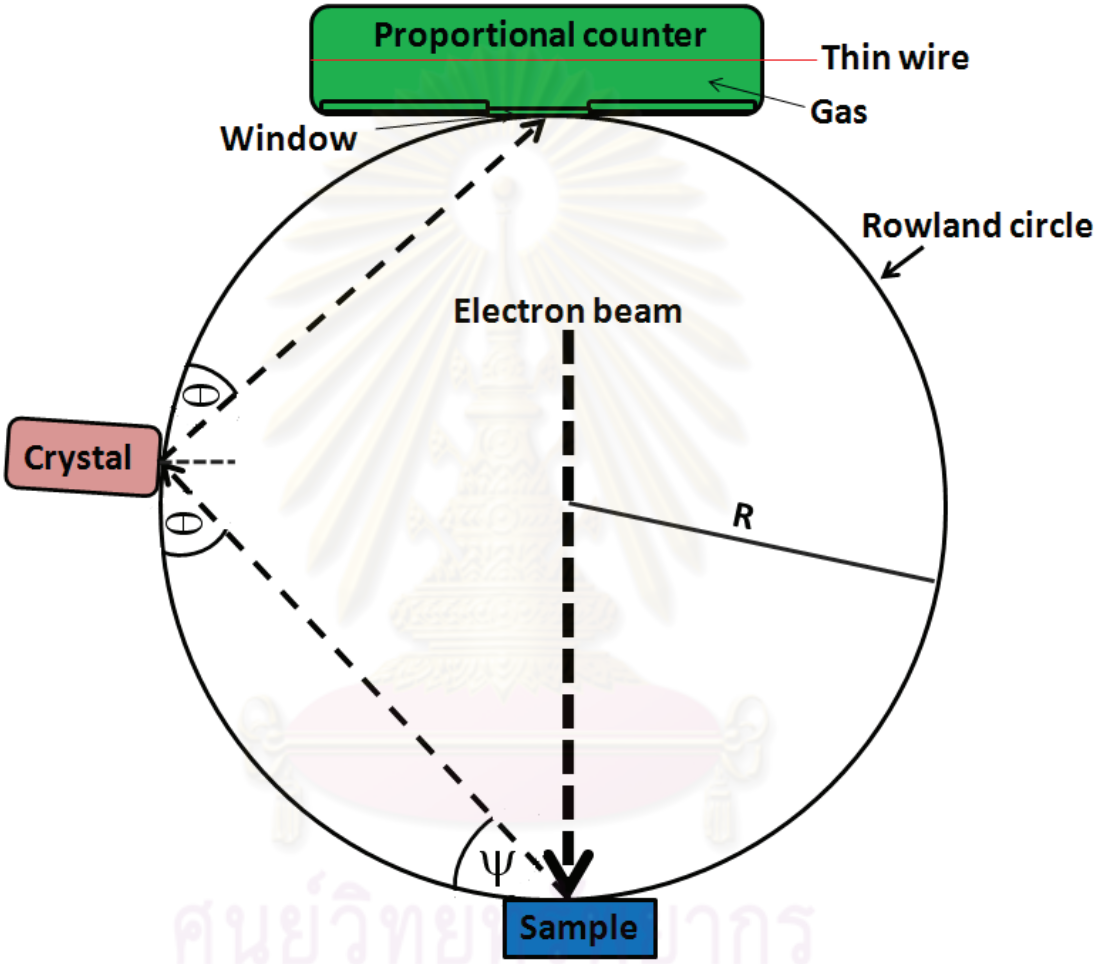


Figure 3.2: Configuration of sample, analytical crystal and detector on the Rowland circle within the WDX spectrometer.

## 3.3 Energy dispersive X-ray spectroscopy

Energy dispersive X-ray spectroscopy (EDX) is an analytical technique used for the elemental analysis or chemical characterization of a sample. It is one of the variation of X-ray fluorescence spectroscopy which depends on the investigation of a sample through interactions between electromagnetic radiation and the matter. Its characterization ability are exactly in large part to the fundamental principle that each element has a unique atomic structure allowing X-rays that are characteristic of an element's atomic structure to be identified uniquely from one another. To stimulate the emission of characteristic X-rays from a specimen, a high-energy beam of charged particles such as electrons or protons, or a beam of X-rays, is focused into the sample being studied. At rest, an atom within the sample contains ground state electrons in discrete energy levels or electron shells bound to the nucleus. The incident beam may excite an electron in an inner shell, ejecting it from the shell while creating an electron hole where the electron was. An electron from an outer, higher-energy shell then fills the hole, and the difference in energy between the higher-energy shell and the lower energy shell may be released in the form of an X-ray as shown in Fig. 3.3. The number and energy of the X-rays emitted from a specimen can be measured by an energy dispersive spectrometer. As the energy of the X-rays are characteristic of the difference in energy between the two shells, and of the atomic structure of the element from which they were emitted, this allows the elemental composition of the specimen to be measured.

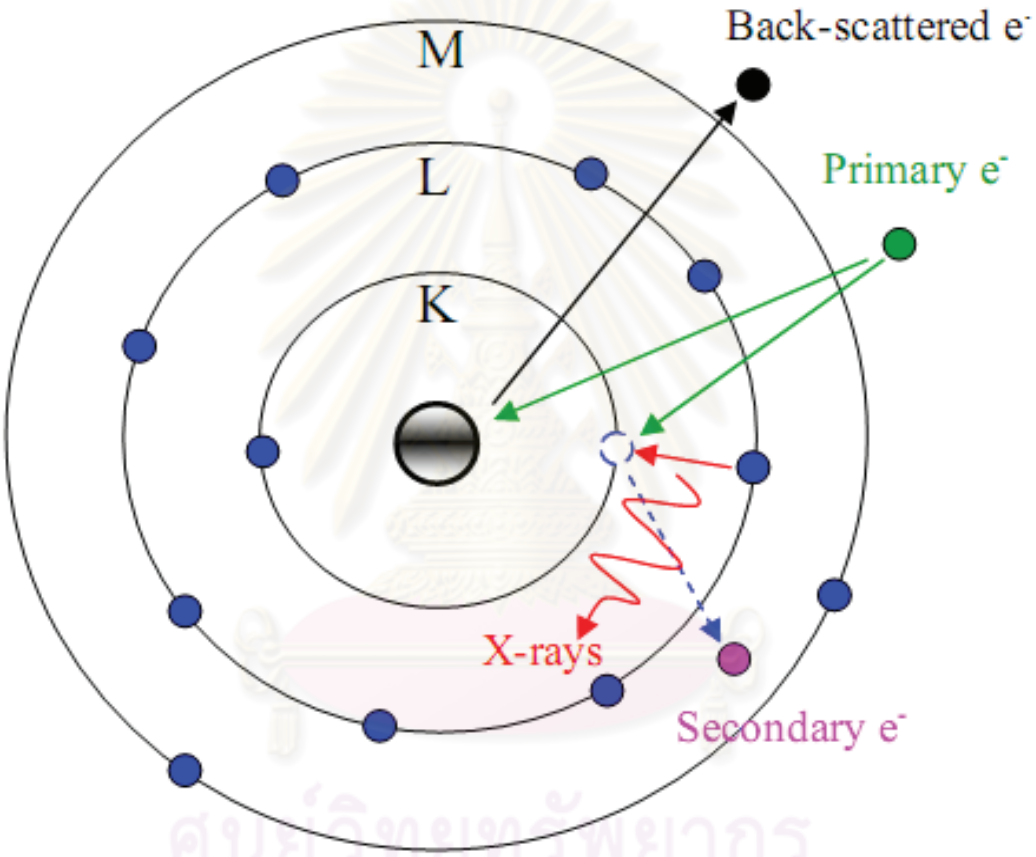


Figure 3.3: Schematic drawings of the x-ray radiation from an atom.

## 3.4 Atomic force microscopy

Atomic Force Microscopy (AFM) is one of the most useful instruments for characterizing surface morphology of materials. The force most commonly associated with atomic force microscopy is an interatomic force called the van der Waals force. AFM process did not use lens and the sample preparation is not difficult. The key of AFM is a cantilever arm. A laser beam is directed toward the back of the cantilever. A sharp tip is on the free end of the cantilever which has a spring constant of the order of 1 N/m. A laser beam reflects off the end of the cantilever onto a photodetector.

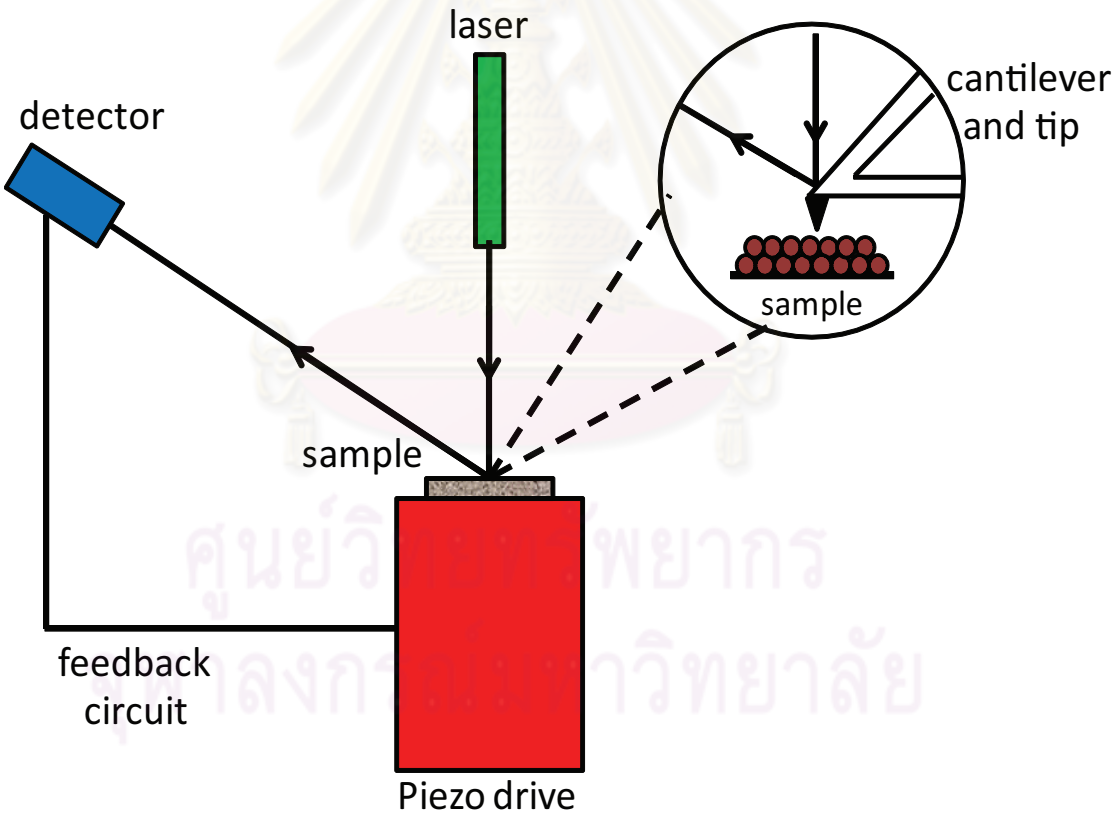


Figure 3.4: Schematic of the atomic force microscope.

The photodetector senses the deflection of cantilever beam as the atom of the sharp tip interacts with the surface atom of the sample. The process of AFM is shown in Fig. 3.4. A piezoelectric scanner pulls the probe across the surface to be imaged. The changes in surface topography cause the probe tip to move up or down, the photodetector senses the motion, and the microscope's computer translates the deflection to surface information in three-dimension. Sample must be cleaned before taking measurements. The interaction force between the cantilever and the sample is replusive when the tip is too close to the sample surface as shown in Fig. 3.5.

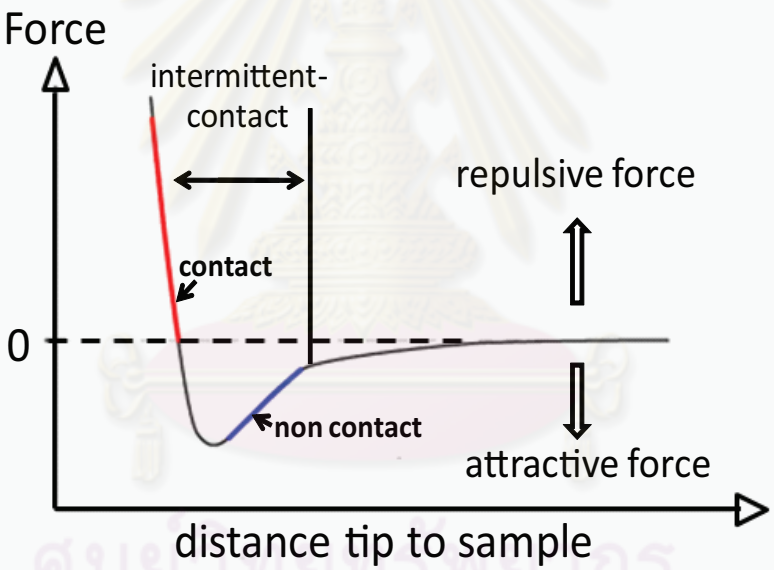


Figure 3.5: AFM operating force regions.

Repulsive forces increase as the probe begins to contact the surface. The repulsive forces in the AFM tend to cause the cantilever to bend up. In the non contact regime, the cantilever is held on the order of 10-100 Å at the resolution in x-y plane range from 0.1 to 1.0 nm and the z direction is 0.01 nm known as atomic resolution. The atomic force between the cantilever and the sample is attractive when the the tip is too far to the sample surface. Attractive forces near the surface are caused by a nanoscopic layer of contamination that is present on all surfaces in surrounding air. The amount of contamination depends on the environment in which the microscope is being operated. In the intermittent contact regime, the vibrating cantilever tip is brought closer to the sample so that the tip just taps the sample. Changing tips and techniques can also provide difference information. The intermittent contact mode or tapping mode was used in this thesis. In tapping mode AFM the cantilever is oscillating close to its resonance frequency. The tips mainly used for tapping mode are silicon probes.

## 3.5 Optical transmission

The optical measurement method is mostly considered to be quick, easy and nondestructive. The principle is based on the interference of two beams of light which the optical path difference is related to the films thickness [43, 44]. The derivation of the thickness of thin film from the transmission spectra was shown in section 2.5. The films need to be grown on a transparent substrate such as glass slices [41] and quartz [45] in order to detect the transmitted beam.

The schematic diagram of the optical system is shown in Fig. 3.6. There are two radiation sources, a deuterium lamp (DL) and halogen lamp (HL) to cover the whole wavelength range of the spectrometer. The operation of optical system can be described as the following.

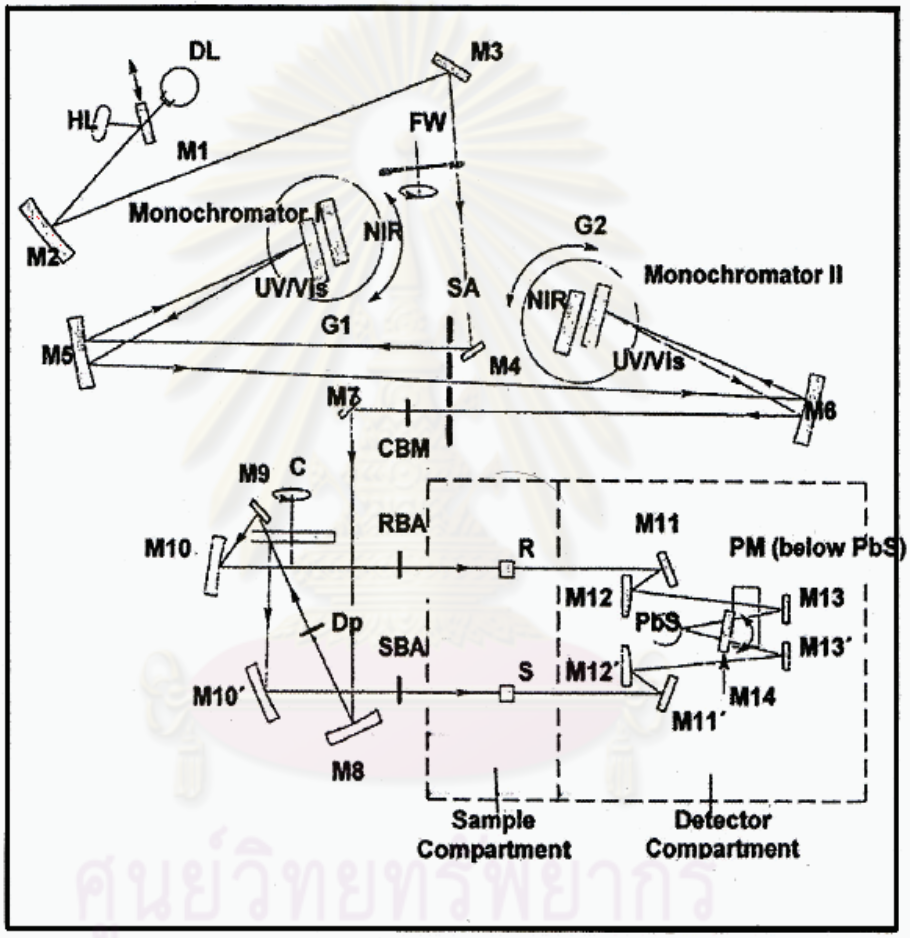


Figure 3.6: Schematic of optical system.

For the operation in the near infrared (NIR) and visible (VIS) ranges, the radiation from halogen lamp is reflected from mirror M1 to M2. At the same time, it blocks the radiation from deuterium lamp. For operation in the ultraviolet (UV) range, mirror M1 is raised to permit radiation from the deuterium lamp to mirror M2. Radiation from the respective source lamp is reflected from mirror M2 to mirror M3 through an optical filter wheel assembly (FW) to mirror M4. The radiation is reflected through the entrance slit of monochromator I, which collimates the radiation. The collimated radiation is reflected at the grating G1. Depending on the current wavelength range, the collimated radiation beam strikes either the UV/VIS grating or the NIR grating.

The radiation is dispersed at the grating to produce a spectrum. The rotational position of the grating effectively selects a segment of spectrum, reflecting this segment to mirror M5 and then through the exit slit serving as the entrance slit of Monochromator II. The radiation is reflected via mirror M6 to the grating on grating table G2 and then back via mirror M6 through the exit slit to mirror M7. The rotational position of grating table G2 is synchronized to that of G1. From mirror M7 the radiation beam is reflected via mirror M8 to the chopper assembly (C).

The chopper separates the radiation into two beams. As the chopper rotates, especially, a mirror segment and a window segment, are brought alternately into the radiation beam. When a window segment enters the beam, radiation passes through to mirror M9 and is then reflected via mirror M10 to create the reference beam (R). On the other hand, when a mirror segment enters, the beam of radiation is reflected via mirror M10́ to from the sample beams (S).

In the sample compartment, a clean substrate is used as a reference and the sample is thin film coated on one side of substrate. The radiation beam passing alternatively through the sample and a reference are reflected by M11, M12, M13 and M11́, M12́, M13́ of the optics in the detector assembly. Mirror M14 is rotated to select the appropriate detector. A photomultiplier (PM) is used in the UV/VIS range while a lead sulfide (PbS) detector is used in the NIR range.

The optical transmission of the films were measured in the percentage ratio of the intensity of the beam passing through the sample to the beam passing through the blank substrate ($I_0$) as shown in Fig. 3.7. The incoming beam is incident normally on the surface of the sample and the reference substrate. The detectors measured the intensity of transmitted beam ($I_t$ and $I_0$), and the percentage of optical transmission can be expressed as

$$T(\%) = \frac{I_t}{I_0} \times 100 \tag{3.4}$$

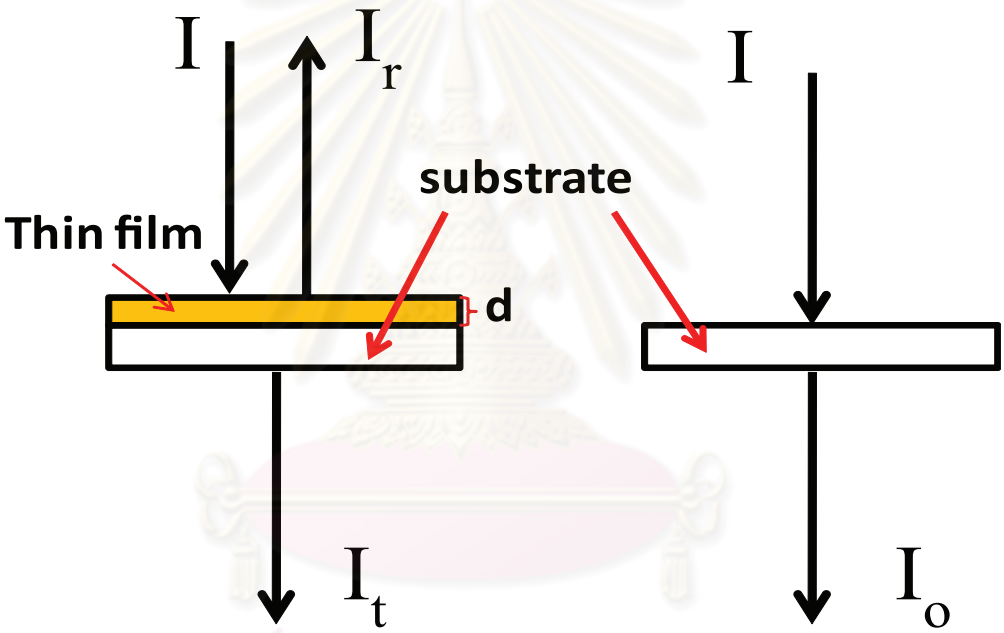


Figure 3.7: Schematic drawing of optical transmission measurement.

The absorbtion coefficient can be calculated directly from the transmission of the films. The transmittance (T) and the reflectance (R) can be expressed in terms of the intensity of transmitted wave $I_0$ from blank substrate, intensity of transmitted wave $I_t$ from thin film and intensity of reflected wave $I_r$ as the followings;

$$T = \frac{I_t}{I_0} = \frac{(1-R)^2 e^{-\alpha d}}{1 + R^2 e^{-2\alpha d}} \tag{3.5}$$

$$R = \frac{I_r}{I_0} = \frac{(n-1)^2 + k^2}{(n+1)^2 + k^2} \tag{3.6}$$

where $\alpha$ is the absorption coefficient; $d$ is the thickness of the film; $n$ is refractive index and $k$ is extinction coefficient.

If the film has a large thickness (d), then

$$R^2 e^{-2\alpha d} \ll 1$$

and equation 3.6 can be reduced to

$$T = (1-R)^2 e^{-\alpha d} \tag{3.7}$$

In general, the changing of photon energy of incident wave affects the reflection (R) slightly. Then, the term $(1\text{-}R)^2$ can be approximated to a constant. From equation 3.7, the absorbtion coefficient is

$$\alpha = \frac{1}{d} In(\frac{I_0}{I_t}) + C \tag{3.8}$$

where $d$ is the thickness of the film and $C$ is a constant.

### 3.5.1 Complex refractive index ($n$ and $k$) and absorption coefficient

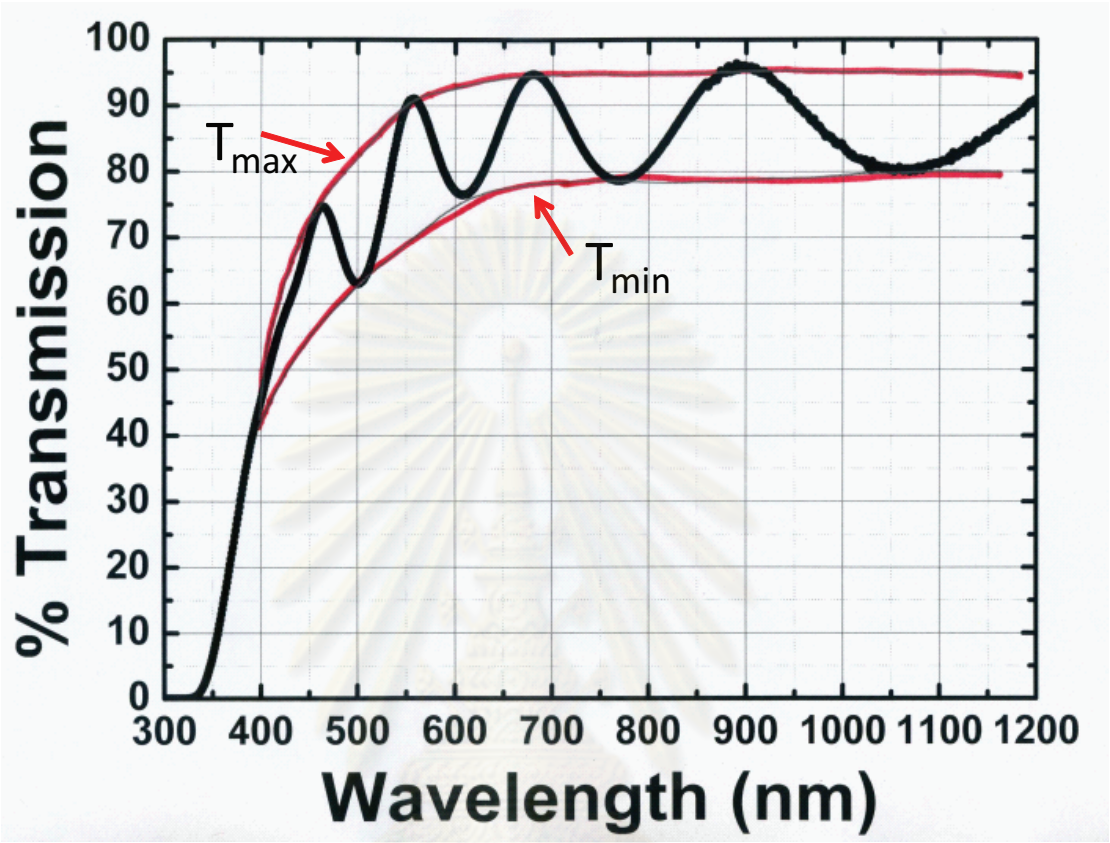


Figure 3.8: Schematic drawing envelope of optical transmission measurement.

When the film has a uniform thickness, the oscillation of transmission spectra can be clearly observed as shown in Figure 3.8. The refractive index can be obtained using an envelope method [41];

$$n(\lambda) = [N + (N^2 - n_s^2)^{1/2}]^{1/2} \tag{3.9}$$

where

$$N = (\frac{n_s^2 + 1}{2}) + 2n_s^2(\frac{T_{\max} - T_{\min}}{T_{\max}T_{\min}})$$

$n_s$ is the refractive index of the substrate, $T_{\max}$ and $T_{\min}$ are the maximum and

minimum transmittances see in Fig. 3.8. The extinction coefficient can be obtained from

$$k = \frac{\alpha\lambda}{4\pi} \tag{3.10}$$

where $\alpha$ is the absorption coefficient;

$$\alpha = \frac{1}{d}\ln\frac{(n-1)(n_s-n)[1+(\frac{T_{\max}}{T_{\min}})^{\frac{1}{2}}]}{(n+1)(n_s+n)[1-(\frac{T_{\max}}{T_{\min}})^{\frac{1}{2}}]}$$

$d$ is the film thickness.

### 3.5.2 Band gap energy

The band gap was also calculated from the transmittance spectra using the Tauc relation [42]. From the transmittance spectra, the energy for the direct gap could be calculated by using the equation

$$(\alpha h\nu)^2 = B(h\nu - E_g) \tag{3.11}$$

where $\alpha$ is the absorption coefficient calculated from equation 3.8, h$\nu$ is the photon energy, $E_g$ is the energy gap as shown in Fig. 3.9 and B is a constant. By plotting $(\alpha \mathrm{h}\nu)^2$ versus h$\nu$, the energy band gap can be obtained from the intercept of graph for direct allowed transition. The photon energy at the point where $(\alpha \mathrm{h}\nu)^2 = 0$ is the energy gap of which value is determined by the extrapolation method. The extrapolation of the linear segment of the spectrum or curve towards the x-axis gives the value of energy gap.

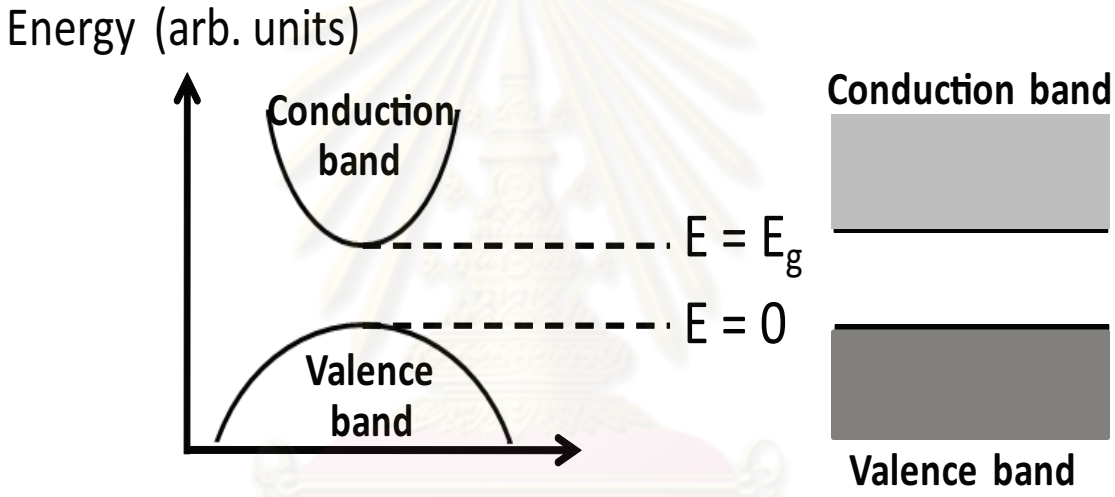


Figure 3.9: Schematic of band diagram.

Fig. 3.10 shows the band diagram of (a) n-type semiconductor and (b) p-type semiconductor, respectively. When an impurity atom with more valence electrons substitutes the atom in lattice inducing electron carriers as major carriers ($n \gg p$), this material is so called n-type semiconductor. In Fig. 3.10(a), n-type semiconductor yields electrons to the conduction band. While the p-type semiconductor occurs when an impurity atom with less valence electrons substitutes the atom in lattice. The state corresponding to the missing electrons is therefore the holes. The number of holes similar to the number of impurities is created. Consequently, the impurities called acceptors, can create holes in the valence band. In Fig. 3.10(b), the impurity levels can be presented at an acceptor level above the valence band edge.

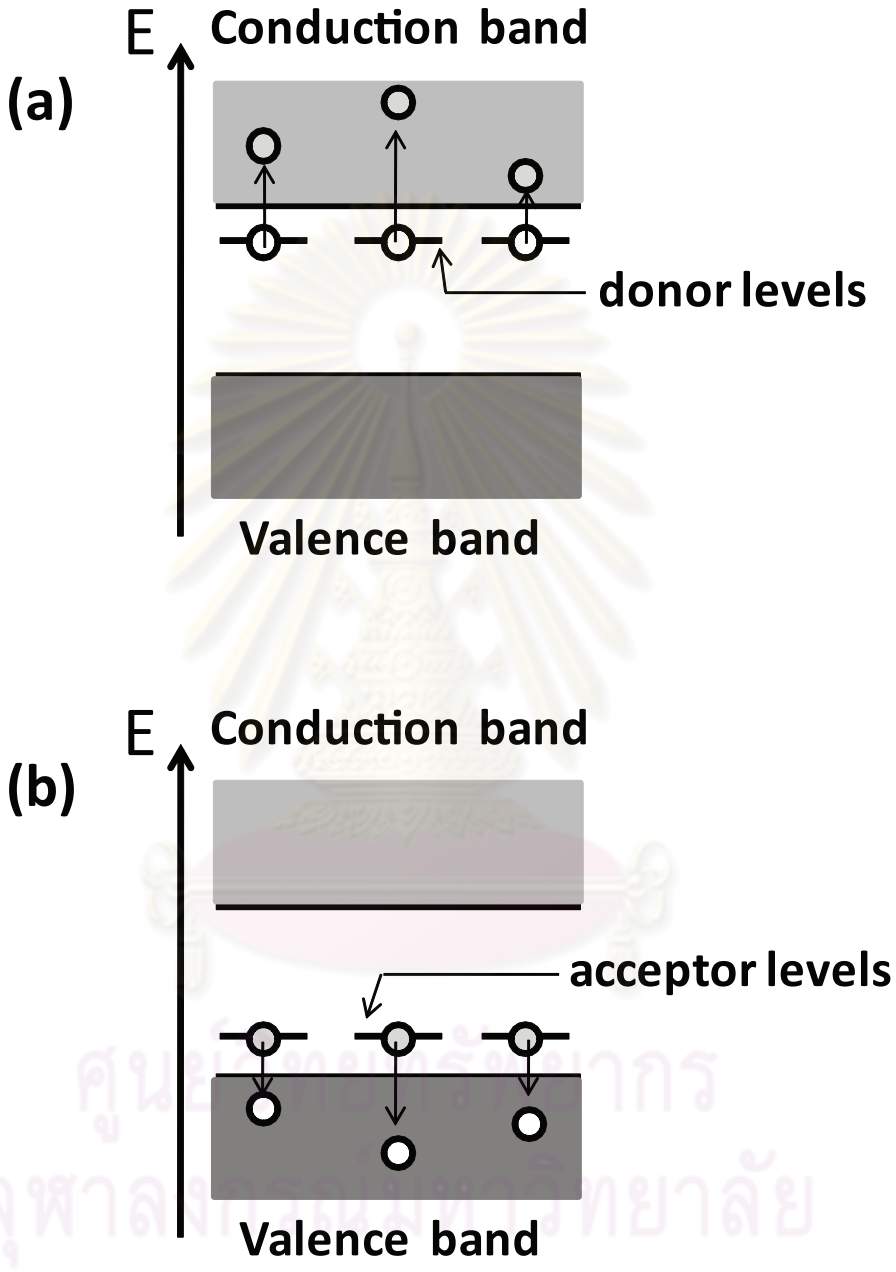


Figure 3.10: The band diagram of (a) n-type semiconductor (b) p-type semiconductor.

# CHAPTER IV

# EXPERIMENTAL METHODS AND SET UP

This chapter presents experimental method and setup. Barium titanate, Fe-doped barium titanate, calcium copper titanate and Fe-doped calcium copper titanate thin films were grown by thermal decomposition of the precursors deposited from a sol-gel system onto quartz substrates. A $^{60}$Co gamma radiation source was used to irradiate our films. The optical transmission spectra of the barium titanate, Fe-doped barium titanate and Fe-doped calcium copper titanate thin films were measured before and after gamma irradiation with different doses using a Perkin-Elmer Lambda 750 UV-Vis-NIR spectrophotometer. The capacitance of a coplanar capacitor made of calcium copper titanate film was measured before and after gamma ray irradiation.

## 4.1 Sample preparation

In this section, we will explain sample preparation of barium titanate, Fe-doped barium titanate, calcium copper titanate and Fe-doped calcium copper titanate precursors and how to deposit the films by a spin-coating sol-gel method.

### 4.1.1 Preparation of BTO and Fe-doped BTO precursors.

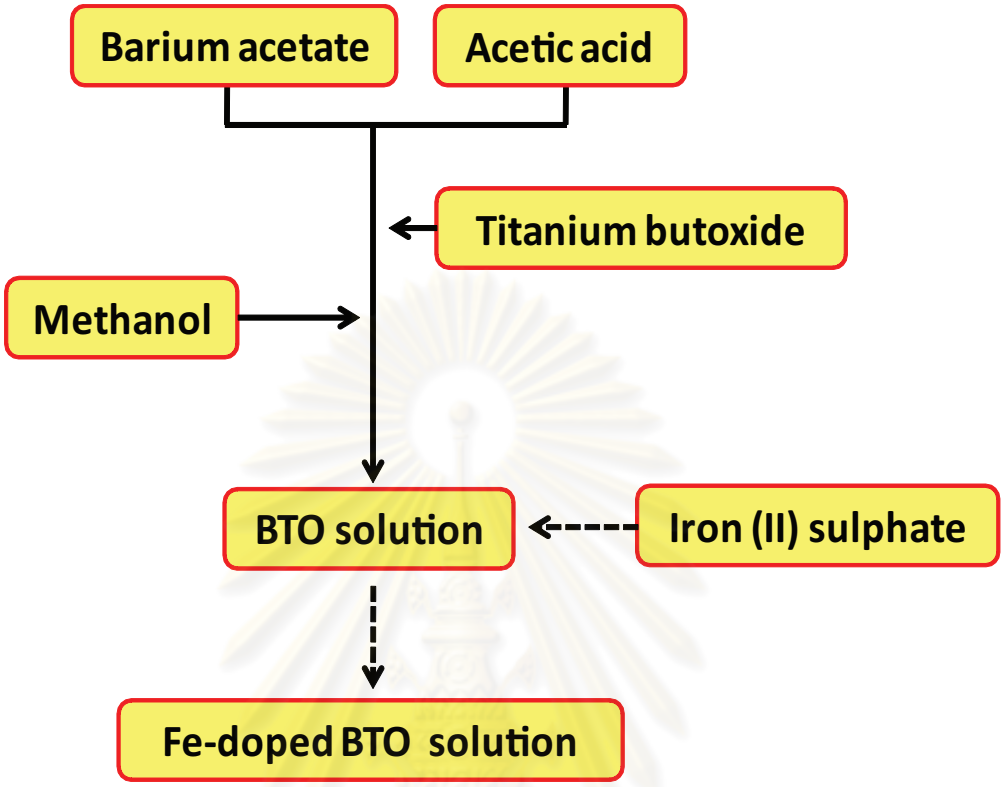


Figure 4.1: Flow chart of preparation of BTO and Fe-doped BTO.

Figure 4.1 shows the flow chart of preparation of BTO and Fe-doped BTO. Firstly, barium acetate ($Ba(CH_3COO)_2$) was dissolved in acetic acid. Then, pure titanium n-butoxide and methanol were added to the solution. In this thesis, 10% by weight of iron (see Appendix B) was done by dissolving iron (II) sulphate ($FeSO_4$) in the $BaTiO_3$ solution. The solution was mixed and stirred in a beaker with the aid of magnetic stirrer. This process was done on a hot plat at 60 $^oC$.

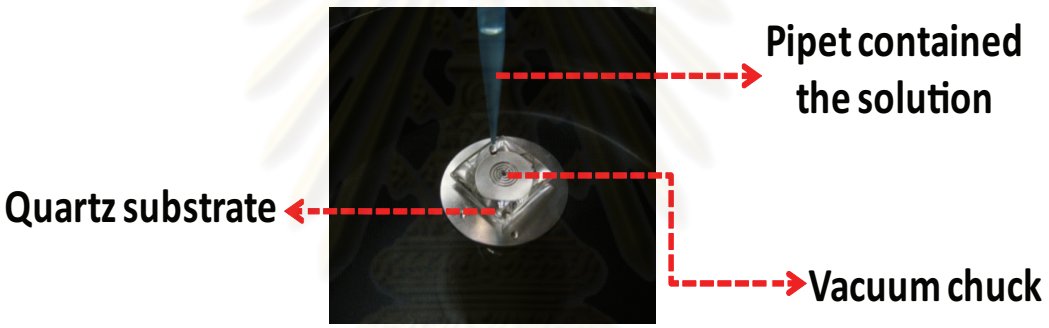


Figure 4.2: Spin coating process on a clean quartz substrate.

BTO or Fe-doped BTO precursor solutions were dropped on the clean quartz substrates as shown in Fig. 4.2 with the spinning speed of 1500 rpm to provide the first layer of each film. We have chosen quartz to be the substrate for our films. Quartz has been suitable substrates for studying the transmission of the materials being supported due to its transparency and high temperature melting point [45].

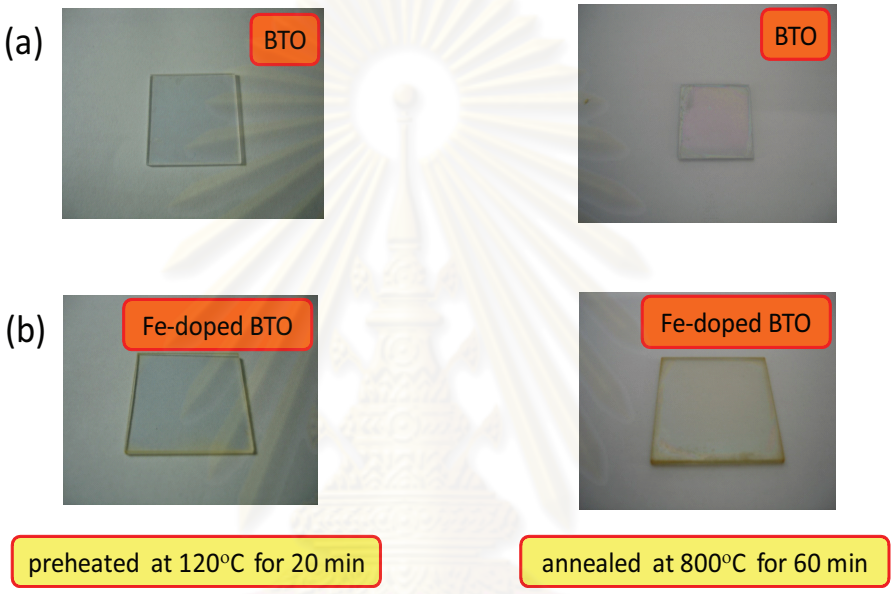


Figure 4.3: (a) BTO thin film after preheated and annealed (b) Fe-doped BTO film after preheated and annealed.

The BTO and Fe-doped BTO films were preheated at 120 $^{o}$C for 20 min before annealing in an atmosphere of air at 800 $^{o}$C for 60 min in order to form the crystalline structure. Figure 4.3(a) shows BTO thin film after preheating and annealing (b). Figure 4.3 shows Fe-doped BTO thin film after preheating and annealing. Different film thicknesses can be obtained by varying the number of deposition cycles. This process was repeated until the desired thickness was obtained. In this thesis, denoted each film by the material formula followed by the number of layers (L). Here, we have the BTO film with 2L, Fe-doped BTO with 4L, 6L and 8L, respectively.

### 4.1.2 Preparation of CCTO and Fe-doped CCTO precursors.

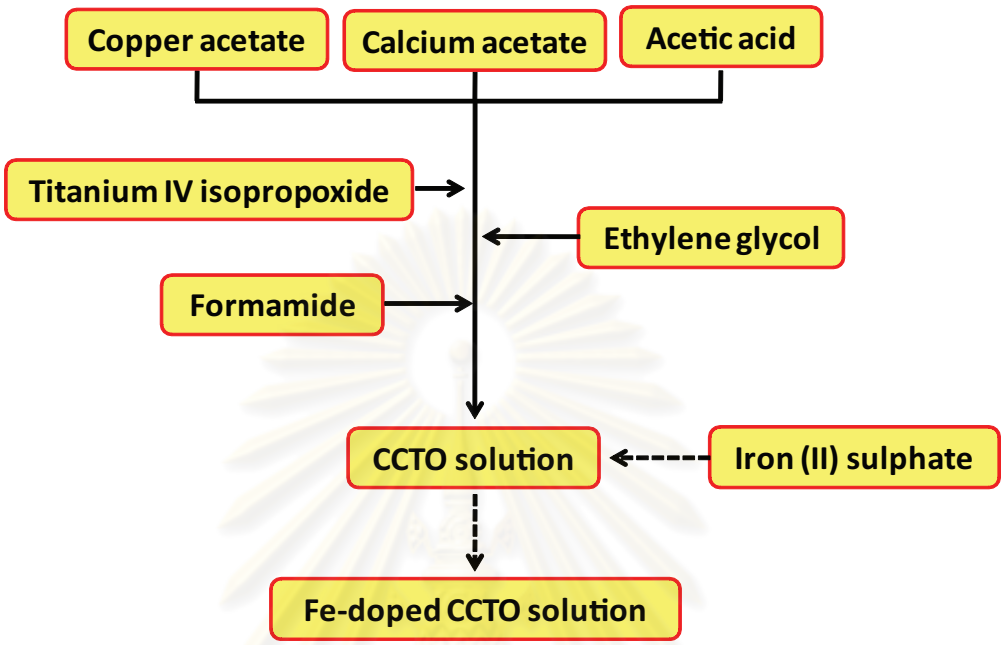


Figure 4.4: Flow chart of preparation of CCTO and Fe-doped CCTO.

Figure 4.4 shows the flow chart of preparation of CCTO and Fe-doped CCTO. Copper acetate ($Cu(CO_2CH_3)_2$) and calcium acetate ($Ca(C_2H_3O_2)_2.H_2O$) were firstly dissolved in acetic acid, and then titanium IV isopropoxide was slowly added. Ethylene glycol and formamide were added into the solution in order to increase solution stability. In this step, the solution viscosity can be also controlled to prevent the film cracking during the baking and annealing. In this thesis, 2% by weight of iron (see Appendix B) was done by dissolving iron (II) sulphate ($FeSO_4$) in the solution. The solution was stirred with a magnetic stirrer on a hot plat at 120 $^oC$. CCTO and Fe-doped CCTO precursor solutions were doped on the quartz substrates with the spinning speed of 1500 rpm to provide the first layer of the film (see Fig. 4.2). The CCTO and Fe-doped CCTO films preheated at 120$^oC$ for 20 min and annealed at 800 $^oC$ for 60 min, respectively. Fig. 4.5(a) shows CCTO thin film after preheating and annealing and Fig. 4.5(b) shows Fe-doped CCTO thin film after preheating and annealing. The film with different thicknesses can

be obtained by repeating this process. In this thesis, we have prepared the CCTO thin film on $Al_2O_3$ with 6L and Fe-doped CCTO on quartz substrate with 2L, respectively.

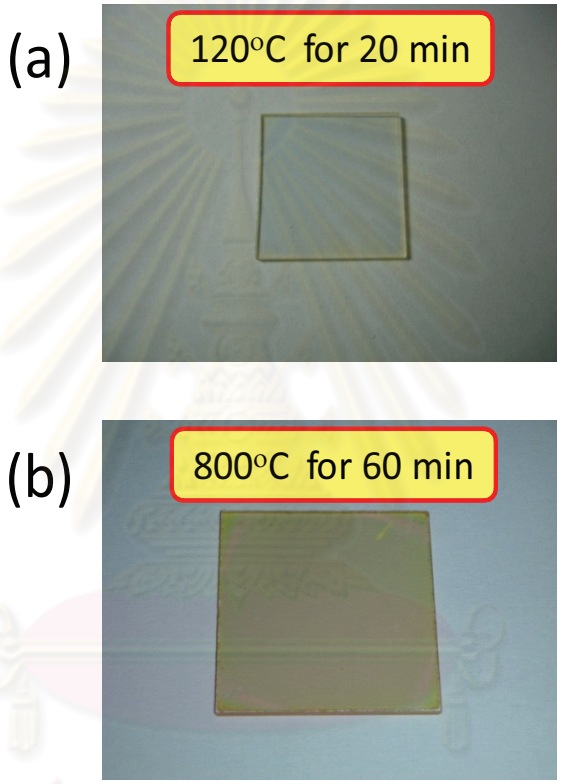


Figure 4.5: (a) Fe-doped CCTO film after preheated at 120$^o$C (b) Fe-doped CCTO film after annealed at 800$^o$C.

## 4.2 Gamma ray irradiation

A $^{60}$Co put gamma radiation with an activity of 10 kCi (Gammacel 220 Excell) at a rate of 10 kGy/hr was used to irradiate our BTO, Fe-doped BTO, CCTO and Fe-doped CCTO thin films. Gammacel 220 Excell has many $^{60}$Co cylinder sources around the aluminium cylinder which we used to hold our samples. Consequently, the positions in Gammacel 220 Excell are not equal doses. A Red Perspex dosimeter was used to calibrate the gamma rays doses at the positions of Gammacel 220 Excell. Figure 4.6 shows the different positions of dosimeter in a aluminium cylinder. The measured radiation doses at several positions are described in Fig. 4.6.

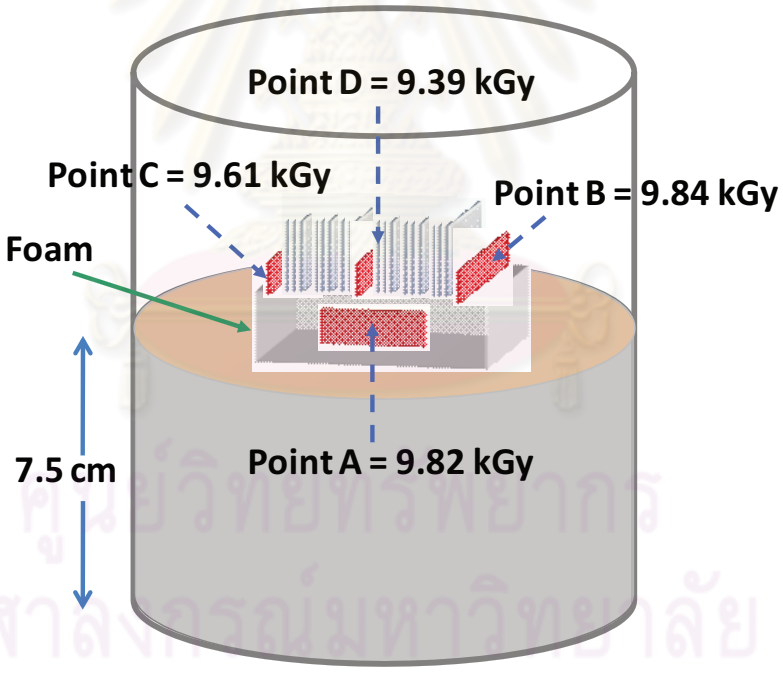


Figure 4.6: The position of dosimeter for dose mapping.

Note that the dose of gamma ray at the Point D was minimum because at this position the sample was blocked by other samples which were placed at the and the front positions. We avoided putting the samples in the middle position. The table 4.1 shows the doses of gamma ray irradiation at different position for 1 hr. We average all three values except the dose value in the middle. The calculated average radiation doses is 9.760 ± 0.161 kGy. For the ease, we used the round number which is approximately 10 kGy. In this thesis, we used approximate doses as shown in the right column of the table 4.1. The radiation doses were varied via the exposure time up to 14.640 ± 0.161 or approximately 15 kGy for about 90 min. We avoided putting the samples in the middle position.

Table 4.1: The doses of gamma ray used in this thesis.

| times (min) | doses (kGy) | approximately doses (kGy) |
|---|---|---|
| 6 | 0.976 ± 0.161 | 1 |
| 18 | 2.928 ± 0.161 | 3 |
| 30 | 4.880 ± 0.161 | 5 |
| 60 | 9.760 ± 0.161 | 10 |
| 90 | 14.640 ± 0.161 | 15 |

Figure 4.7 shows the process of gamma ray irradiation. Foam was used to hold the film at different positions. The reason for choosing foam is because it is a cheap insulator and it is not difficult to machine. The foam which was used to hold the films was put in the middle of the aluminium cylinder and send it in Gammacel 220 Excell.


Figure 4.7: The $^{60}$Co gamma radiation source (Gammacel 220 Excell).

## 4.3 UV-VIS-NIR preparation

A Perkin-Elmer Lambda 750 UV-Vis-NIR spectrophotometer was used to determine transmission spectra of the film. The samples (quartz substrates and the thin films) are held with a box acelic. Quartz substrate as a reference was put at R position (shown in Fig. 3.6) and the thin film was put at S position (shown in Fig. 3.6). The wavelength used in the experiment was in the range of 300 nm to 1200 nm with the increment 0.1 nm. The light source is on the left side and the detector is on the right side of the Fig. 4.8, respectively. The results of optical properties of Fe-doped BTO and Fe-doped CCTO thin films before and after gamma ray irradiation will be shown in section 5.2 and 5.4, respectively.

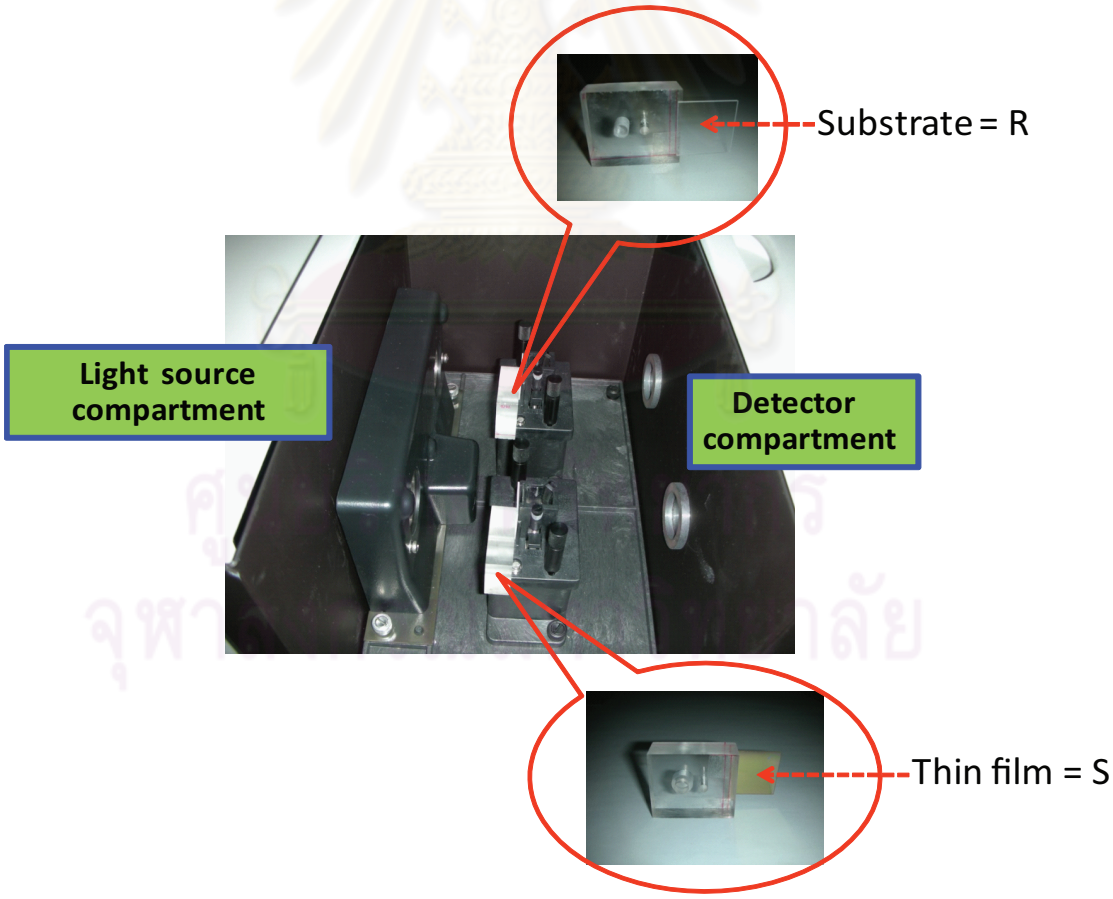


Figure 4.8: The set up process of UV-VIS-NIR spectrometer.

# CHAPTER V

# RESULTS AND DISCUSSION

## 5.1 Structural properties of BTO and Fe-doped BTO thin films

In this section, first we will briefly explain the X-ray diffraction result of BTO and Fe-doped BTO thin films, then the surface morphology of the BTO film with 6 layer compare with Fe-doped BTO thin films with 8 layer. Finally, the composition of Fe-doped BTO thin films will be presented.

### 5.1.1 X-ray diffraction pattern of BTO and Fe-doped BTO thin films

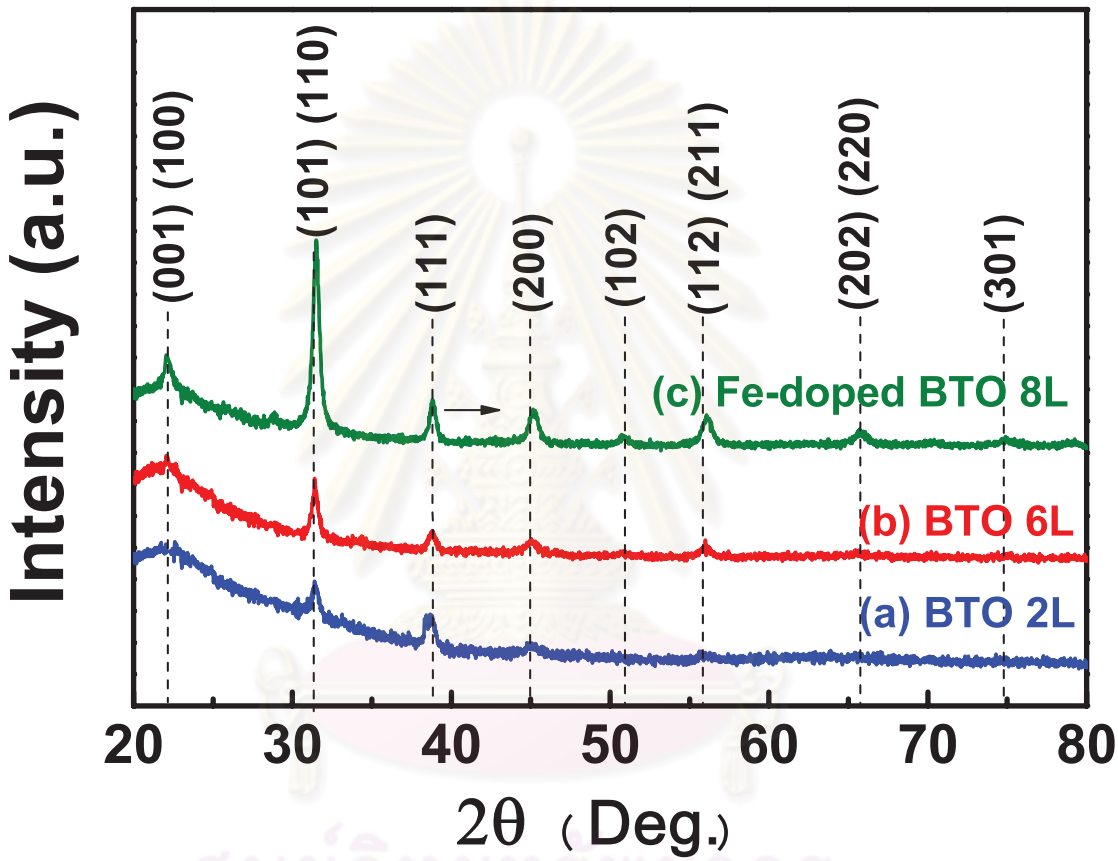


Figure 5.1: X-ray diffraction patterns of (a) BTO film with 2 layers (b) BTO film with 6 layers (c) Fe-doped BTO film with 8 layers.

The X-ray diffraction patterns of BTO and Fe-doped BTO films were recorded to determine their crystal structures. Figure 5.1 shows the XRD patterns of BTO with 2 and 6 layers as well as that for Fe-doped BTO films with 8 layers, derived from a sol-gel method. We denoted each film by the material formula followed by the number of layers (L). The tetragonal phase of BTO was identified in our films and it is indicated in Fig. 5.1 by the peaks with the indices of its crystallographic planes. The diffraction peaks are sharper and more intense as the films grow thicker through the deposition of more layers. The peak positions slightly shifted to higher diffraction angles after doping Fe in the film indicating that the lattice constants slightly decreased. From equation 3.2, the peak position for (200) and (101) was used to calculated the lattice constant (a-axis and c-axis)of BTO and Fe-doped BTO. The lattice constants of BTO with 6L are 4.005 Å and 4.021 Å for a-axis and c-axis. The lattice constants of Fe-doped BTO with 8L are 3.994 Å and 4.033 Å, respectively. This could be attributed to the substitution of ions with smaller size $Fe^{3+}$ (0.64 Å) to ions with bigger size $Ba^{2+}$ (1.34 Å). These results are consistent with the work of other groups [4, 46]. Figure 5.2 shows X-Ray diffraction patterns of (a) $BaTiO_3$ film before and after gamma ray dose of 1 kGy (b) Fe-doped BTO film before and after gamma ray dose of 1 kGy, respectively. The XRD pattern of both films did not change after gamma irradiation dose of 1 kGy. In Fig. 5.2, the diffraction peaks are sharper and more intense and the peak position slightly shifted to higher diffraction angles (see in Fig. 5.3) after BTO doped with Fe.

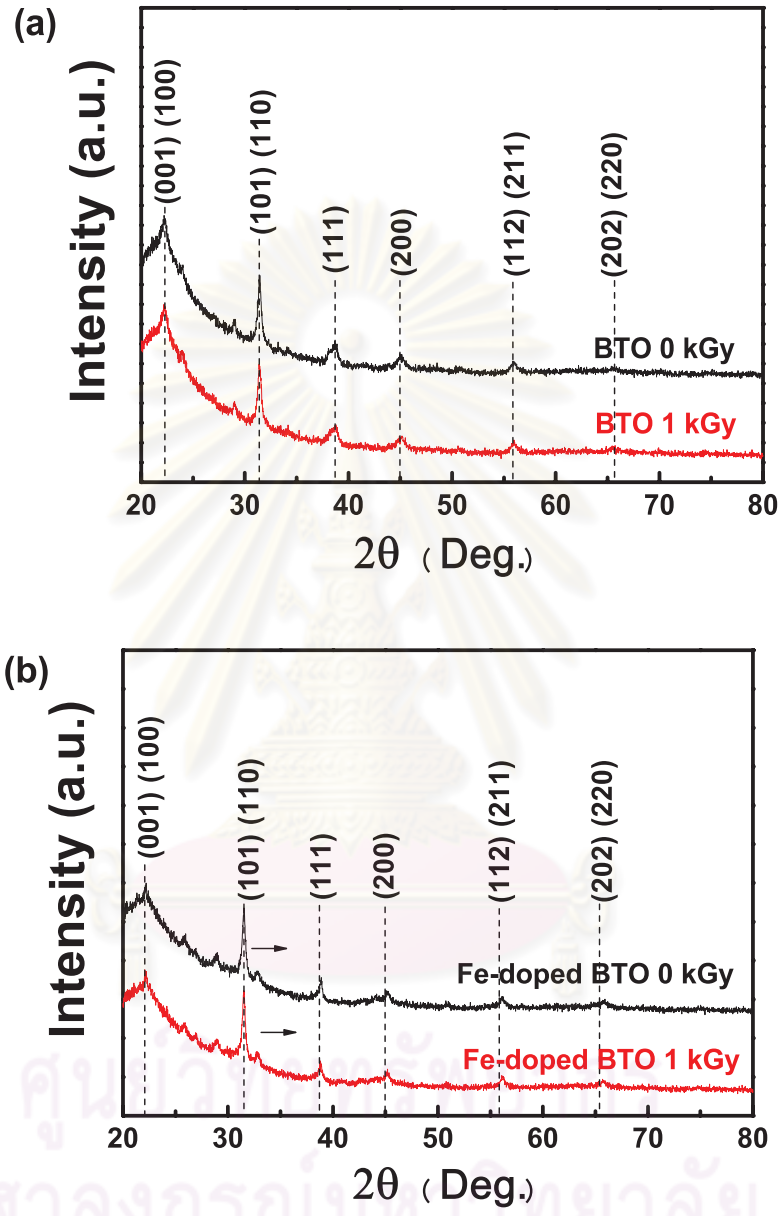


Figure 5.2: X-ray diffraction patterns of (a) BTO film before and after gamma ray dose of 1 kGy (b) Fe-doped BTO film before and after gamma ray dose of 1 kGy.

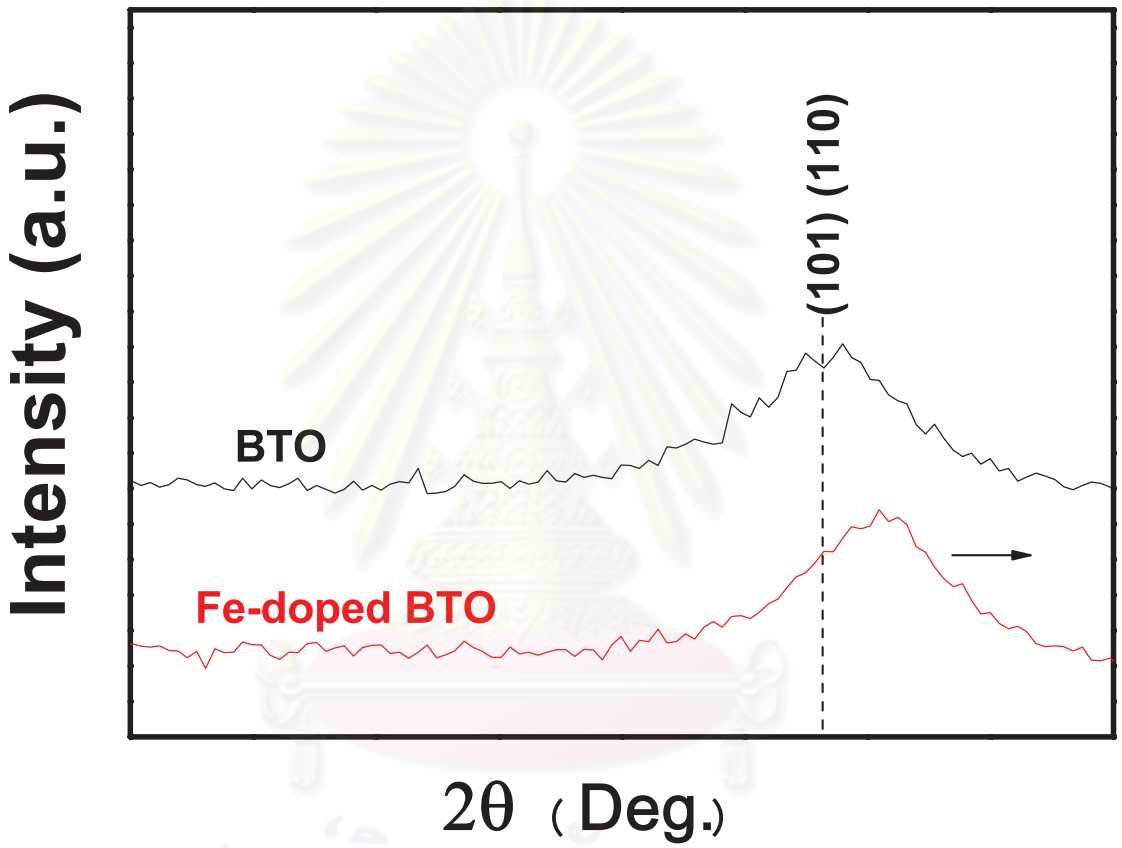


Figure 5.3: X-ray diffraction patterns of BTO and Fe-doped BTO film before and after gamma ray dose of 1 kGy zoom at (101), (110).

### 5.1.2 Surface morphology of BTO and Fe-doped BTO thin films

The surface morphology of the BTO and Fe-doped BTO films was observed using a Veeco Nanoscope IV atomic force microscope (AFM). The estimated average grain size of the Fe-doped BTO 8L film is 40 nm which is smaller than the 54 nm grain size for the 6L film as seen in Fig. 5.4. Devan et al. observed similar results with a decrease in grain size with doping concentrations [46]. Indeed, many research groups have reported that increasing the dopant concentration could reduce the grain size due to competition between different phase structures in the materials [2, 4].

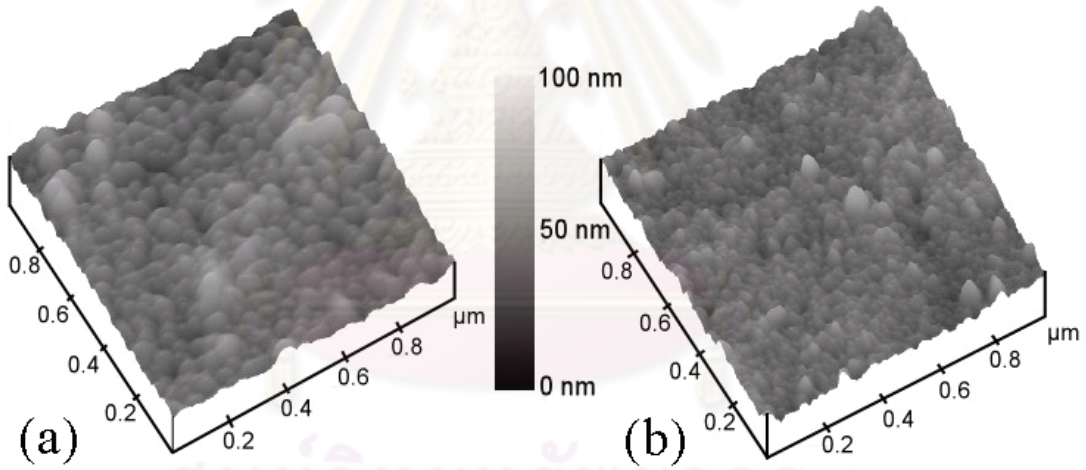


Figure 5.4: Atomic force microscopy images (1.0 × 1.0 $\mu$m) of the films comprised of (a) BTO with 6L (b) Fe-doped BTO with 8L.

### 5.1.3 Composition of Fe-doped BTO thin films

The compositions of the films were obtained using a WDX equipped with an electron probe microscopic spectrometer (EPMS: JEOL model JXA-8100). In the beginning, we have planned to dope Fe with 10% by weight for BTO. However, the quantity of Fe in our films was not the same as the calculation, and later is confirmed from WDX experiment. The obtained concentration of Fe is 7% by weight instead of 10% by weight. The substitution site for the dopant cation depends more strongly on its concentration and on the Ba/Ti molar ratio than on its size. The ionic radius of $Fe^{3+}$ (0.64 Å) is comparable with the ionic radius of $Ti^{4+}$ (0.68 Å) but is significantly different from that for $Ba^{2+}$ (1.34 Å) [4]. However, the WDX shows signals that are consistent with $Ba_{0.8}Fe_{0.2}TiO_3$ as shown in Table 5.1 with the Fe doping occurring by substitution of Ba sites in BTO yielding a Ba/Ti ratio slightly smaller than 1. The oxidation state determined from the energy of the X-ray absorption edge (7130.5 eV) corresponds to $Fe^{3+}$. The X-ray absorption experiment was done by Thidarat Supasai, a Ph.D student at Department of physics, Chulalongkorn University. In our case the $Fe^{3+}$ dopant acts as a donor when it substitutes the $Ba^{2+}$ site that means our doped BTO films are n-type semiconductor. A similar result for this substitution was found in the work of Battisha et al. [1].

Table 5.1: Mass (%), Atom (%) and Ratio of Fe-doped BTO.

| | Mass (%) | Atom (%) | Ratio |
|---|---|---|---|
| Ba | 66.293 | 41.159 | 0.8 |
| Fe | 4.552 | 6.9471 | 0.2 |
| Ti | 29.154 | 51.8939 | 1 |
| | 100 | 100 | |

## 5.2 Optical properties of BTO and Fe-doped BTO thin film

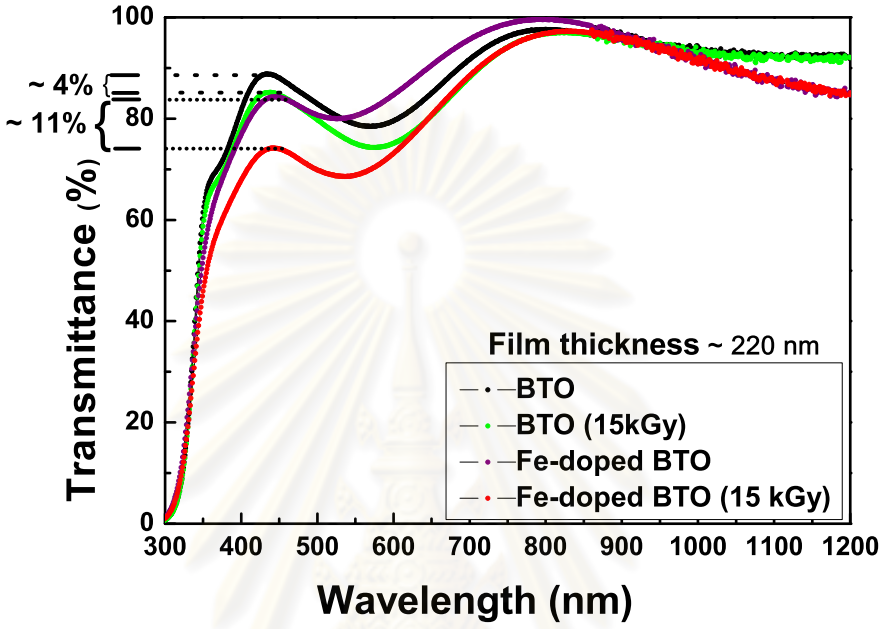


Figure 5.5: The transmission spectra of BTO and Fe-doped BTO thin films before and after gamma irradiation at a dose of 15 kGy.

The optical transmittance spectra of the films using a Perkin-Elmer Lambda 750 UV-Vis-NIR spectrophotometer were measured after gamma irradiation immediately. Figure 5.5 shows the optical transmission spectra in the 300 - 1200 nm wavelength range of the BTO and Fe-doped BTO films of comparable thickness (ca. 220 nm) before and after gamma irradiation at 15 kGy. The oscillation in the transmission curve is due to interference between light reflecting from the film surface and from the film-substrate interface. The depth of modulation indicates good homogeneity of the films across the light beam (ca. 1 cm in diameter). The transmittance of both BTO and Fe-doped BTO films were reduced after the irradiation, and a brownish tint could be seen by the naked eye in the irradiated films (Fig. 5.6). It is believed that structural defects after gamma irradiation causes a

change in the color of films as well as the change in color observed in jewelry. This phenomena is called color center. From the Section 2.4, the color center occurs when the gamma ray kicks out Ba or Ti or O atoms leaving atom vacancies. The atom vacancy are often occur at O site rather than Ba or Ti sites in $BaTiO_3$.

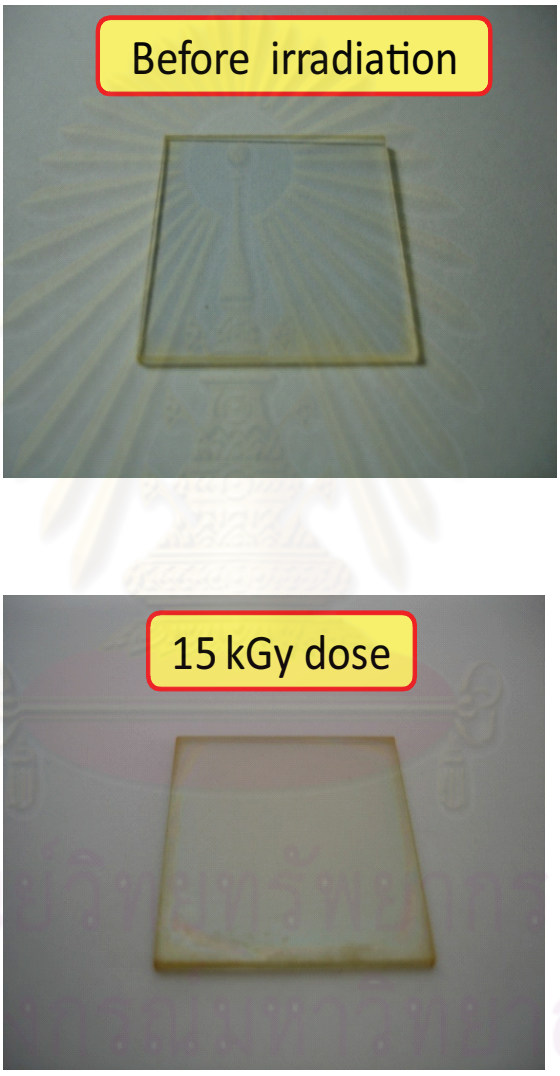


Figure 5.6: Fe-doped BTO thin films before and after gamma irradiation at a dose of 15 kGy.

However, our results revealed that gamma irradiation causes a more marked change on the transmittance of the Fe-doped BTO film than to the BTO film. For comparison, following gamma irradiation at 15 kGy, the transmittance decreased by 4% in the BTO film but by 11% for the Fe-doped BTO film. It seems that the trapping process in the films after irradiation occurs more readily in the doped films, presumably because they have more defects than in BTO films.

Fig. 5.7(a) shows the optical transmission spectra of Fe-doped BTO films with 4L and 6L (denoted by Fe-doped BTO 4L and Fe-doped BTO 6L, respectively) in the 300 - 1200 nm wavelength range and Fig. 5.7(b) shows the same trend for the Fe-doped BTO film with 8L (denoted by Fe-doped BTO 8L). As expected, the thicker film shows deeper oscillations in the transmission spectrum than the thinner film. The transmittance also decreased with the increasing gamma radiation doses. The doses used in this study were 1, 5, 10 and 15 kGy, respectively. We observed that the transmittance of the films did not change any further for gamma radiation doses higher than ca. 10 kGy. The absorption edge shifted to a lower energy as the films got thicker (Fig. 5.7(a)), because the films with a larger number of layers accumulated longer heating times (800 $^0$C for 60 min for each layer) causing the growth of bigger grains. However, there was little variation in the absorption edge between the Fe-doped BTO 4L film annealed for four hours and Fe-doped BTO 8L film annealed for eight hours. The film thickness of Fe-doped BTO ranging from four to eight layers were calculated via the envelope method derived by Swanepoel [47] and were approximately 220 nm (4L), 375 nm (6L) and 520 nm (8L).

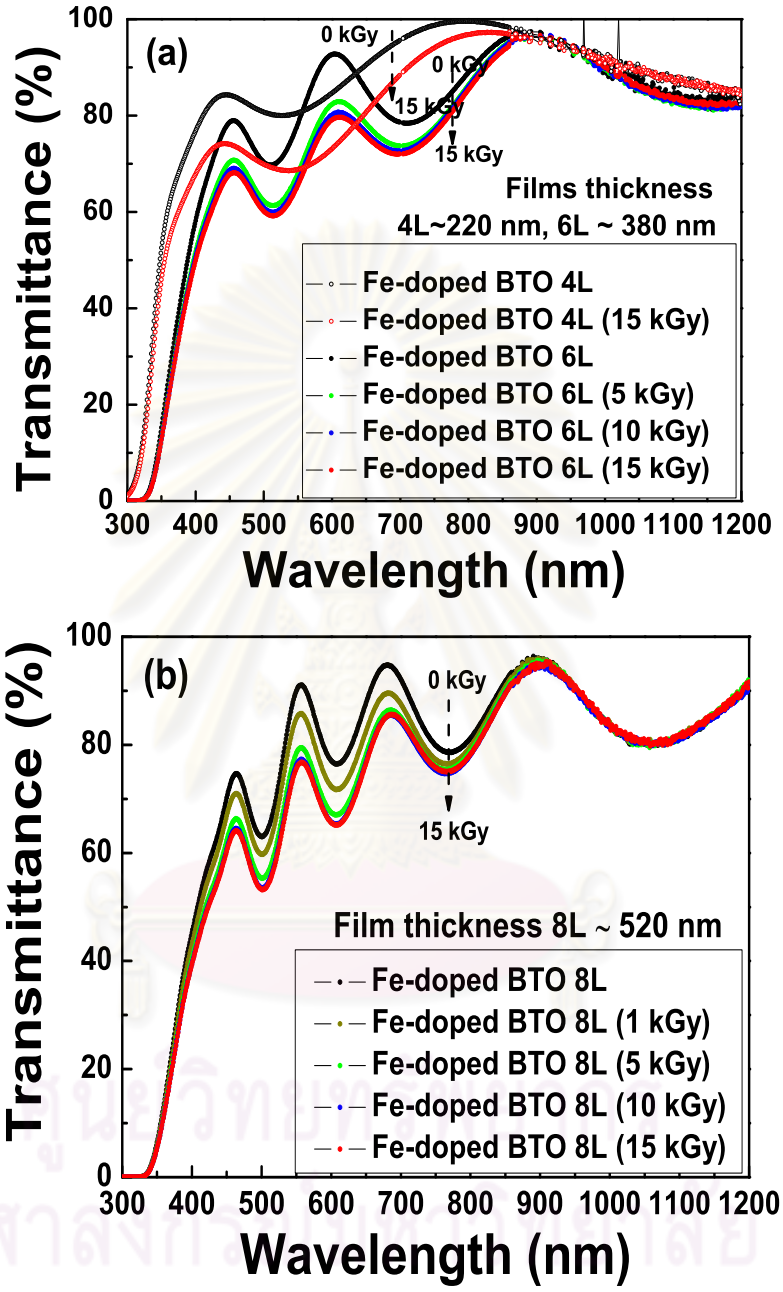


Figure 5.7: The transmission spectra of (a) Fe-doped BTO films with 4L, 6L and (b) Fe-doped BTO films with 8L, after exposure to different gamma radiation doses.

From the transmittance spectra, the energy for the direct gap could be calculated by using the Equation 3.11: $(\alpha h\nu)^2 = B(h\nu - E_g)$ where $\alpha$ is the absorption coefficient, $h\nu$ is the photon energy, $E_g$ is the energy gap and B is a constant.

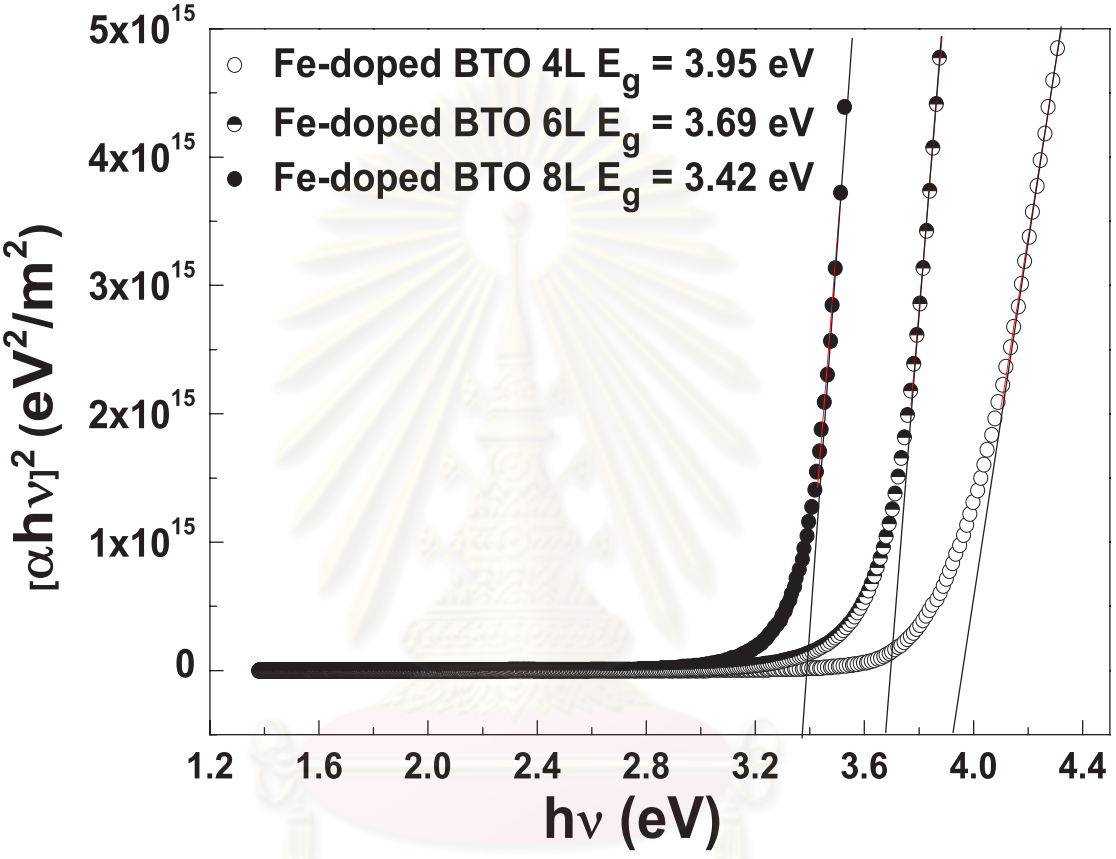


Figure 5.8: Plot between $(\alpha h\nu)^2$ versus $h\nu$ of Fe-doped BTO thin films with 4L 6L and 8L, respectively.

The energy band gap of Fe-doped BTO with 4L, 6L and 8L did not change after gamma exposure to different gamma radiation doses as shown in Fig. 5.9.

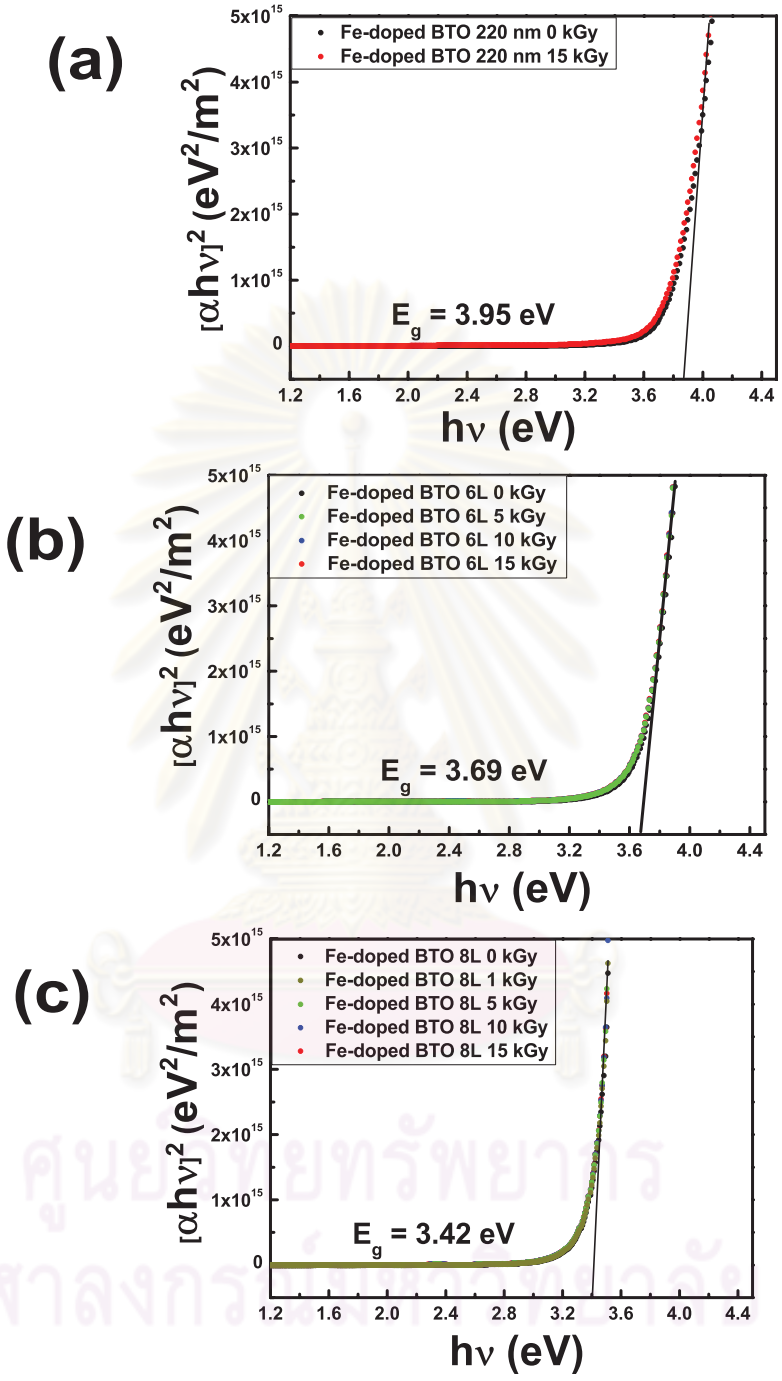


Figure 5.9: Plot between $(\alpha h\nu)^2$ versus $h\nu$ of Fe-doped BTO thin films before and after exposure to different gamma radiation doses (a) 4L (b) 6L and (c) 8L, respectively.

Figure 5.10, 5.11 and 5.12 show the plot between ln$\alpha$ versus h$\nu$ of Fe-doped BTO with 4L, 6L and 8L, respectively. The measurement of the band edge characteristic can be obtained from the so called Urbach rule. In general, an exponentially increasing absorption edge can be seen in various types of materials;

$$\alpha = \alpha_0 \mathrm{e}^{(\frac{\sigma(h\nu - E_0)}{kT})} = \alpha_0 \mathrm{e}^{(\frac{h\nu - E_0}{E_u})} \tag{5.1}$$

where $\alpha_0$ and $E_0$ are the Urbach bundle convergence point coordinates, $E_u$ is the absorption edge energy width interpreted as the width of the tails of localized states in the band gap as shown in Fig. 3.9, Section 3.5.2 and $\sigma$ is the steepness parameter, $k$ is the Boltzmann constant and $T$ is the temperature.

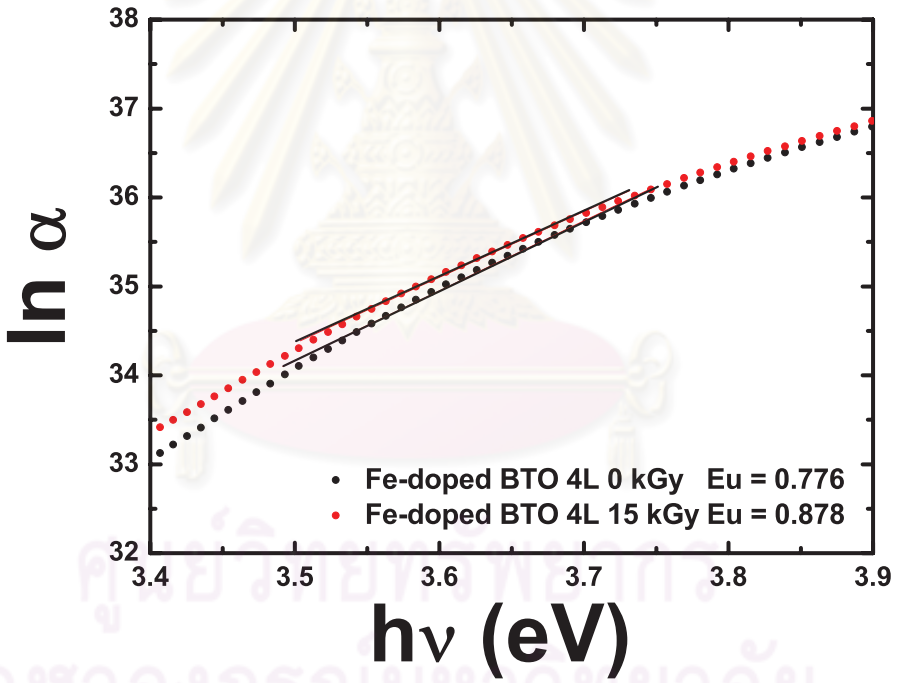


Figure 5.10: Determination of the Urbach energy for Fe-doped BTO 4L with gamma irradiation doses of 15 kGy.

As the gamma radiation dose increased, the absorption edge energy width of Fe-doped BTO with 4L increase from 0.776 to 0.878 eV after 15 kGy indicating that the gamma ray induced more defects.

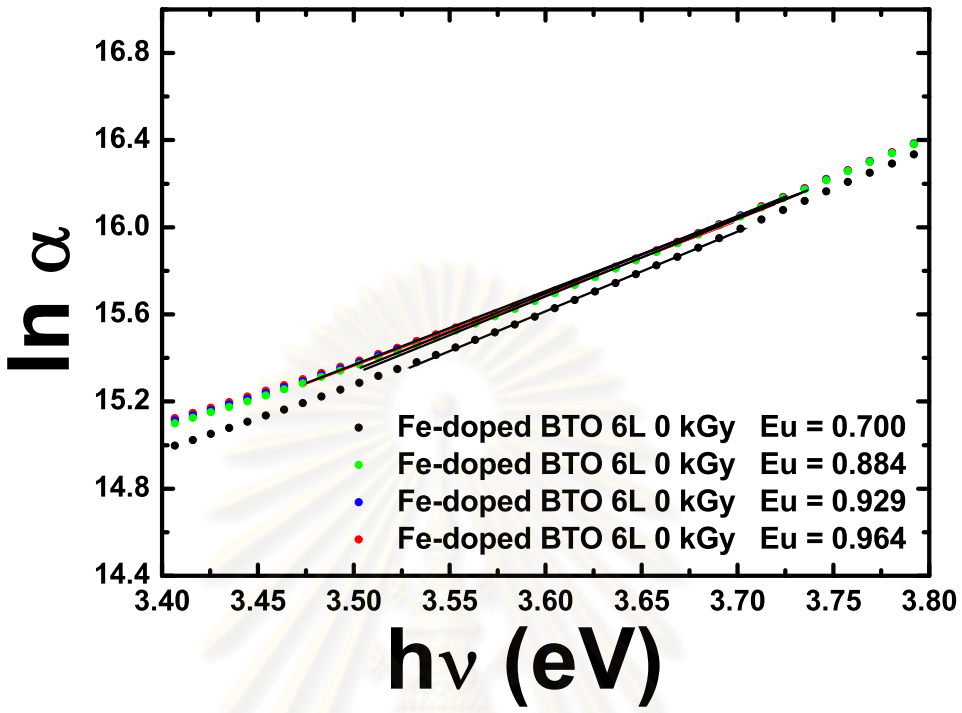


Figure 5.11: Determination of the Urbach energy for Fe-doped BTO 6L with different gamma irradiation doses.

In the similar way, the absorption edge energy width increases with the gamma radiation dose. The absorption edge energy width of Fe-doped BTO with 6L increase from 0.700 to 0.964 eV after 15 kGy indicating that the gamma ray induced more defects.

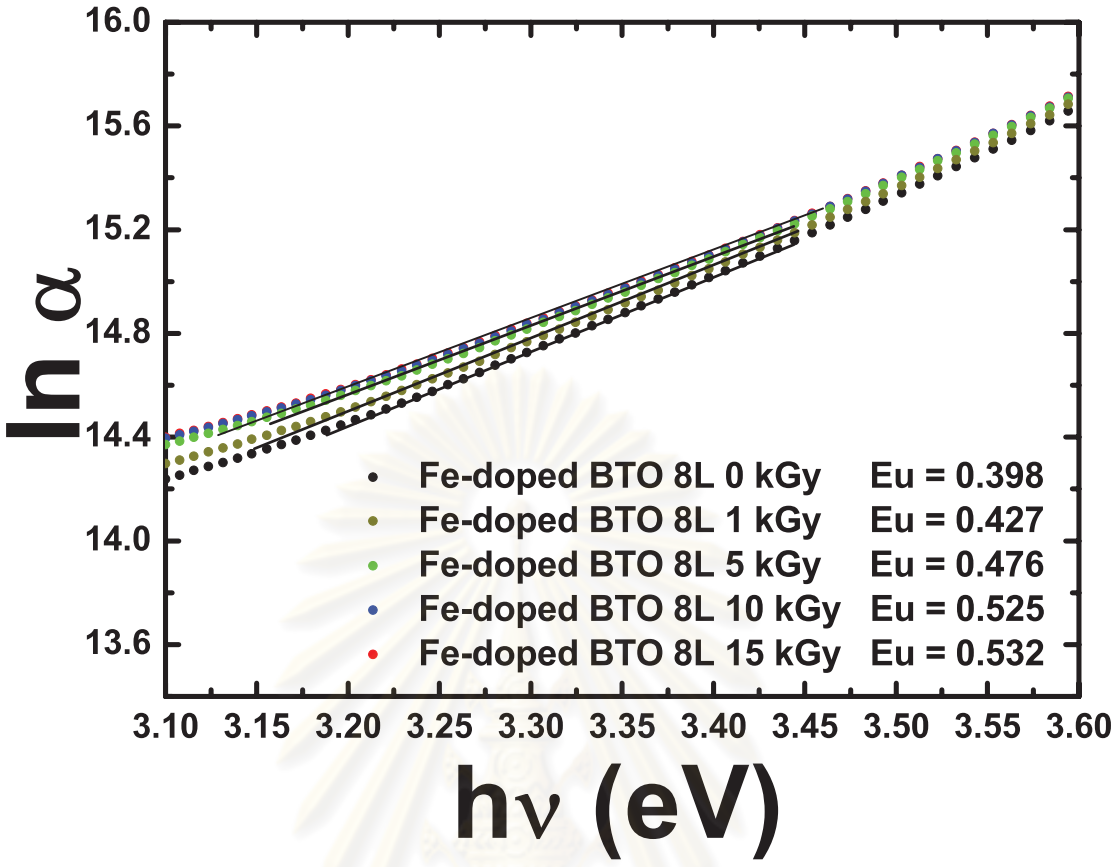


Figure 5.12: Determination of the Urbach energy for Fe-doped BTO 8L with different gamma irradiation doses.

The same trend can be seen in the data of Fe-doped BTO with 8L. The absorption edge energy width of Fe-doped BTO with 8L increase from 0.398 to 0.532 eV after 15 kGy.

Figure 5.8 shows a plot between $(\alpha h\nu)^2$ versus $h\nu$ of the Fe-doped BTO thin films with 4, 6 and 8 layers. The resulting energy band gaps were 3.42 eV, 3.69 eV and 3.95 eV for Fe-doped BTO with 8, 6 and 4 layers, respectively. For comparison, the energy band gap value of pure BTO powder, BTO single crystal, and BTO thin films are 3.92 eV [48], 3.6 eV [49] and 3.72-3.77 eV [50], respectively. The particle size in these films increases as the annealing cycle increases [51]. The corresponding reduction in band gap energy with increasing particle size can be explained by quantum confinement [37, 52]. By way of comparison, we used the quantum confinement prediction for energy gap.

$$E_g(r) = E_g(bulk) + \frac{2\pi^2 h^2}{r^2}\left(\frac{1}{|m_e|} + \frac{1}{|m_h|}\right) \tag{5.2}$$

$$E_g(r) = E_g(bulk) + \frac{2\pi^2 h^2}{r^2 \mu} \tag{5.3}$$

where $m_e$, $m_h$, $\mu$ and $r$ are the effective mass of electron, the effective mass of hole, the reduced mass and the diameter of nanoparticle, respectively. Normally, if the particle size is smaller than the corresponding DeBroglie wavelength, the size quantization effects can be observed in the band gap. The theoretical calculated DeBroglie wavelength for BTO is about 15 nm,

$$a_B = (4\pi\varepsilon_0\varepsilon_r\hbar^2)/\mu e^2$$

Analysis of the variation of the dispersion curves of Fe-doped BTO films after different gamma irradiation doses (0-15 kGy) reveal that the refractive index and the extinction coefficient increase with the wavelength rising more rapidly toward short wavelengths and following a typical dispersion curve shape (Fig. 5.13). When measured in the 350 - 750 nm wavelength range, the refractive index ($n$) for the Fe-doped BTO 4L increased from 2.17 - 1.88 range to 2.34 - 1.95 range upon the gamma irradiation at a dose of 15 kGy, with a corresponding increase in the extinction coefficient ($k$) (Fig. 5.13(a) and (b)). The value of the extinction

coefficient for this film prior to gamma irradiation was in the order of $10^{-2}$ and this increase after the irradiation with higher doses, indicating that higher optical losses result directly from the irradiation. With thicker films, the refractive index is also increased due to the increased film density and better crystallinity as shown in Fig. 5.14. While the extinction coefficient of BTO 4L, 6L and 8L films did not change much. The extinction coefficient follows an approximately linear function of the wavelength. The dispersion curves near the electronic band transition were significantly altered by the gamma irradiation. One of the main results of these experiments is that the complex refractive index of the films can be tuned by exposure to various gamma rays doses. These observed phenomena could be useful for the development of gamma irradiation dosimeters based on simple optical detection properties.

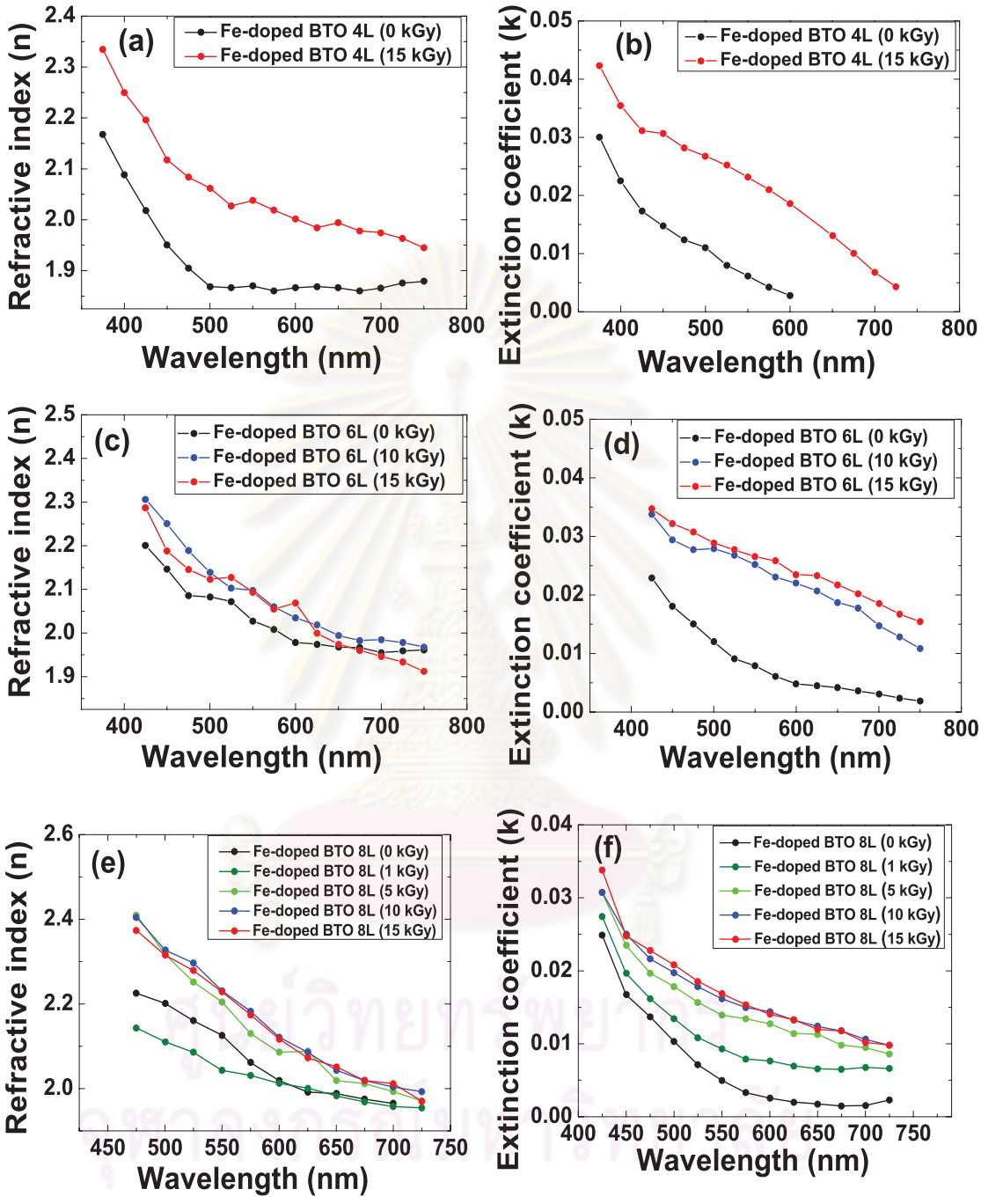


Figure 5.13: (a,c,e) The refractive index of Fe-doped BTO thin films with 4L 6L and 8L, respectively and (b,d,f) the extinction coefficient of Fe-doped BTO thin films with 4L 6L and 8L, respectively.

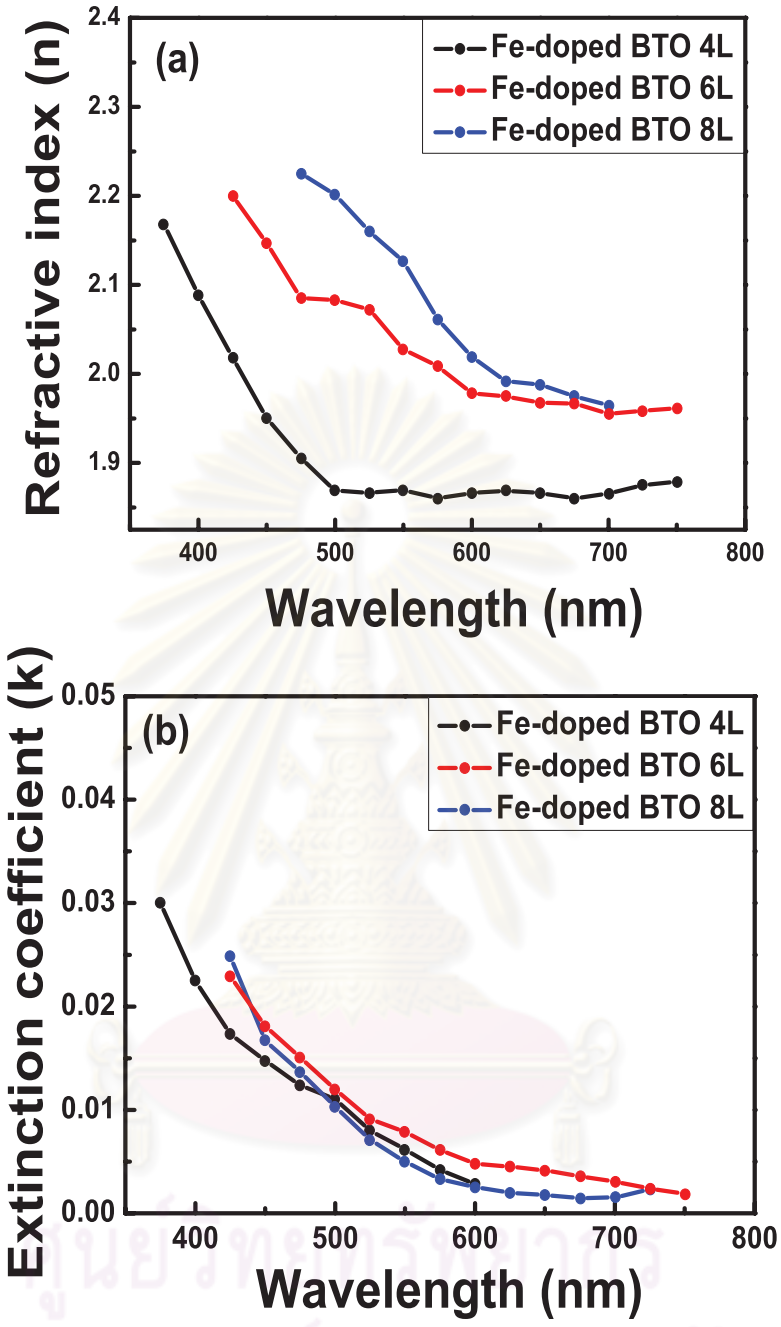


Figure 5.14: The refractive index of Fe-doped BTO thin films with 4L 6L and 8L, respectively.

## 5.3 Structural properties of CCTO and Fe-doped CCTO thin films

In this section, the XRD patterns of CCTO and Fe-doped CCTO thin films were used to confirm the crystalline of the film and EDX used to confirm the composition for Fe in the Fe-doped CCTO films.

### 5.3.1 X-ray diffraction pattern of CCTO and Fe-doped CCTO thin films

The X-ray diffraction patterns of CCTO and Fe-doped CCTO thin films were recorded to determine their crystal structures. Figure 5.15 shows the XRD patterns of CCTO and Fe-doped CCTO films. From equation 3.3, peak (220) was used to calculate the lattice constants of the films. The lattice constant of CCTO is 7.3877 Å while Fe-doped CCTO with lattice constant is 7.3799 Å, respectively. In Fig. 5.15, the peak positions of CCTO film slightly change after doping Fe in the film indicating that Fe substituting for Cu (see Section 5.3.2) and Fig. 5.16 shows X-ray diffraction pattern of Fe-doped CCTO thin films before and after gamma ray dose of 1 kGy. The XRD pattern of Fe-doped CCTO films did not change after gamma irradiation dose of 1 kGy.

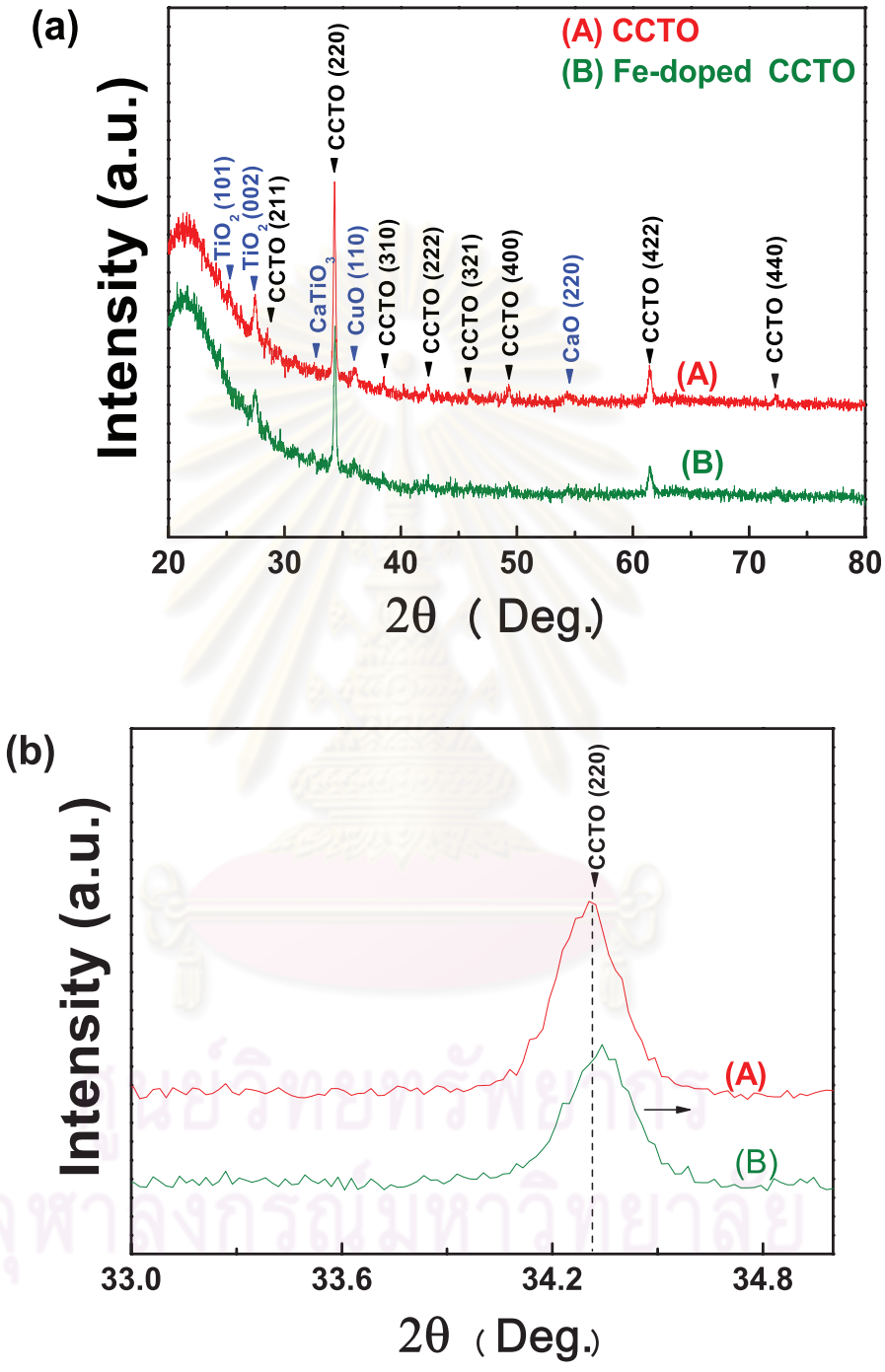


Figure 5.15: X-ray diffraction patterns of CCTO and Fe-doped CCTO thin films.

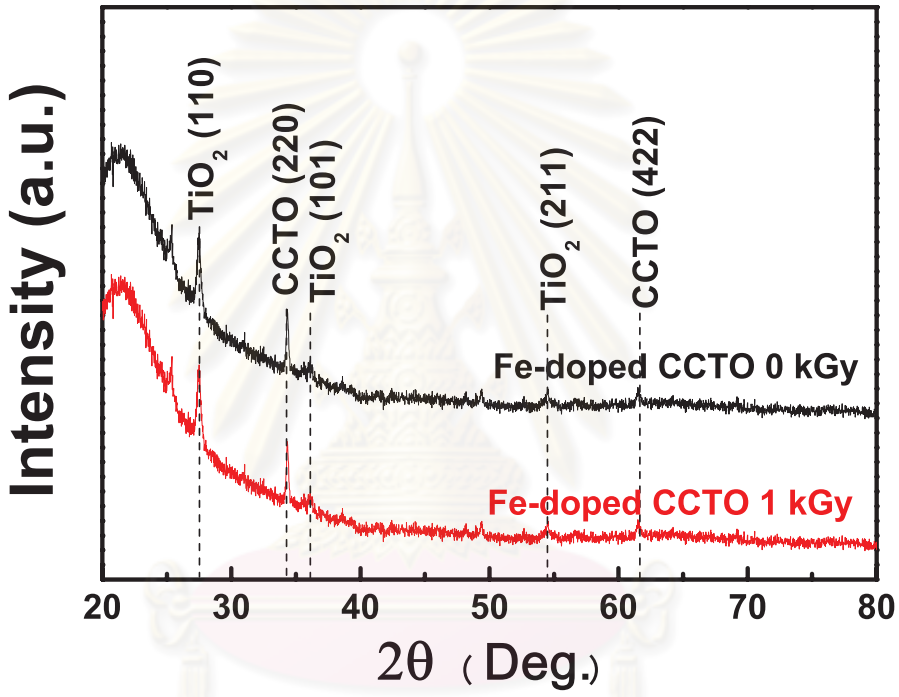


Figure 5.16: X-ray diffraction patterns of Fe-doped CCTO thin films before and after gamma ray dose of 1 kGy.

### 5.3.2 Energy dispersive X-ray data of Fe-doped CCTO

The compositions of the films were obtained using a EDX equipped with Field Emission Scanning Electron Microscopy (FSEM: HITASHI model S-4700). Table 5.2 shows the ratio of intensity and weight (%) of each atom in CCTO. The concentration of Fe doped 2% by weight for CCTO were choosed in this thesis. EDX experiment shown that Fe concentration of CCTO is 2.44%. Table 5.2 shows the intensity, weight (%) and rtatio of each atom in CCTO. The ratio of Ca:Cu:Ti:O is 1:1.5:5.2:10.3 indicating the excess Ti and the insucient Cu and O constitutions. The excess of Ti obtained from EDX consistent with the $TiO_2$ phase formation in XRD result. Table 5.3 shows the intensity, weight (%) and ratio of each atom in Fe-doped CCTO. The ratio of Ca:Cu:Fe:Ti:O is 1:1.5:0.4:3.6:8.6 indicating that Fe atoms are present in the film by substitution of Cu sites in the CCTO film. However, from this result we found that the amount of Cu was insufficient in the film.

Table 5.2: Intensity, Weight (%) and Ratio of CCTO.

| | Intensity (c/s) | Weight (%) | Ratio |
|---|---|---|---|
| Ca | 61.72 | 8.273 | 1 |
| Cu | 2.44 | 20.264 | 1.5 |
| Ti | 172.47 | 39.555 | 5.2 |
| O | 100.56 | 27.575 | 10.3 |
| | | 100 | |

Table 5.3: Intensity, Weight (%) and Ratio of Fe-doped CCTO.

| | Intensity (c/s) | Weight (%) | Ratio |
|---|---|---|---|
| Ca | 57.57 | 8.215 | 1 |
| Cu | 1.73 | 15.419 | 1.5 |
| Fe | 6.52 | 5.782 | 0.4 |
| Ti | 169.55 | 41.644 | 3.6 |
| O | 96.12 | 28.939 | 8.6 |
| | | 100 | |

## 5.4 Optical properties of Fe-doped CCTO

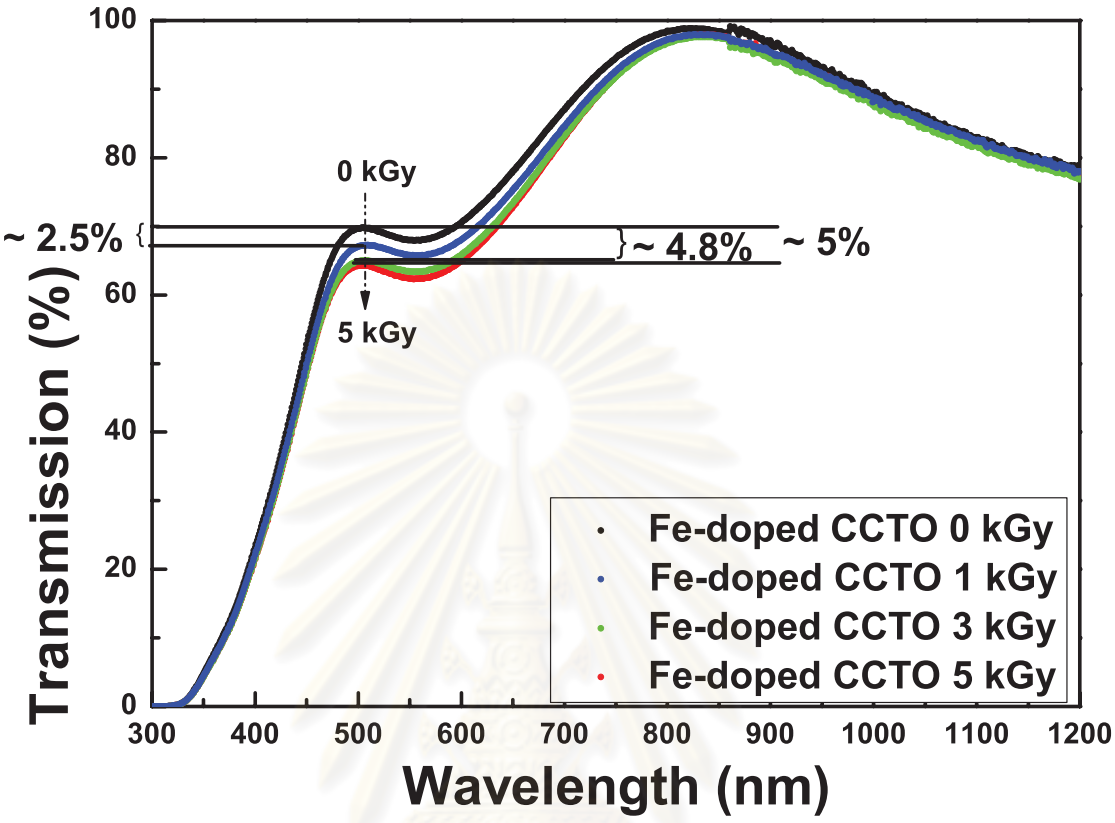


Figure 5.17: The transmission spectra of Fe-doped CCTO thin films for different gamma radiation dose.

Figure 5.17 shows the optical transmission spectra in the 300-1200 nm wavelength range of Fe-doped CCTO films before and after gamma irradiation at 1, 3 and 5 kGy dose, respectively. The depth of modulation normally indicates that the films are homogeneous.

We have found the reduction in transmittance decreasing to 2.5%, 4.8% and 5.0% after exposure with gamma irradiation dose of 1 kGy, 3 kGy and 5 kGy, respectively. We observed that the transmittance of the films did not change after the gamma radiation dose is higher than ca. 3 kGy. In another word, there was not much change in the transmittance for the film exposed with 3 kGy and 5 kGy. This could be due to the saturation of activity of color centers phenomena. There were not much change in the percentage transmission of Fe-doped CCTO film as

compared with BTO and Fe-doped BTO film. For example, BTO and Fe-doped BTO with thickness 220 nm decrease 4% and 11% after gamma irradiation with 15 kGy, while CCTO films with thickness of 360 nm decrease 5%, after irradiation with 5 kGy dose, respectively.

After gamma ray irradiation, the films became brownish tint. This color changes can be seen by naked eye (see in Fig. 5.18) but with less change in color compared to that of BTO and Fe-doped BTO films.

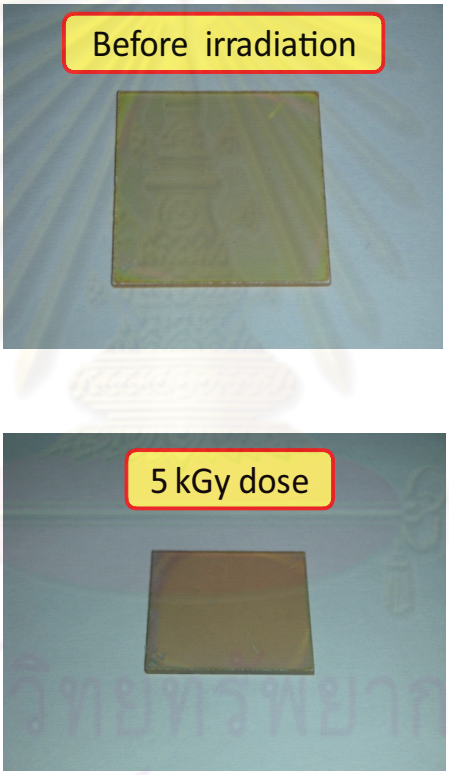


Figure 5.18: Fe-doped CCTO thin films before and after gamma irradiation at a dose of 5 kGy.

### 5.4.1 Energy gap

From the transmittance spectra in Fig. 5.17, the energy gap for direct gap could be calculated by using the equation 3.11. Figure 5.19 shows plot between$(\alpha h\nu)^2$ versus h$\nu$ of Fe-doped CCTO thin films. The resulting energy band gaps were 3.67 eV. The discrepancy will be further investigated. The refractive index can be obtained using envelope method from equation 3.9. The extinction coefficient can be obtained from equation 3.10. However, we focused on absorption region to extract some information as shown in Fig. 5.20

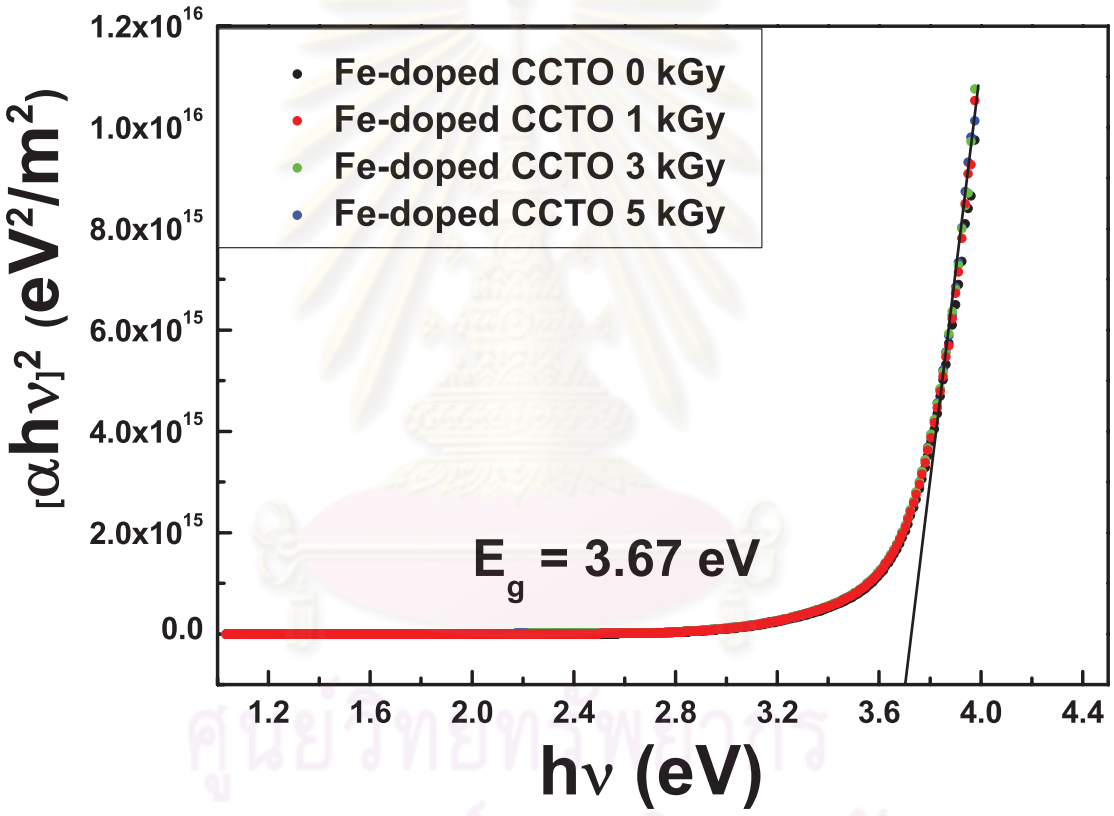


Figure 5.19: Plot between $(\alpha h\nu)^2$ versus h$\nu$ of Fe-doped CCTO thin films.

Figure 5.20 show the plot between ln$\alpha$ versus h$\nu$ of Fe-doped CCTO films. As the gamma radiation dose increased, the absorption edge energy width increased from 0.2298 to 0.2778 eV after 5 kGy indicating that the gamma ray induced more defects.

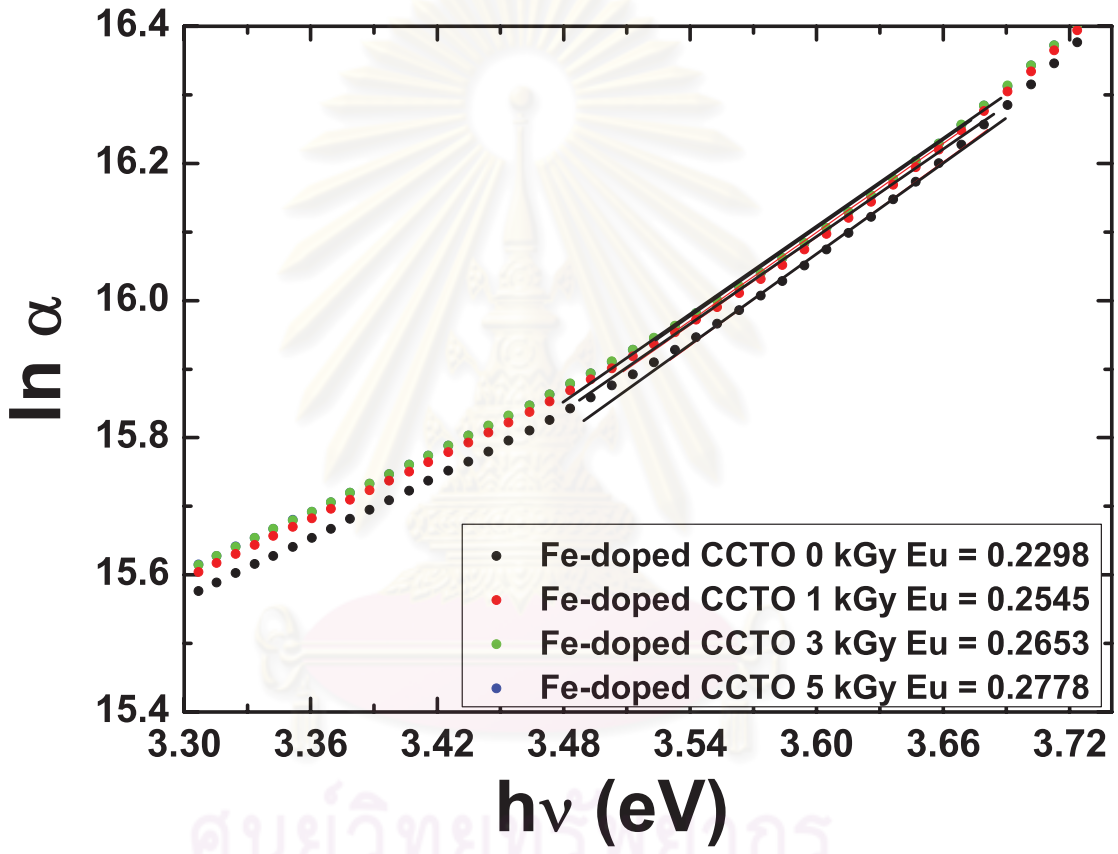


Figure 5.20: Determination of the Urbach energy for Fe-doped CCTO with difference gamma irradiation doses.

### 5.4.2 Complex refractive index (n and k) of Fe-doped CCTO

Figure 5.21 shows the refractive index and the extinction coefficient of the Fe-doped CCTO film measured in the 450-700 nm wavelength range. The refractive index of the films measured in this wavelength range increased from 2.24 - 2.00 range to 2.30 - 2.00 range for Fe-doped CCTO film upon the gamma irradiation with a 3 kGy dose with a corresponding increase in the extinction coefficient as shown in Figure 5.22. There was not much change in the refractive index of the films until the dose increased to 3 kGy. The increasing in the extinction coefficient with the irradiation dose indicates that high optical losses causing by the irradiation. The value of the extinction coefficient of the films before and after gamma irradiation was still on the order of $10^{-2}$. The shape of refractive index was similar to the result of Raffaella et al.'s group [53].

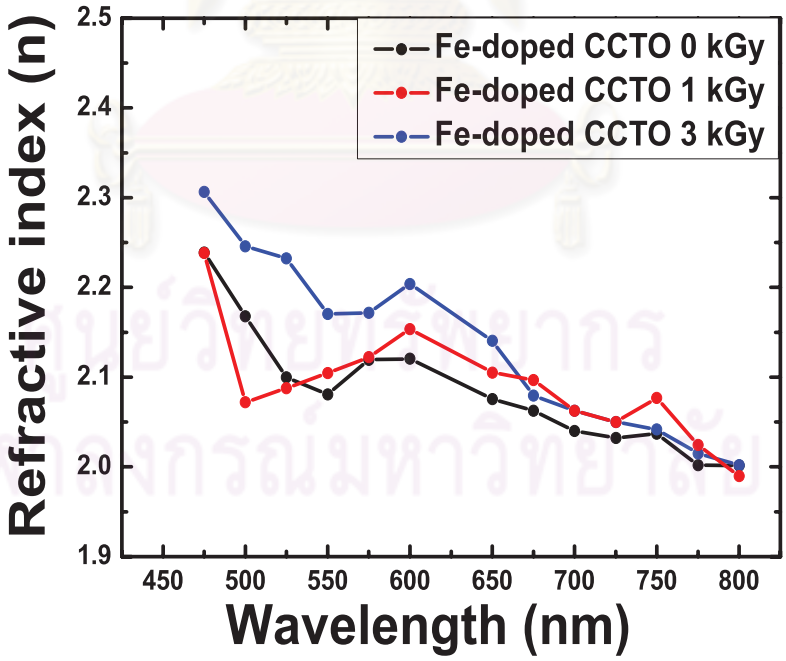


Figure 5.21: The refractive index of Fe-doped CCTO thin films for different gamma radiation dose.

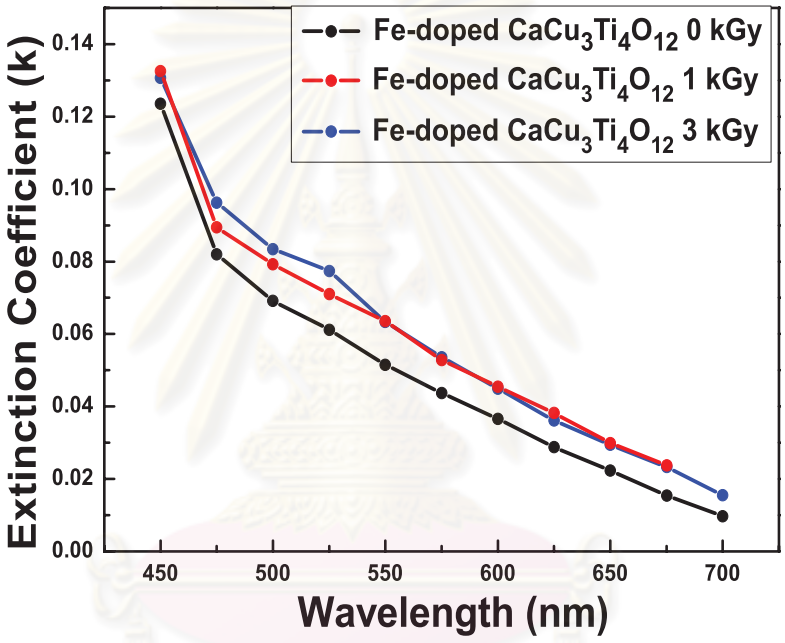


Figure 5.22: The extinction coefficient of Fe-doped CCTO thin films for different gamma radiation dose.

### 5.4.3 Capacitance of CCTO capacitor

CCTO film was grown on $Al_2O_3$ substrate which has insulator property. A HEWELETT PACKARD (HP): Model 4192A LCR IMPEDANCE ANALYZER was used to measure the capacitance of CCTO capacitor. When the electrodes are on the top of the film and on the same plane, the capacitor is so called a coplarnar capacitor. In general, the electrodes are in the form of interdigitate electrodes. The processing of interdigitated electrodes for this film can be read form Yamairoh Kasa's thesis [54]. Fig. 5.23 shows CCTO thin films with interdigitated electrodes. The gap width is 10$\mu$m and the overall size of capacitor is about 2×3 mm$^2$.

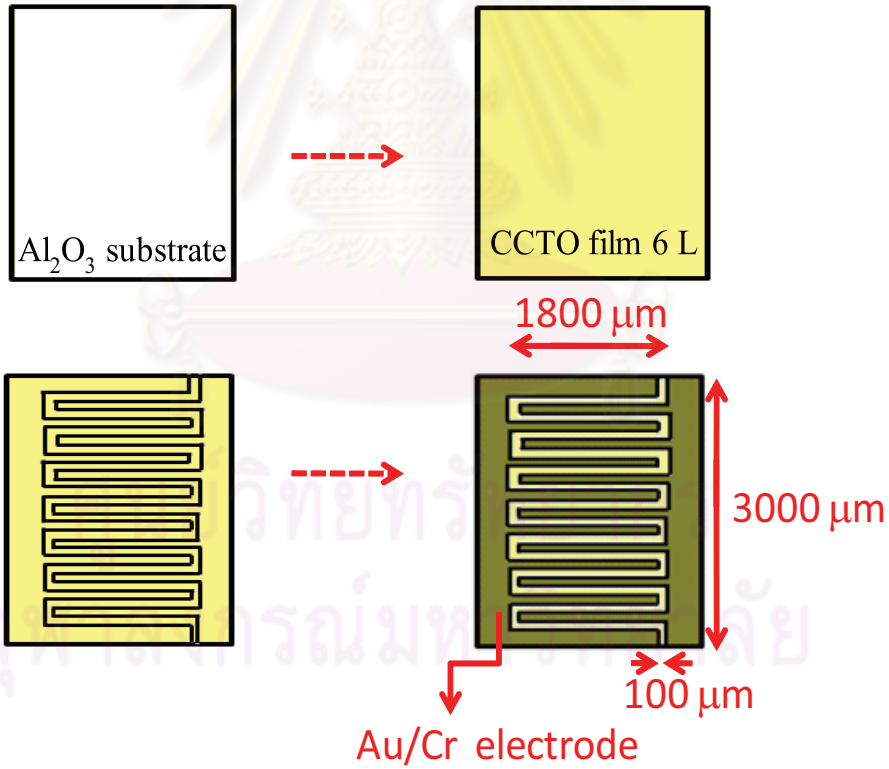


Figure 5.23: CCTO thin films with interdigitated electrode.

Figure 5.24 shows (a) the capacitance (b) dielectric constant and (c) loss tangent of the CCTO films before gamma radiation. Figure 5.25 shows (a) the capacitance (b) dielectric constant and (c) loss tangent of the CCTO films after gamma radiation dose of 5 kGy, respectively. From Fig. 5.24(a) and Fig. 5.25(a), the capacitance of the film before gamma ray irradiation which increases from 1.36 - 1.22 pF to 1.62 - 1.36 pF in 10 kHz - 1 MHz frequency range after gamma ray irradiation with 5 kGy doses. Our results increasing of capacitance values are consistant with other works [13]. Arshak et al. [13] found that the capacitance for ZnO thick film exhibited from 21.58 pF at a dose of 1 mGy to 28.33 pF at 2.3 mGy dose and thick films of $SnO_2$ also showed an increase in the capacitance from 5.05 pF before irradiation to 8.69 pF at a dose 0.46 mGy. However, our CCTO film based on the change of capacitance is not that sensitive to gamma rays like as ZnO and $SnO_2$. From Fig. 5.24(b) and (c) and Fig. 5.25(b) and (c), the dielectric constant of the CCTO film increasing from 314 - 280 to 552 - 308 and loss tangent of CCTO film increasing from 0.020 - 0.013 to 0.138 - 0.030. The observed increase in dielectric constant values with increasing dose may be attributed to a gradual formation of mobile charge carriers or easily orientable dipolar molecules that are capable of conducting the electric current. These charge carriers or dipolar molecules could be formed from structural modifications caused by gamma ray irradiation [55, 56, 57].

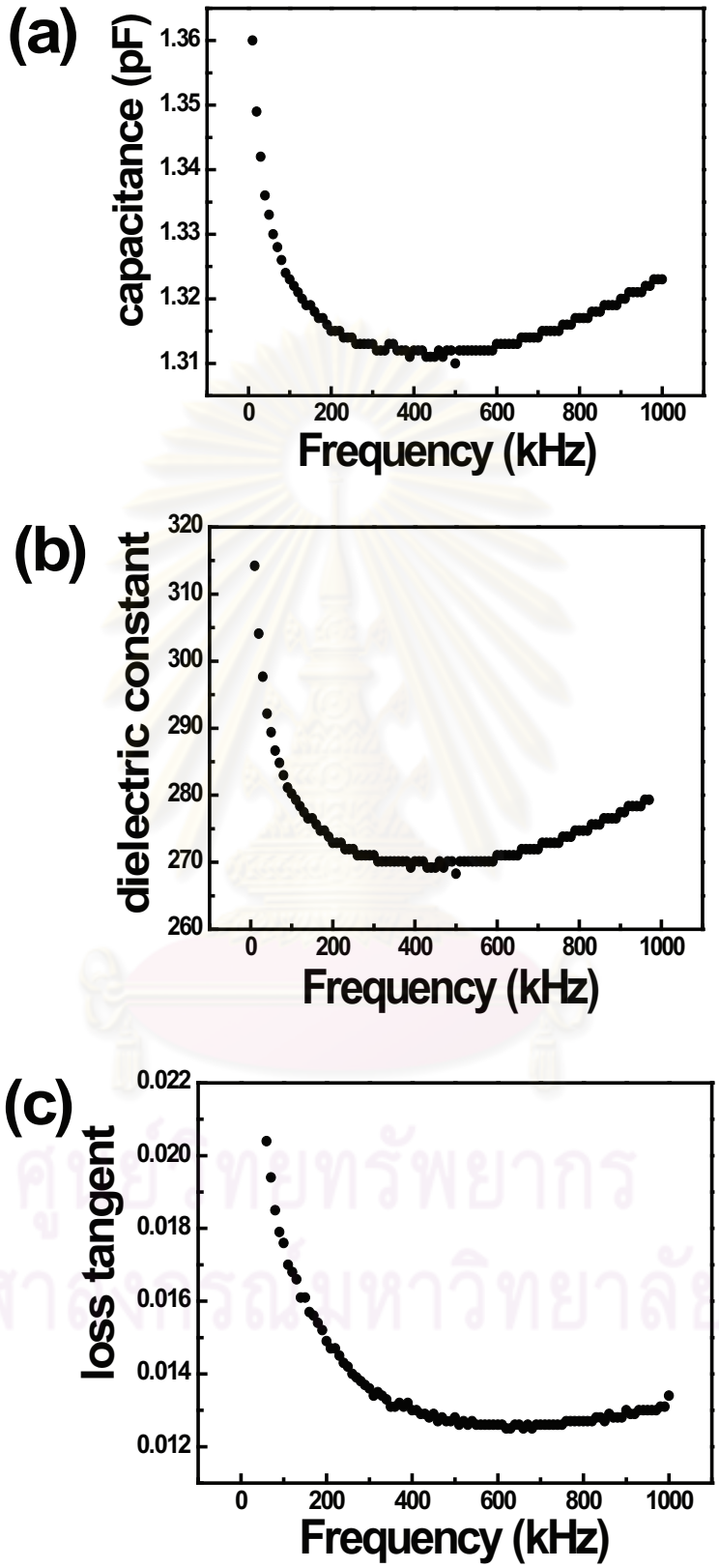


Figure 5.24: The (a) capacitance (b) dielectric constant and (C) loss tangent of CCTO films before gamma radiation.

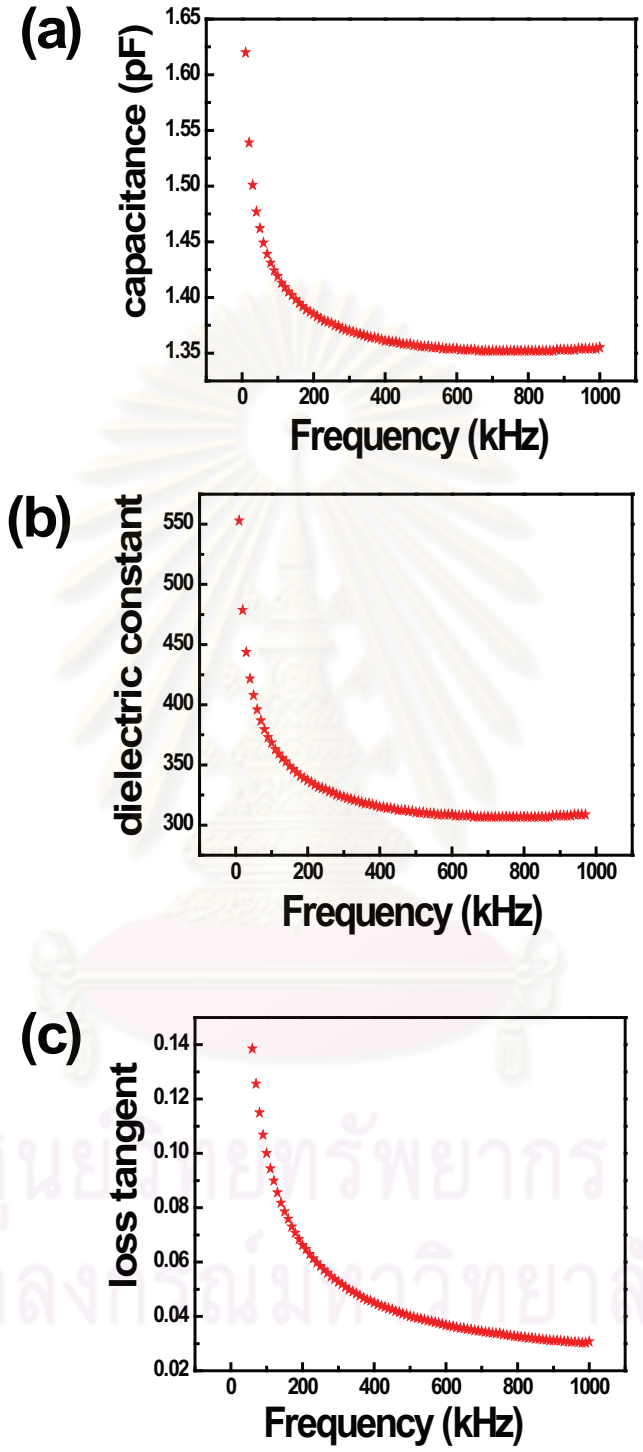


Figure 5.25: The (a) capacitance (b) dielectric constant and (C) loss tangent of CCTO films after gamma radiation dose of 5 kGy.

# CHAPTER VI

# CONCLUSIONS

In this thesis, we focus on the effect of gamma ray irradiation on optical properties of BTO, Fe-doped BTO and Fe-doped CCTO and electrical properties of CCTO thin films. We prepared the BTO, Fe-doped BTO, CCTO and Fe-doped CCTO thin films by a sol-gel spin coating technique with the annealing temperature of 800 $^{o}$C. BTO, Fe-doped BTO and Fe-doped CCTO thin films were grown on the quartz substrate for investigating the optical properties, while the CCTO thin film were grown on the $Al_2O_3$ in order to investigate the electrical properties, respectively. The conclusion of this thesis is as follows:

For BTO and Fe-doped BTO, the WDX shows signals that are consistent with $Ba_{0.8}Fe_{0.2}TiO_3$ with the Fe doping occurring by substitution of Ba sites in BTO. Gamma irradiation effects were found to be more pronounced for the Fe-doped BTO films than for the undoped BTO. The transmittance in the UVvisible range of Fe-doped BTO decreased by 11%, while that of BTO films decreased to 4% after 15 kGy irradiation respectively. The refractive index of the films, as measured in the 350 - 750 nm wavelength range was in the 2.24 - 2.00 range to 2.30 - 2.00 range after gamma irradiation at 15 kGy for Fe-doped BTO. The extinction coefficient of Fe-doped BTO films was in the order of $10^{-2}$ and increased after gamma irradiation. These changes are due to the formation of colour centers and the concomitant change in the complex refractive index for the irradiated Fe-doped BTO films.

The transmittance of Fe-doped CCTO films was reduced to 2.5%, 4.8% and 5.0% after exposure with gamma irradiation dose of 1 kGy, 3 kGy and 5 kGy, respectively. The refractive index increased from 1.76 - 1.99 range to 1.91 - 2.08 range for Fe-doped CCTO upon the gamma irradiation with a 3 kGy dose, respectively. The extinction coefficient of the Fe-doped CCTO film was in the order of $10^{-2}$ and increased after gamma irradiation. The capacitance of the CCTO film before gamma ray irradiation which increases from 1.36 - 1.22 pF to 1.62 - 1.36 pF after gamma ray irradiation dose of 5 kGy. The dielectric constant of the CCTO film increase from 314 - 280 to 552 - 308 after gamma ray irradiation dose of 5 kGy and loss tangent of CCTO film increase from 0.020 - 0.013 to 0.138 - 0.030 after gamma ray irradiation dose of 5 kGy, respectively.

Effects of gamma ray irradiation on fundamental properties of perovskite thin films prepared by a sol-gel spin coating techniques can be applied in design of modern radiation dosimeters based on the change in their optical and electrical properties.

# References


[1] Battish, I., Hamad, A., and Mahani, R. Structure and dielectric studies of nano-composite $Fe_2O_3$: $BaTiO_3$ prepared by sol-gel method. *Physica B* 404 (2009): 2274–2279.

[2] Brzozowski, E. and Castro, M. Grain growth control in Nb-doped $BaTiO_3$. *J. Mater. Process. Technol.* 168 (2005): 464–470.

[3] Daoudi, K., Tsuchiya, T., and Kumagai, T. Pulsed-laser crystallization and epitaxial growth of metal-organic films of Ca-doped $LaMnO_3$ on STO and LSAT substrates. *Appl. Surf. Sci.* 253 (2007): 6527–6530.

[4] Ye, Y. and Guo, T. Dielectric properties of Fe-doped $Ba_{0.65}Sr_{0.35}TiO_3$ thin films fabricated by the sol-gel method. *Ceram. Int.* 35 (2009): 2761–2765.

[5] Sulaimana, M., Hutagalunga, S., Ainb, M., and Ahmada, Z. Dielectric properties of Nb-doped $CaCu_3Ti_4O_{12}$ electroceramics measured at high frequencies. *J. Alloys Compd.* 493 (2010): 486–492.

[6] Chiodelli, G. et al. Electric and dielectric properties of pure and doped $CaCu_3Ti_4O_{12}$ perovskite materials. *Solid State Commun.* 132 (2004): 241–246.

[7] Kundu, T., Jana, A., and Barik, P. Doped barium titanate nanoparticles. *Bull. Mater. Sci.* 31 (2008): 501–505.

[8] Lina, F., Jianga, D., Maa, X., and Shi, W. Effect of annealing atmosphere on magnetism for Fe-doped $BaTiO_3$ ceramic. *Physica B* 403 (2008): 2525–2529.

[9] Lin, F., Jiang, D., Ma, X., and Shi, W. Influence of doping concentration on room-temperature ferromagnetism for Fe-doped $BaTiO_3$ ceramics. *J. Magn. Magn. Mater.* 320 (2008): 691–691.

[10] Hemer, S., Selmi, F., Varadan, V., and Varadan, V. The effect of various dopants on the dielectric properties of barium strontium titanate. *Mater. Lett.* 15 (1993): 317–324.

[11] Gao, J., Zheng, L., Song, Z., Lin, C., and Zhu, D. $\gamma$ ray irradiation effects of $Au/PbTiO_3/YBa_2Cu_3O_{7-\delta}$ capacitors under different bias voltage. *Mater. Lett.* 42 (2000): 345–349.

[12] Arshak, K. et al. Properties of BGO thin films under the influence of gamma radiation. *Thin Solid Films* 516 (2008): 1493–1498.

[13] Arshak, K. et al. Gamma Radiation Sensing Using ZnO and $SnO_2$ Thick Film Interdigitated Capacitors. *Electronics Technology, 2006. ISSE '06. 29th International Spring Seminar on* (2006): 483–488.

[14] Ta, M., Briand, D., Boudart, B., and Guhel, Y. $^{60}$Co gamma irradiation effects on electrical characteristics of $Al/Y_2O_3$/n-Si/Al capacitors. *Microelectron. Eng.* 87 (2010): 2158–2162.

[15] Fasasi, A. et al. Thermoluminescence properties of barium titanate prepared by solid-state reaction. *Sens. Actuator A-Phys.* 135 (2007): 598–604.

[16] Arshak, K. and Korostynska, O. Preliminary studies of properties of oxide thin/thick films for gamma radiation dosimetry. *Mater. Sci. Eng., B* 107 (2004): 224?232.

[17] Ke, S., Huang, H., Fan, H., Chan, H., and Zhou, L. Structural and electric properties of barium strontium titanate based ceramic composite as a humidity sensor. *Solid State Ion.* 179 (2008): 1632–1635.

[18] Zimmermann, F., Voigts, M., Menesklou, W., and Ivers-Tiffee, E. $Ba_{0.6}Sr_{0.4}TiO_3$ and $BaZr_{0.3}Ti_{0.7}O_3$ thick films as tunable microwave dielectrics. *J. Eur. Ceram. Soc.* 24 (2004): 1729–1733.

[19] Kumar, A. and Manavalan, S. Characterization of barium strontium titanate thin films for tunable microwave and DRAM applications. *Surf. Coat. Technol.* 198 (2005): 406–413.

[20] Li, W., Xu, Z., Chu, R., Fu, P., and Hao, J. Structure and electrical properties of $BaTiO_3$ prepared by sol-gel process. *J. Alloys Compd.* 482 (2009): 137–140.

[21] Wang, X., Zhang, L., Liu, H., Zhai, J., and Yao, X. Dielectric nonlinear properties of $BaTiO_3$-$CaTiO_3$-$SrTiO_3$ ceramics near the solubility limit. *Mater. Chem. Phys.* 112 (2008): 675–678.

[22] Xiao, C., Jin, C., and Wang, X. Crystal structure of dense nanocrystalline $BaTiO_3$ ceramics. *Mater. Chem. Phys.* 111 (2008): 209–212.

[23] Jaffe, B., Cook, W., and Jaffe, H.. *Piezoelectric Ceramics.* Academic Press, London 1971.

[24] Chen, K. and Chen, Y. Preparation of barium titanate ultrafine particles from rutile titania by a hydrothermal conversion. *Powder Technol.* 141 (2004): 69–74.

[25] Maier, R. and Cohn, J. Ferroelectric and ferrimagnetic iron-doped thin-?lm $BaTiO_3$ : Influence of iron on physical properties. *J. Appl. Phys.* 92 (2002): 5429–5436.

[26] Stashans, A. and Castillo, D. Simulation of iron impurity in $BaTiO_3$ crystals. *Physica B* 404 (2009): 1571–1575.

[27] Onodera, A., Takesada, M., Kawatani, K., and Hiramatsu, S. Dielectric Properties and Phase Transition in $CaCu_3Ti_4O_{12}$ at High Temperatures. *J. Appl. Phys.* 47 (2008): 7753–7756.

[28] Homes, C., Vogt, T., Shapiro, S., Wakimoto, S., and Ramirez, A. Optical Response of High-Dielectric-Constant Perovskite-Related Oxide. *Science* 293 (2001): 673–676.

[29] Barber, P. et al. Polymer Composite and Nanocomposite Dielectric Materials for Pulse Power Energy Storage. *J. Mater. Sci. Technol.* 2 (2009): 1697–1733.

[30] Fanga, L., Shen, M., and Cao, W. Effects of postanneal conditions on the dielectric properties of $CaCu_3Ti_4O_{12}$ thin films prepared on $Pt/Ti/SiO_2/Si$ substrates. *J. Appl. Phys.* 95 (2004): 6483–6485.

[31] Homes, C. et al. Charge transfer in the high dielectric constant materials $CaCu_3Ti_4O_{12}$ and $CdCu_3Ti_4O_{12}$. *Phys. Rev. B* 67 (2003): 092106(1)–092106(4).

[32] Fiorenza, P. et al. Perovskite $CaCu_3Ti_4O_{12}$ thin films for capacitive applications: From the growth to the nanoscopic imaging of the permittivity. *J. Appl. Phys.* 105 (2009): 061634 – 061634–6.

[33] Srivastava, A. et al. Dielectric relaxation in pulsed laser ablated $CaCu_3Ti_4O_{12}$ thin film. *J. Appl. Phys.* 100 (2006): 034102–034102–6.

[34] Krohns, S. et al. Correlations of structural, magnetic, and dielectric properties of undoped and doped $CaCu_3Ti_4O_{12}$. *Eur. Phys. J. B* 72 (2009): 173–182.

[35] Hernandez, M. et al. Eu-Doped $BaTiO_3$ Powder and Film from Sol-Gel Process with Polyvinylpyrrolidone Additive. *Int. J. Mol. Sci.* 10 (2009): 4088–4101.

[36] Voll, D., Bera, A., and Schneider, H. Temperature-Dependent sol-gel-derived mullite spectroscopic study dehydration of precursors: an FTIR. *J. Eur. Ceram. Soc.* 18 (1998): 1101–1106.

[37] Supasai, T. et al. Influence of temperature annealing on optical properties of $SrTiO_3/BaTiO_3$ multilayered films on indium tin oxide. *Appl. Surf. Sci.* 256 (2010): 4462–4467.

[38] Kovacs, E. and Keresztesb, A. Effect of gamma and UV-B/C radiation on plant cells. *Micron* 33 (2002): 199–210.

[39] Arshak, K. and Korostynska, O. Thin- and thick-film real-time gamma radiation detectors. *IEEE Sens. J.* 5 (2005): 574–580.

[40] Shimoyama, K., Kubo, K., Maeda, T., and Yamabe, K. Epitaxial Growth of $BaTiO_3$ Thin Film on $SrTiO_3$ Substrate in Ultra High Vacuum without Introducing Oxidant. *J. Appl. Phys.* 40 (2001): L463–L464.

[41] Caglar, M., Caglar, Y., and Ilican, S. The determination of the thickness and optical constants of the ZnO crystalline thin film by using envelope method. *J. Optoelectron. Adv. Mater.* 8 (2006): 1410–1413.

[42] Tauc, J. and Menth, A. States In The Gap. *J. Non-Cryst. Solids* 569 (1972): 8–10.

[43] Elshabini, A. and Barlow, F.. *Thin films technology handbook.*. New York 1998.

[44] Serway, R. and Beichner, R.. *Physics for scientists and engineers with modern physics.* 5th ed. Philadephia 2000.

[45] Dejene, F. and Ocaya, R. lectrical, optical and structural properties of pure and gold-coated $VO_2$ thin films on quartz substrate. *Curr. Appl. Phys.* 10 (2010): 508–512.

[46] Devan, R., Ma, Y., and Chougule, B. Effective dielectric and magnetic properties of (Ni-Co-Cu)ferrite/BTO composites. *Mater. Chem. Phys.* 115 (2009): 263–268.

[47] Swanepoel, R. Determination of the thickness and optical constants of amorphous silicon. *J. Phys. E. Sci. Instrum.* 16 (1983): 1214–1222.

[48] Mansingh, A. and Vasanta, C. Effect of the target on the structure and optical properties of radio-frequency sputtered barium titanate films. *J. Mater. Sci. Lett.* 7 (1988): 1104–1106.

[49] Onton, A., Marello, V., Lucovsky, G., and Galeener, F.. in *AIP Conf. Proc. No. 31, AIP, New York,* 1967.

[50] Zhang, H. et al. Optical and electrical properties of sol-gel derived $BaTiO_3$ films on ITO coated glass. *Mater. Chem. Phys.* 63 (2000): 174–177.

[51] Lu, X., Zhu, J., Zhang, W., Ma, G., and Wang, Y. The energy gap of r.f.-sputtered $BaTi0_3$ thin films with different grain size. *Thin Solid Films* 274 (1996): 165–168.

[52] Burs, L. Electronic Wave Functions in Semiconductor Clusters: Experiment and Theory. *J. Phys. Chem.* 90 (1986): 2555–2560.

[53] Nigro, R. et al. Calcium Copper-Titanate Thin Film Growth: Tailoring of the Operational Conditions through Nanocharacterization and Substrate Nature Effects. *J. Phys. Chem. B* 110 (2006): 17460–17467.

[54] Kasa, Y.. *Microstructural and dielectric properties of calcium copper titanate thin films prepared by a sol-gel method.* Master's thesis Chulalongkorn University 2010.

[55] A-Karmi, A. Impedance spectroscopy of gamma irradiated PM-355. *Radiat. Meas.* 41 (2006): 209–212.

[56] Tataroglu, A. and Altndal, S. The effects of frequency and c-irradiation on the dielectric properties of MIS type Schottky diodes. *Nucl. Instrum. Methods Phys. Res. Sect. B-Beam Interact. Mater. Atoms* 254 (2007): 113–117.

[57] A. Al-Karmi Impedance spectroscopy of gamma irradiated PM-355. *Radiat. Meas.* 41 (2006): 209–212.

# APPENDICES

# Appendix A
# XRD database

The XRD peak position of barium titanate, calcium copper titanate, contamination substances ($TiO_2$, $CaTiO_3$) thin films were confirmed by XRD database from The International Centre for Diffraction Data (ICDD) which shown as follows:

***Pattern :*** 00-005-0626 ***Radiation =*** 1.540598 ***Quality :*** High

$BaTiO_3$

Barium Titanium Oxide

***Lattice :*** Tetragonal
***S.G. :*** P4mm (99)

***a =*** 3.99400
***c =*** 4.03800

***Z =*** 1

***Mol. weight =*** 233.23
***Volume [CD] =*** 64.41
***Dx =*** 6.012
***I/Icor =*** 8.34

***Color:*** Colorless
***Additionnal diffraction line(s):*** Plus 10 additional reflections.
***Sample source or locality:*** Sample from National Lead Company.
***Sample preparation:*** Annealed at 1480 C in MgO.
***Analysis:*** Spectroscopic analysis: <0.1% Bi, Sr; <0.01% Al, Ca, Fe, Mg, Pb, Si; <0.001% Mn, Sn.
***General comments:*** Inverts to cubic form at 120 C.
***Temperature of data collection:*** X-ray pattern at 26 C.
***General comments:*** Merck Index, 8th Ed., p. 122.
***Data collection flag:*** Ambient.

Swanson, Fuyat., Natl. Bur. Stand. (U.S.), Circ. 539, volume 3, page 45 (1954)

CAS Number: 12047-27-7

***Radiation :*** CuKa1
***Lambda :*** 1.54050
***SS/FOM :*** F30= 19(0.0490,32)

***Filter :*** Beta
***d-sp :*** Not given

| *2th* | *i* | *h* | *k* | *l* |
|---|---|---|---|---|
| 22.039 | 12 | 0 | 0 | 1 |
| 22.263 | 25 | 1 | 0 | 0 |
| 31.498 | 100 | 1 | 0 | 1 |
| 31.647 | 100 | 1 | 1 | 0 |
| 38.888 | 46 | 1 | 1 | 1 |
| 44.856 | 12 | 0 | 0 | 2 |
| 45.378 | 37 | 2 | 0 | 0 |
| 50.614 | 6 | 1 | 0 | 2 |
| 50.978 | 8 | 2 | 0 | 1 |
| 51.100 | 7 | 2 | 1 | 0 |
| 55.955 | 15 | 1 | 1 | 2 |
| 56.253 | 35 | 2 | 1 | 1 |
| 65.755 | 12 | 2 | 0 | 2 |
| 66.123 | 10 | 2 | 2 | 0 |
| 70.359 | 5 | 2 | 1 | 2 |
| 70.662 | 2 | 3 | 0 | 0 |
| 74.336 | 5 | 1 | 0 | 3 |
| 75.094 | 7 | 3 | 0 | 1 |
| 75.164 | 9 | 3 | 1 | 0 |
| 78.768 | 3 | 1 | 1 | 3 |
| 79.472 | 5 | 3 | 1 | 1 |
| 83.492 | 7 | 2 | 2 | 2 |
| 86.965 | 1 | 2 | 0 | 3 |
| 87.287 | 1 | 3 | 0 | 2 |
| 88.069 | 1 | 3 | 2 | 0 |
| 91.586 | 7 | 2 | 1 | 3 |
| 92.060 | 12 | 3 | 1 | 2 |
| 92.327 | 12 | 3 | 2 | 1 |
| 99.494 | 1 | 0 | 0 | 4 |
| 100.984 | 2 | 4 | 0 | 0 |
| 103.869 | 1 | 1 | 0 | 4 |
| 104.502 | 1 | 2 | 2 | 3 |
| 104.991 | 1 | 3 | 2 | 2 |
| 105.362 | 1 | 4 | 1 | 0 |
| 108.256 | 3 | 1 | 1 | 4 |
| 108.946 | 1 | 3 | 0 | 3 |
| 109.733 | 5 | 4 | 1 | 1 |
| 113.556 | 2 | 3 | 1 | 3 |
| 114.362 | 2 | 3 | 3 | 1 |
| 117.506 | 3 | 2 | 0 | 4 |

***Pattern :*** 01-075-1149 ***Radiation =*** 1.540598 ***Quality :*** Alternate

$CaCu_3Ti_4O_{12}$

Calcium Copper Titanium Oxide
***Also called:*** Calcium tricopper tetratitanium oxide

***Lattice :*** Body-centered cubic
***S.G. :*** Im-3m (229)

***Mol. weight =*** 614.31
***Volume [CD] =*** 404.08

***a =*** 7.39300
***Dx =*** 5.049

***Z =*** 2
***I/Icor =*** 5.33

***ICSD collection code:*** 030592
***Test from ICSD:*** No R value given.
***Test from ICSD:*** At least one TF missing.
***Cancel:***
Data collection flag: Ambient.

Deschanvres, A., Raveau, B., Tollemer, F., Bull. Soc. Chim. Fr., volume 1967, page 4077 (1967)
Calculated from ICSD using POWD-12++ (1997)

***Radiation :*** CuKa1
***Lambda :*** 1.54060
***SS/FOM :*** F22=1000(0.0000,22)

***Filter :*** Not specified
***d-sp :*** Calculated spacings

| *2th* | *i* | *h* | *k* | *l* |
|---|---|---|---|---|
| 16.947 | 20 | 1 | 1 | 0 |
| 24.056 | 13 | 2 | 0 | 0 |
| 29.573 | 10 | 2 | 1 | 1 |
| 34.279 | 999 | 2 | 2 | 0 |
| 38.475 | 4 | 3 | 1 | 0 |
| 42.315 | 141 | 2 | 2 | 2 |
| 45.891 | 5 | 3 | 2 | 1 |
| 49.262 | 406 | 4 | 0 | 0 |
| 52.470 | 2 | 4 | 1 | 1 |
| 55.545 | 1 | 4 | 2 | 0 |
| 58.512 | 1 | 3 | 3 | 2 |
| 61.386 | 248 | 4 | 2 | 2 |
| 64.184 | 2 | 5 | 1 | 0 |
| 69.597 | 1 | 5 | 2 | 1 |
| 72.230 | 159 | 4 | 4 | 0 |
| 74.824 | 1 | 5 | 3 | 0 |
| 77.387 | 1 | 4 | 4 | 2 |
| 79.926 | 1 | 5 | 3 | 2 |
| 82.443 | 76 | 6 | 2 | 0 |
| 84.947 | 1 | 5 | 4 | 1 |
| 87.440 | 16 | 6 | 2 | 2 |
| 89.929 | 1 | 6 | 3 | 1 |

***Pattern :*** 03-065-1156 ***Radiation =*** 1.540598 ***Quality :*** Deleted

$TiO_2$

Titanium Oxide

***Lattice :*** Monoclinic ***Mol. weight =*** 79.90

***S.G. :*** P21/m (11) ***Volume [CD] =*** 284.23

***a =*** 12.17870 ***Dx =*** 1.867

***b =*** 3.74120 ***beta =*** 107.05

***c =*** 6.52490

***a/b =*** 3.25529 ***Z =*** 4 ***I/Icor =*** 7.54

***c/b =*** 1.74407

***NIST M&A collection code:*** N 2978 8216
***Temperature factor:*** IB=O,Ti
***Deleted and rejected by:*** Deleted: calculated density look very unusual for the given system, SK 2/02.
***Data collection flag:*** Ambient.

T.P.Feist & P.K.Davies, J. Solid State Chem., volume 101, page 275-2 (1992)
Calculated from NIST using POWD-12++

***Radiation :*** CuKa1 ***Filter :*** Not specified

***Lambda :*** 1.54060 ***d-sp :*** Calculated spacings

***SS/FOM :*** F30=1000(0.0000,34)

| 2th | i | h | k | l |
|---|---|---|---|---|
| 7.587 | 999 | 1 | 0 | 0 |
| 13.991 | 7 | -1 | 0 | 1 |
| 14.186 | 57 | 0 | 0 | 1 |
| 15.207 | 38 | 2 | 0 | 0 |
| 17.512 | 6 | -2 | 0 | 1 |
| 17.979 | 23 | 1 | 0 | 1 |
| 22.895 | 22 | 3 | 0 | 0 |
| 23.152 | 26 | -3 | 0 | 1 |
| 23.748 | 8 | 2 | 0 | 1 |
| 24.979 | 298 | 1 | 1 | 0 |
| 27.324 | 7 | -1 | 0 | 2 |
| 27.783 | 4 | 0 | 1 | 1 |
| 28.334 | 97 | 2 | 1 | 0 |
| 28.596 | 52 | 0 | 0 | 2 |
| 29.673 | 11 | -2 | 1 | 1 |
| 29.799 | 36 | -4 | 0 | 1 |
| 29.959 | 26 | 1 | 1 | 1 |
| 30.461 | 4 | 3 | 0 | 1 |
| 30.690 | 10 | 4 | 0 | 0 |
| 31.050 | 3 | -3 | 0 | 2 |
| 31.777 | 2 | 1 | 0 | 2 |
| 33.235 | 12 | 3 | 1 | 0 |
| 33.846 | 11 | 2 | 1 | 1 |
| 35.451 | 5 | -4 | 0 | 2 |
| 36.521 | 31 | -1 | 1 | 2 |
| 37.006 | 2 | -5 | 0 | 1 |
| 37.199 | 8 | -2 | 1 | 2 |
| 37.512 | 1 | 0 | 1 | 2 |
| 37.710 | 6 | 4 | 0 | 1 |
| 38.465 | 7 | -4 | 1 | 1 |
| 38.633 | 4 | 5 | 0 | 0 |
| 38.996 | 1 | 3 | 1 | 1 |
| 39.181 | 1 | 4 | 1 | 0 |
| 39.472 | 1 | -3 | 1 | 2 |
| 40.065 | 19 | 1 | 1 | 2 |
| 40.976 | 1 | -5 | 0 | 2 |
| 41.796 | 2 | -1 | 0 | 3 |
| 42.120 | 1 | 3 | 0 | 2 |
| 42.863 | 1 | -3 | 0 | 3 |
| 43.128 | 1 | -4 | 1 | 2 |
| 43.486 | 28 | 0 | 0 | 3 |
| 43.955 | 4 | 2 | 1 | 2 |
| 44.456 | 54 | -5 | 1 | 1 |
| 44.613 | 43 | -6 | 0 | 1 |
| 45.063 | 1 | 4 | 1 | 1 |
| 45.351 | 1 | 5 | 0 | 1 |
| 45.537 | 1 | -4 | 0 | 3 |
| 46.525 | 8 | 1 | 0 | 3 |
| 46.775 | 2 | 6 | 0 | 0 |
| 47.323 | 3 | -6 | 0 | 2 |
| 47.917 | 7 | -5 | 1 | 2 |
| 48.635 | 39 | 0 | 2 | 0 |
| *48.635 | 39 | -1 | 1 | 3 |
| 49.300 | 11 | 1 | 2 | 0 |
| 49.427 | 6 | -5 | 0 | 3 |
| 49.594 | 1 | -3 | 1 | 3 |
| 50.152 | 1 | 0 | 1 | 3 |
| 50.726 | 3 | 2 | 0 | 3 |
| 50.923 | 3 | -1 | 2 | 1 |
| *50.923 | 3 | 0 | 2 | 1 |
| 51.165 | 18 | -6 | 1 | 1 |
| 51.256 | 11 | 2 | 2 | 0 |
| 51.832 | 11 | 5 | 1 | 1 |
| 52.000 | 7 | -4 | 1 | 3 |
| 52.264 | 3 | 1 | 2 | 1 |
| 52.581 | 14 | -7 | 0 | 1 |
| 52.897 | 27 | 1 | 1 | 3 |
| 53.124 | 15 | 6 | 1 | 0 |
| 53.353 | 5 | 6 | 0 | 1 |
| 54.347 | 6 | -6 | 0 | 3 |
| *54.347 | 6 | 3 | 2 | 0 |
| 54.527 | 7 | -3 | 2 | 1 |
| 54.818 | 1 | 4 | 1 | 2 |
| *54.818 | 1 | 2 | 2 | 1 |
| 55.175 | 3 | 7 | 0 | 0 |
| 55.554 | 8 | -5 | 1 | 3 |
| 55.711 | 5 | 5 | 0 | 2 |
| 55.908 | 6 | 3 | 0 | 3 |
| 56.379 | 1 | -2 | 0 | 4 |
| 56.753 | 24 | -3 | 0 | 4 |
| *56.753 | 24 | 2 | 1 | 3 |
| 57.168 | 2 | -2 | 2 | 2 |
| *57.168 | 2 | -1 | 0 | 4 |
| 57.393 | 10 | 0 | 2 | 2 |
| 58.087 | 7 | -4 | 2 | 1 |
| 58.311 | 9 | -4 | 0 | 4 |
| 58.476 | 8 | -7 | 1 | 1 |
| *58.476 | 8 | 3 | 2 | 1 |
| 58.614 | 4 | 4 | 2 | 0 |
| 58.830 | 2 | -3 | 2 | 2 |
| 59.196 | 3 | 6 | 1 | 1 |
| *59.196 | 3 | 1 | 2 | 2 |
| 60.145 | 7 | -6 | 1 | 3 |
| *60.145 | 7 | -7 | 0 | 3 |
| 60.903 | 1 | 7 | 1 | 0 |
| *60.903 | 1 | -5 | 0 | 4 |
| 61.407 | 4 | 5 | 1 | 2 |
| 61.611 | 5 | 3 | 1 | 3 |
| *61.611 | 5 | -4 | 2 | 2 |
| 61.738 | 3 | 7 | 0 | 1 |
| 61.933 | 5 | -8 | 0 | 2 |
| *61.933 | 5 | 4 | 0 | 3 |
| 62.036 | 7 | -2 | 1 | 4 |
| 62.256 | 3 | 2 | 2 | 2 |
| *62.256 | 3 | 1 | 0 | 4 |
| 62.389 | 1 | -3 | 1 | 4 |
| 62.650 | 1 | -5 | 2 | 1 |
| 62.816 | 4 | -1 | 1 | 4 |
| 63.129 | 3 | 4 | 2 | 1 |
| 63.390 | 3 | 6 | 0 | 2 |
| 63.863 | 2 | -4 | 1 | 4 |
| *63.863 | 2 | 8 | 0 | 0 |
| 64.730 | 4 | 0 | 1 | 4 |
| *64.730 | 4 | -6 | 0 | 4 |
| 65.605 | 1 | -7 | 1 | 3 |
| 65.867 | 1 | -2 | 2 | 3 |
| 66.022 | 1 | -1 | 2 | 3 |
| 66.418 | 15 | 2 | 0 | 4 |
| *66.418 | 15 | -5 | 1 | 4 |
| 66.807 | 1 | -3 | 2 | 3 |
| 67.125 | 2 | 7 | 1 | 1 |
| 67.270 | 11 | 0 | 2 | 3 |
| *67.270 | 11 | 4 | 1 | 3 |
| 68.117 | 9 | -6 | 2 | 1 |
| 68.708 | 4 | 6 | 1 | 2 |
| *68.708 | 4 | 5 | 0 | 3 |
| 69.208 | 3 | 8 | 1 | 0 |
| 69.427 | 3 | -7 | 0 | 4 |
| 69.580 | 4 | 1 | 2 | 3 |
| 69.774 | 3 | -9 | 0 | 1 |
| *69.774 | 3 | 6 | 2 | 0 |
| 69.996 | 3 | -6 | 1 | 4 |
| *69.996 | 3 | -9 | 0 | 2 |
| 70.202 | 3 | -6 | 2 | 2 |
| 71.206 | 1 | 4 | 2 | 2 |
| 71.642 | 4 | 2 | 1 | 4 |
| *71.642 | 4 | 7 | 0 | 2 |
| 71.913 | 3 | -5 | 2 | 3 |
| *71.913 | 3 | -8 | 1 | 3 |
| 72.638 | 1 | -2 | 0 | 5 |
| 72.909 | 1 | 2 | 2 | 3 |
| 73.084 | 1 | 9 | 0 | 0 |
| *73.084 | 1 | -4 | 0 | 5 |
| 73.848 | 3 | 5 | 1 | 3 |
| *73.848 | 3 | -1 | 0 | 5 |
| 74.027 | 2 | -9 | 0 | 3 |
| 74.425 | 7 | -7 | 2 | 1 |
| 74.817 | 2 | -9 | 1 | 1 |
| 75.064 | 4 | 6 | 2 | 1 |
| *75.064 | 4 | -9 | 1 | 2 |
| 75.651 | 1 | 8 | 1 | 1 |
| 75.894 | 3 | -7 | 2 | 2 |
| *75.894 | 3 | -6 | 2 | 3 |
| 76.255 | 2 | 6 | 0 | 3 |
| *76.255 | 2 | 0 | 0 | 5 |
| 76.495 | 1 | 3 | 1 | 4 |
| 76.589 | 2 | 7 | 2 | 0 |
| 76.811 | 7 | 1 | 3 | 0 |
| 77.043 | 3 | 5 | 2 | 2 |
| 77.210 | 4 | 3 | 2 | 3 |
| 77.366 | 2 | 4 | 0 | 4 |
| *77.366 | 2 | -3 | 1 | 5 |
| 77.611 | 1 | -2 | 2 | 4 |
| *77.611 | 1 | -2 | 1 | 5 |
| 77.929 | 4 | -6 | 0 | 5 |
| *77.929 | 4 | -3 | 2 | 4 |
| 78.102 | 2 | 9 | 1 | 0 |
| *78.102 | 2 | -4 | 1 | 5 |
| 78.352 | 4 | -1 | 2 | 4 |
| *78.352 | 4 | 2 | 3 | 0 |
| 78.797 | 1 | -10 | 0 | 2 |
| 78.932 | 2 | -1 | 1 | 5 |
| 79.024 | 2 | -9 | 1 | 3 |
| *79.024 | 2 | -10 | 0 | 1 |
| 79.271 | 5 | -4 | 2 | 4 |
| 79.575 | 3 | 1 | 0 | 5 |
| 80.042 | 1 | -5 | 1 | 5 |
| *80.042 | 1 | 0 | 2 | 4 |
| 80.532 | 1 | 8 | 0 | 2 |
| 80.870 | 3 | -7 | 2 | 3 |
| *80.870 | 3 | 3 | 3 | 0 |
| 81.190 | 2 | 6 | 1 | 3 |
| *81.190 | 2 | 0 | 1 | 5 |
| 81.560 | 1 | -9 | 0 | 4 |
| *81.560 | 1 | -8 | 2 | 1 |
| 81.719 | 1 | -7 | 0 | 5 |
| 82.090 | 1 | -10 | 0 | 3 |
| 82.279 | 1 | 7 | 2 | 1 |
| *82.279 | 1 | 4 | 1 | 4 |
| 82.452 | 3 | -8 | 2 | 2 |
| *82.452 | 3 | 4 | 2 | 3 |
| 82.800 | 3 | -1 | 3 | 2 |
| *82.800 | 3 | 10 | 0 | 0 |
| 83.209 | 1 | -2 | 3 | 2 |
| 83.400 | 1 | 0 | 3 | 2 |
| 83.756 | 2 | -10 | 1 | 2 |
| *83.756 | 2 | 6 | 2 | 2 |
| 83.963 | 2 | -10 | 1 | 1 |
| *83.963 | 2 | -4 | 3 | 1 |

***Pattern :*** 00-042-0423 ***Radiation =*** 1.540598 ***Quality :*** High

$CaTiO_3$

Calcium Titanium Oxide
Perovskite, syn

***Lattice :*** Orthorhombic
***S.G. :*** Pnma (62)

***a =*** 5.44240
***b =*** 7.64170
***c =*** 5.38070
***a/b =*** 0.71220
***c/b =*** 0.70412
***Z =*** 4

***Mol. weight =*** 135.98
***Volume [CD] =*** 223.78
***Dx =*** 4.036
***Dm =*** 4.030

***Sample preparation:*** Prepared from Ti O2 and Ca C O3 at 1100 C for 16 hours, reground, and then 1300 C for 16 hours.
***Analysis:*** Chemical analysis (wt.%): Ca 28.82, Tl 26.54, Al 0.103, Si <0.04, Cr <0.002, Fe 0.044, Sr 0.013, Zr 0.533, Mo <0.004, Pd <0.004, Ag <0.004, Cd 0.008, Ba 0.011, Ce <0.03, Nd <0.03, U <0.07.
***General comments:*** High resolution comparison of CuKα and CoKα patterns to obtain high accuracy cell parameters.
***Optical data:*** B=2.38
***Data collection flag:*** Ambient.

Ball, C., Napier, J., Aust. Nucl. Sci. Technol. Organ. (1988)

***Radiation :*** CuKa1
***Lambda :*** 1.54060
***SS/FOM :*** F30=169(0.0057,31)

***Filter :*** Not specified
***d-sp :*** Debye-Scherrer

| *2th* | *i* | *h* | *k* | *l* |
|---|---|---|---|---|
| 23.230 | 10 | 1 | 0 | 1 |
| 23.260 | 5 | 0 | 2 | 0 |
| 26.030 | 3 | 1 | 1 | 1 |
| 32.900 | 26 | 2 | 0 | 0 |
| 33.110 | 100 | 1 | 2 | 1 |
| 33.270 | 24 | 0 | 0 | 2 |
| 34.980 | 1 | 2 | 1 | 0 |
| 37.000 | 1 | 2 | 0 | 1 |
| 37.250 | 2 | 1 | 0 | 2 |
| 38.890 | 2 | 2 | 1 | 1 |
| 39.090 | 4 | 0 | 3 | 1 |
| 39.140 | 3 | 1 | 1 | 2 |
| 40.680 | 5 | 2 | 2 | 0 |
| 40.990 | 4 | 0 | 2 | 2 |
| 42.610 | 2 | 1 | 3 | 1 |
| 44.160 | 2 | 2 | 2 | 1 |
| 44.380 | 1 | 1 | 2 | 2 |
| 47.490 | 44 | 2 | 0 | 2 |
| 47.560 | 23 | 0 | 4 | 0 |
| 48.950 | 2 | 2 | 3 | 0 |
| 49.050 | 2 | 2 | 1 | 2 |
| 51.990 | 1 | 2 | 3 | 1 |
| 52.190 | 1 | 1 | 3 | 2 |
| 52.350 | 1 | 0 | 1 | 3 |
| 53.260 | 2 | 3 | 0 | 1 |
| 53.530 | 2 | 2 | 2 | 2 |
| 53.580 | 2 | 1 | 4 | 1 |
| 53.770 | 1 | 1 | 0 | 3 |
| 54.700 | 4 | 3 | 1 | 1 |
| 55.200 | 1 | 1 | 1 | 3 |
| 58.880 | 15 | 3 | 2 | 1 |
| 59.040 | 10 | 2 | 4 | 0 |
| 59.280 | 10 | 0 | 4 | 2 |
| 59.350 | 22 | 1 | 2 | 3 |
| 61.910 | 1 | 1 | 4 | 2 |
| *61.920 | 1 | 2 | 0 | 3 |
| 63.190 | 1 | 0 | 5 | 1 |
| 65.460 | 1 | 3 | 3 | 1 |
| 68.990 | 4 | 4 | 0 | 0 |
| 69.480 | 18 | 2 | 4 | 2 |
| 69.860 | 4 | 0 | 0 | 4 |
| 70.230 | 1 | 4 | 1 | 0 |
| 71.490 | 1 | 4 | 0 | 1 |
| 72.290 | 1 | 1 | 0 | 4 |
| 73.000 | 1 | 3 | 3 | 2 |
| 73.110 | 1 | 2 | 5 | 1 |
| 73.270 | 1 | 1 | 5 | 2 |
| *73.270 | 1 | 2 | 3 | 3 |
| 73.510 | 1 | 1 | 1 | 4 |
| 73.910 | 1 | 4 | 2 | 0 |
| 74.160 | 1 | 3 | 4 | 1 |
| 75.520 | 1 | 3 | 1 | 3 |
| 77.120 | 1 | 1 | 2 | 4 |
| 78.780 | 3 | 4 | 0 | 2 |
| 79.110 | 5 | 3 | 2 | 3 |
| 79.200 | 6 | 1 | 6 | 1 |
| 79.400 | 1 | 2 | 0 | 4 |
| 79.970 | 1 | 4 | 1 | 2 |
| 80.350 | 1 | 2 | 5 | 2 |
| 80.590 | 1 | 2 | 1 | 4 |
| 82.930 | 1 | 0 | 5 | 3 |
| 83.040 | 1 | 1 | 3 | 4 |
| 84.830 | 1 | 3 | 5 | 1 |
| 84.990 | 1 | 3 | 3 | 3 |
| 85.240 | 1 | 1 | 5 | 3 |
| 88.090 | 3 | 4 | 4 | 0 |
| 88.910 | 3 | 0 | 4 | 4 |
| 89.330 | 1 | 4 | 3 | 2 |
| 92.110 | 1 | 0 | 7 | 1 |
| *92.120 | 1 | 3 | 1 | 4 |
| 92.480 | 1 | 5 | 0 | 1 |
| 93.649 | 1 | 5 | 1 | 1 |
| 97.160 | 2 | 5 | 2 | 1 |
| 97.500 | 3 | 4 | 4 | 2 |
| 97.670 | 3 | 3 | 6 | 1 |
| 98.080 | 4 | 1 | 6 | 3 |
| 98.120 | 3 | 2 | 4 | 4 |
| 98.399 | 5 | 1 | 2 | 5 |
| 98.599 | 1 | 4 | 5 | 0 |
| 103.070 | 1 | 5 | 3 | 1 |
| 107.290 | 2 | 4 | 0 | 4 |
| 107.490 | 1 | 0 | 8 | 0 |
| 108.520 | 1 | 4 | 1 | 4 |
| 111.620 | 1 | 5 | 4 | 1 |
| 111.790 | 1 | 5 | 0 | 3 |

| *2th* | *i* | *h* | *k* | *l* |
|---|---|---|---|---|
| 112.240 | 1 | 4 | 2 | 4 |
| 112.440 | 1 | 1 | 8 | 1 |
| 112.670 | 1 | 3 | 0 | 5 |
| 113.050 | 1 | 5 | 1 | 3 |
| 113.430 | 1 | 3 | 7 | 1 |
| 113.940 | 1 | 3 | 1 | 5 |
| 116.320 | 1 | 6 | 0 | 0 |
| 116.900 | 3 | 5 | 2 | 3 |
| 117.450 | 3 | 2 | 8 | 0 |
| *117.470 | 3 | 3 | 6 | 3 |
| 117.680 | 3 | 0 | 8 | 2 |
| 117.820 | 5 | 3 | 2 | 5 |
| 118.390 | 1 | 0 | 0 | 6 |
| 118.700 | 1 | 4 | 3 | 4 |

# Appendix B
# Fe-doping concentration

The concentration of Fe doped 10% by weight for BTO and Fe doped 2% by weight for CCTO were choosed in this thesis. The process of calculation as shown in equation 1. From WDX experiment shown that Fe concentration of BTO is 7% (data shown in Subsection 5.1.3) and EDX experiment show that Fe concentration of CCTO about 2.5% (data shown in Subsection 5.3.2) by weight instead of 10% and 2% by weight, respectively.

$$\left(\frac{\frac{gFe}{MW_{Fe}}}{\frac{g(Ba/Ca)}{MW_{(Ba/Ca)}}}\right)\left(\frac{MW_{Fe}}{MW_{(BTO/CCTO)}}\right)\times 100 = .....\% \qquad (1)$$

where $gFe$ is weight of Fe, $MW_{Fe}$ is molecular weight of $Fe$, $g(Ba/Ca)$ is weight of $Ba$ for Fe-doped BTO or weight of $Ca$ for Fe-doped CCTO, $MW_{Ba/Ca}$ is molecular weight of $Ba$ for BTO or $Ca$ for Fe-doped CCTO and $MW_{(BTO/CCTO)}$ is molecular weight of BTO or CCTO, respectively.

# Appendix C
# Definition

Gray (Gy) is the SI unit of energy for the absorbed dose of radiation.

Absorbed dose is defined as the deposited energy from incident radiation per unit mass of target material, such as air or body tissue.

One gray is the absorption of one joule of radiation energy by one kilogram of matter.

The curie temperature (Tc) is the critical temperature which a previously ferromagnetic material becomes paramagnetic.

# Appendix D
# Conference presentations

## International Presentations:

**Kongwut, O.** , Kornduangkaeo, A. , Jangsawang, N. and Hodak, S.K. Influence of gamma irradiation on refractive index of Fe-doped barium titanate thin films. Poster presentation at The Fifth Mathematics and Physical Sciences Graduate Congress, Faculty of Science, Chulalongkorn University, Bangkok (7-9 December 2009)

**O. Kongwut**, A. Kornduangkaeo, N. Jangsawang and S.K. Hodak, Influence of gamma irradiation on refractive index of Fe-doped barium titanate thin films. Oral presentation at TACT 2009 International Thin Films Conference, National Taipei University of Technology, Taipei, Taiwan (14-16 December 2009)

## Local Presentation:

**O. Kongwut**, W. Dharmavanij, A. Kornduangkaeo and S. K. Hodak. Effects of gamma ray irradiation on optical properties of $BaTiO_3$ thin films prepared by a sol-gel methode. Oral presentation at The Science forum 2009, Faculty of Science, Chulalongkorn University, Bangkok (12-13 March 2009)

**O. Kongwut**, W. Dharmavanij, A. Kornduangkaeo and S.K. Hodak. Effects of gamma ray irradiation on optical properties of $BaTiO_3$ thin films prepared

by a sol-gel method. Poster presentation at Siam Physics Congress 2009, Cha am beach, Phetchaburi (19-21 March 2009)

**O. Kongwut**, N. Jangsawang, A. Kornduangkaeo and S.K. Hodak. Optical properties of Fe-doped calcium copper titanate thin films under gamma irradiation. Poster presentation at The 16th national graduate Research Conference, Maejo University, Sansai, Chiang Mai (11-12 March 2010)

Satreerat K. Hodak, **O. Kongwut**, N. Jangsawang and A. Kornduangkaeo. Optical properties of Fe-doped barium titanate thin films under gamma irradiation. Oral presentation at The Science forum 2009, Faculty of Science, Chulalongkorn University, Bangkok (11-12 March 2010)

**O. Kongwut**, N. Jangsawang, A. Kornduangkaeo and S.K. Hodak. Optical properties of Fe-doped calcium copper titanate thin films under gamma irradiation. Oral presentation at Siam Physics Congress 2010, River Kwai Village Hotel, Kanchanaburi (25-27 March 2010)

# Appendix E
# Publications

**O. Kongwut**, A. Kornduangkaeo, N. Jangsawang and S.K. Hodak, Influence of gamma irradiation on refractive index of Fe-doped barium titanate thin films. (Thin Solid Films).

**O. Kongwut**, A. Kornduangkaeo, N. Jangsawang and S.K. Hodak, Optical properties of Fe-doped calcium copper titanate thin films under gamma irradiation. (Proceeding).

Thin Solid Films 518 (2010) 7407–7411

Contents lists available at ScienceDirect

Thin Solid Films

journal homepage: www.elsevier.com/locate/tsf

# Influence of gamma irradiation on the refractive index of Fe-doped barium titanate thin films

O. Kongwut [a], A. Kornduangkeaw [b], N. Jangsawang [b], Satreerat K. Hodak [a,c,*]

[a] Department of Physics, Faculty of Science, Chulalongkorn University, Bangkok, 10330, Thailand
[b] Thailand Institute of Nuclear Technology (TINT), Bangkok, 10900, Thailand
[c] Center of Innovative Nanotechnology, Chulalongkorn University, Bangkok, 10330, Thailand

ARTICLE INFO

Available online 10 May 2010

*Keywords:*
Gamma irradiation
Fe-doped $BaTiO_3$
Sol–gel method
Refractive index

ABSTRACT

Polycrystalline Fe-doped barium titanate (Fe-doped $BaTiO_3$) thin films were grown by thermal decomposition of the precursors deposited from a sol–gel system onto quartz substrates. The changes in the transmittance spectra induced by gamma irradiation on the Fe-doped $BaTiO_3$ thin films were quantified. The values for the optical energy band gap were in the range of 3.42–3.95 eV depending on the annealing time. The refractive index of the film, as measured in the 350–750 nm wavelength range was in the 2.17–1.88 range for the as prepared film, and this increased to 2.34–1.95 after gamma irradiation at 15 kGy. The extinction coefficient of the film was in the order of $10^{-2}$ and increased after gamma irradiation. We obtained tuneable complex refractive index of the films by exposure to various gamma rays doses.



## 1. Introduction

Recently, the effects of the inclusion of different transition metals on the structural, optical, electrical and magnetic properties of perovskite ($ABO_3$) thin films have been investigated. Various types of dopants and cations of different sizes can be accommodated in the $ABO_3$ sites [1–4]. Barium titanate ($BaTiO_3$) is a ferroelectric material with a perovskite structure ($Ba^{2+}$ as A and $Ti^{4+}$ as B) that has gained much interest due to its many potential applications, such as high dielectric constant capacitors, dynamic random access memories, and piezoelectric and optical wave guide devices [5–7]. In addition, doping Fe ions into the $BaTiO_3$ lattice leads to the acquisition of both ferromagnetic and ferroelectric properties [8]. The ferromagnetism of Fe-doped $BaTiO_3$ ceramics was reported to be dependent upon the annealing atmosphere and Fe-doping concentration, with the substitution by $Fe^{3+}$ occurring in Ti sites being confirmed by Mossbauer measurements [9,10]. Herner et al. showed that doping barium strontium titanate ($BaSrTiO_3$) with Fe could reduce the loss tangent [11], by means of improving the dielectric properties compared to pure $BaSrTiO_3$. Another way to change the fundamental properties of these materials is by exposure to high energy electromagnetic radiation or high energy particles, such as X-rays, gamma rays, electron or neutron bombardment. The retained polarization, dielectric constant and coercive field of lead titanate films decreased upon increasing gamma irradiation doses, but the material was less sensitive to neutron irradiation [12]. Recently, Arshak et al. observed that the energy gap of a bismuth germanate film decreased from 1.95 eV to 1.76 eV after exposure to gamma irradiation with a 0.228 mGy of gamma irradiation [13]. Fasasi et al. have reported the use of high dose gamma irradiation to study the thermoluminescence glow curve characteristic of $BaTiO_3$ ceramics and the dose dependence on the glow curve [14]. These radiation imparted changes in $BaTiO_3$ are extremely useful for the effective design of modern radiation dosimeters.

In this work, the effect of gamma ray irradiation on the optical properties of Fe-doped and undoped $BaTiO_3$ thin films was investigated. The changes in transmittance spectra induced by gamma irradiation, and the corresponding changes in the film refractive index and extinction coefficient, were measured as a function of the gamma irradiation dose.

## 2. Experimental details

$BaTiO_3$ and Fe-doped $BaTiO_3$ thin films were deposited on quartz substrates by a sol–gel method. The Fe-doping process was done by dissolving iron (II) sulphate ($FeSO_4$) in a mixture of barium acetate ($Ba(CH_3COO)_2$) and acetic acid. Then, pure titanium n-butoxide and methanol were added to the solution. The precursor solution was dropped onto the clean quartz substrate with a spinning speed of 1500 rpm to provide the first layer of the film. The film was preheated at 120 °C for 20 min before annealing in an atmosphere of air at 800 °C for 60 min in order to form the crystalline structure. This process was repeated until the desired thickness was obtained. Different film thicknesses can be obtained by varying the number of deposition cycles. A $^{60}Co$ gamma radiation source with an activity of 10 kCi (Gammacel 220 Excell) was used to irradiate the $BaTiO_3$ and Fe-doped $BaTiO_3$ thin films. The radiation doses were varied via the exposure time up to 15 kGy at a rate of 10 kGy/h. The optical transmittance

* Corresponding author. Department of Physics, Faculty of Science, Chulalongkorn University, Bangkok, 10330, Thailand.
*E-mail address:* satreerat.h@chula.ac.th (S.K. Hodak).

0040-6090/$ – see front matter © 2010 Elsevier B.V. All rights reserved.
doi:10.1016/j.tsf.2010.05.023

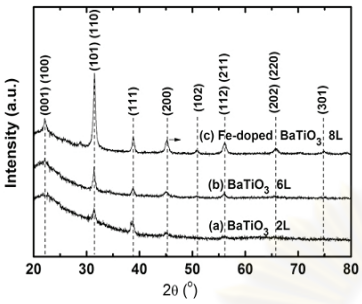


**Fig. 1.** X-ray diffraction patterns of (a) $BaTiO_3$ film with 2 layers (b) $BaTiO_3$ film with 6 layers (c) Fe-doped $BaTiO_3$ film with 8 layers.

spectra of the films were measured using a Perkin-Elmer Lambda 750 UV–Vis–NIR spectrophotometer. The refractive index and the extinction coefficient of the films before and after gamma irradiation as a function of the gamma dose were extracted from the transmittance spectra using the envelope method [15]. The band gap was also calculated from the transmittance spectra using the Tauc relation [16].

The compositions of the films were obtained using a wavelength dispersive X-ray spectrometer (WDX) equipped with an electron probe microscopic spectrometer (EPMS: JEOL model JXA-8100). The oxidation state of Fe in the Fe-doped $BaTiO_3$ films was examined by X-ray absorption spectroscopy near the edge structure (XANES) using a synchrotron source. The X-ray diffraction (XRD: Bruker model D8-Discover) patterns of $BaTiO_3$ and Fe-doped $BaTiO_3$ films were recorded to determine their crystal structures. The surface morphology of the films was observed using a Veeco Nanoscope IV atomic force microscopy (AFM).

## 3. Results and discussion

### 3.1. Structural properties

The substitution site for the dopant cation depends more strongly on its concentration and on the Ba/Ti molar ratio than on its size [17]. The ionic radius of $Fe^{3+}$ (0.64 Å) is comparable with the ionic radius of $Ti^{4+}$ (0.68 Å) but is significantly different from that of $Ba^{2+}$ (1.34 Å) [4]. However, the WDX shows signals that are consistent with $Ba_{0.8}Fe_{0.2}TiO_3$ with the Fe doping occurring by substitution of Ba sites in $BaTiO_3$ yielding a Ba/Ti ratio slightly smaller than 1. The oxidation state determined from the energy of the X-ray absorption edge (7130.5 eV) corresponds to $Fe^{3+}$. In our case the $Fe^{3+}$ dopant acts as a donor when it substitutes the $Ba^{2+}$ site. A similar result for this substitution was found in the work of Battisha et al. [1].

The crystallinity of the films was investigated using X-ray diffraction. Fig. 1 shows the XRD patterns of undoped $BaTiO_3$ with two and six layers as well as that for Fe-doped $BaTiO_3$ films with eight layers, derived from a sol–gel method. We denoted each film by the material formula followed by the number of layers ($L$). The tetragonal phase of $BaTiO_3$ was identified in our films and it is indicated in Fig. 1 by the peaks with the indices of its crystallographic planes. The diffraction peaks are sharper and more intense as the films grow thicker through the deposition of more layers. The peak positions slightly shifted to higher diffraction angles after doping Fe in the film indicating that the lattice constants slightly decreased. This could be attributed to the substitution of ions with smaller size ($Fe^{3+}$) to ions with bigger size ($Ba^{2+}$). These results are consistent with the work of other groups [4,18].

The surface of morphology of $BaTiO_3$ and Fe-doped $BaTiO_3$ films was investigated by atomic force microscopy (AFM), where the estimated average grain size of the $Ba_{0.8}Fe_{0.2}TiO_3$ 8 L film at 40 nm is smaller than the 54 nm grain size for the 6 L film as seen in Fig. 2. Devan et al. observed similar results with a decrease in grain size with doping concentrations [18]. Indeed, many research groups have reported that increasing the dopant concentration could reduce the grain size due to competition between different phase structures in the materials [2,4,19,20].

### 3.2. Optical properties

Fig. 3 shows the optical transmission spectra in the 300–1200 nm wavelength range of the undoped $BaTiO_3$ and Fe-doped $BaTiO_3$ films of comparable thickness (ca. 220 nm) before and after gamma irradiation at 15 kGy. The oscillation in the transmission curve is due to interference between light reflecting from the film surface and from the film–substrate interface. The depth of modulation indicates good homogeneity of the films across the light beam (ca. 1 cm in diameter). The transmittance of both undoped and Fe-doped films was reduced after the irradiation, and a brownish tint could be seen by the naked eye in the irradiated films. However, our results revealed that gamma irradiation causes a more marked change on the transmittance of the Fe-doped $BaTiO_3$ film than to the undoped film. For comparison, following gamma irradiation at 15 kGy, the transmittance decreased by ~4% in the undoped $BaTiO_3$ film but by ~11% for the $Ba_{0.8}Fe_{0.2}TiO_3$ film. It seems that the trapping process in the films after irradiation occurs more readily in the doped films, presumably because they have more defects than in undoped films. There are two types of defects in barium titanate; the type that preserves the stoichiometry (Schottky) and the type that changes the stoichiometry that occurs at the dopant substituted cells. Oxygen vacancy defects are commonly found in

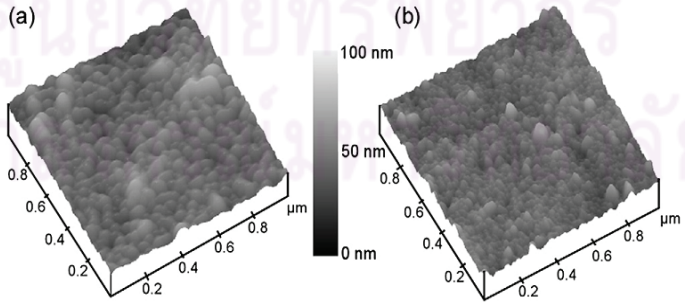


**Fig. 2.** Atomic force microscopy images (1.0×1.0 μm) of the films comprised of (a) $BaTiO_3$ with 6 layers (b) Fe-doped $BaTiO_3$ with 8 layers.

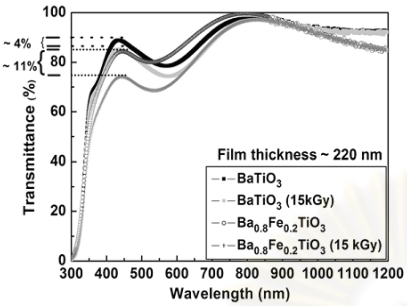


**Fig. 3.** The transmission spectra of $BaTiO_3$ and $Ba_{0.8}Fe_{0.2}TiO_3$ thin films before and after gamma irradiation at a dose of 15 kGy.

$BaTiO_3$ due to an insufficient oxygen supply during the film processing [21]. Intrinsic Schottky defects in $BaTiO_3$ are believed to form according to the following process: [14].

$$Ba_{Ba} + Ti_{Ti} + 3O_o \Rightarrow V''_{Ba} + V''''_{Ti} + 3V^{\bullet\bullet}_o + Ba_s + Ti_s + 3O_s$$

where $Ba_{Ba}$, $Ti_{Ti}$, $3O_o$ are occupied Ba, Ti and O sites, respectively, $V''_{Ba}$, $V''''_{Ti}$ and $3V^{\bullet\bullet}_o$ are vacancies of Ba, Ti and O atoms, respectively, and $Ba_s$, $Ti_s$ and $3O_s$ are the Schottky defects, respectively. Upon irradiation there are a number of phenomena that can give rise to trap sites in $BaTiO_3$. For example, a negative ion could be removed and this ion vacancy can subsequently trap an electron which constitutes the so-called F-center [14]. Another pathway is the self-trapping of holes [22]. Fig. 4(a) shows the optical transmission spectra of Fe-doped $BaTiO_3$ films with four and six layers (denoted by $Ba_{0.8}Fe_{0.2}TiO_3$ 4 L and $Ba_{0.8}Fe_{0.2}TiO_3$ 6 L, respectively) in the 300–1200 nm wavelength range and Fig. 4(b) shows the same trend for the Fe-doped $BaTiO_3$ film with eight layers (denoted by $Ba_{0.8}Fe_{0.2}TiO_3$ 8 L). As expected, the thicker film shows deeper oscillations in the transmission spectrum than the thinner film. The transmittance also decreased with the increasing gamma radiation doses. The doses used in this study were 1, 5, 10 and 15 kGy, respectively. We observed that the transmittance of the films did not change any further for gamma radiation doses higher than ca. 10 kGy. The absorption edge shifted to a lower energy as the films got thicker (Fig. 4(a)), because the films with a larger number of layers accumulated longer heating times (800 °C for 60 min for each layer) causing the growth of bigger grains. However, there was little variation in the absorption edge between the $Ba_{0.8}Fe_{0.2}TiO_3$ 4 L film annealed for 4 h and $Ba_{0.8}Fe_{0.2}TiO_3$ 8 L film annealed for 8 h. The film thickness of $Ba_{0.8}Fe_{0.2}TiO_3$ ranging from four to eight layers was calculated via the envelope method derived by Swanepoel [23] and was approximately 220 nm (4 L), 375 nm (6 L) and 520 nm (8 L). From the transmittance spectra, the energy for the direct gap could be calculated by using the Eq. (1)

$$(\alpha h\nu)^2 = B\left(h\nu - E_g\right) \tag{1}$$

Where $\alpha$ is the absorption coefficient calculated by $\alpha = \frac{1}{d}\ln\frac{1}{T}$, $h\nu$ is the photon energy, $E_g$ is the energy gap and $B$ is a constant [16]. Fig. 5 shows a plot between $(\alpha h\nu)^2$ versus $h\nu$ (eV) of the Fe-doped $BaTiO_3$ thin films with 4, 6 and 8 layers of thin films. The resulting energy band gaps were 3.42 eV, 3.69 eV and 3.95 eV for $Ba_{0.8}Fe_{0.2}TiO_3$ with 8, 6 and 4 layers, respectively. For comparison, the energy band gap value of pure $BaTiO_3$ powder, $BaTiO_3$ single crystal, and $BaTiO_3$ thin films are 3.92 eV [24], 3.6 eV [25] and 3.72–3.77 eV [26], respectively. The particle size in these films increases as the annealing cycle increases

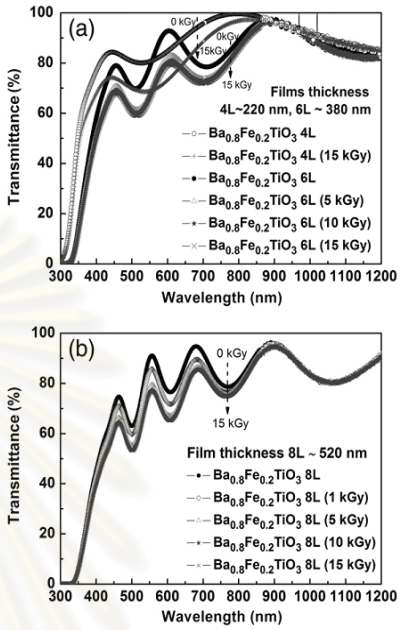


**Fig. 4.** The transmission spectra of (a) $Ba_{0.8}Fe_{0.2}TiO_3$ films with 4 and 6 layers and (b) $Ba_{0.8}Fe_{0.2}TiO_3$ films with 8 layers, after exposure to different gamma radiation doses.

[27]. The corresponding reduction in band gap energy with increasing particle size can be explained by quantum confinement [28,29]. The refractive index can be obtained using an envelope method;

$$n(\lambda) = \left[N + \left(N^2 - n_s^2\right)^{1/2}\right]^{1/2} \tag{2}$$

where $N = \left(\frac{n_s^2+1}{2}\right) + 2n_s^2\left(\frac{T_{max}-T_{min}}{T_{max}T_{min}}\right)$, $n_s$ is the refractive index of the substrate, $T_{max}$ and $T_{min}$ are the maximum and minimum transmittances. The extinction coefficient can be obtained from

$$k = \frac{\lambda\alpha}{4\pi} \tag{3}$$

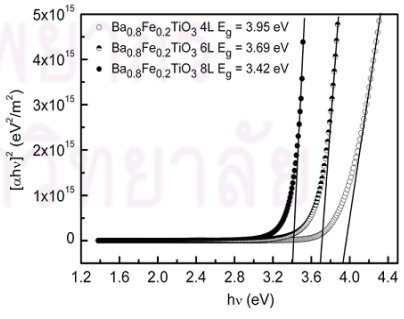


**Fig. 5.** Plot between $(\alpha h\nu)^2$ versus $h\nu$ (eV) of $Ba_{0.8}Fe_{0.2}TiO_3$ thin films with 4, 6 and 8 layers.

where λ is the wavelength, $\alpha$ is the absorption coefficient $\left(\alpha = \frac{1}{d} ln \frac{(n-1)(n_s-n)}{(n+1)(n_s+n)} \frac{\left[1+(T_{max}/T_{min})^{1/2}\right]}{\left[1-(T_{max}/T_{min})^{1/2}\right]}\right)$ and $d$ is the film thickness.

Analysis of the variation of the dispersion curves of $Ba_{0.8}Fe_{0.2}TiO_3$ films after different (0–15 kGy) gamma irradiation doses reveal that the refractive index and the extinction coefficient increase with the wavelength rising more rapidly toward short wavelengths and following a typical dispersion curve shape (Fig. 6). When measured in the 350–750 nm wavelength range, the refractive index for the $Ba_{0.8}Fe_{0.2}TiO_3$ 4 L increased from the 2.17–1.88 range to the 2.34–1.95 range upon the gamma irradiation at a dose of 15 kGy, with a corresponding increase in the extinction coefficient (Fig. 6(a) and (b)). The value of the extinction coefficient for this film prior to gamma irradiation was in the order of $10^{-2}$ and this increased after the irradiation with higher doses, indicating that higher optical losses result directly from the irradiation. With thicker films, the refractive index is also increased due to the increased film density and better crystallinity. The extinction coefficient follows an approximately linear function of the wavelength. The dispersion curves near the electronic band transition were significantly altered by the gamma irradiation. One of the main results of these experiments is that the complex refractive index of the films can be tuned by exposure to various gamma rays doses. These observed phenomena could be useful for the development of gamma irradiation dosimeters based on simple optical detection properties.

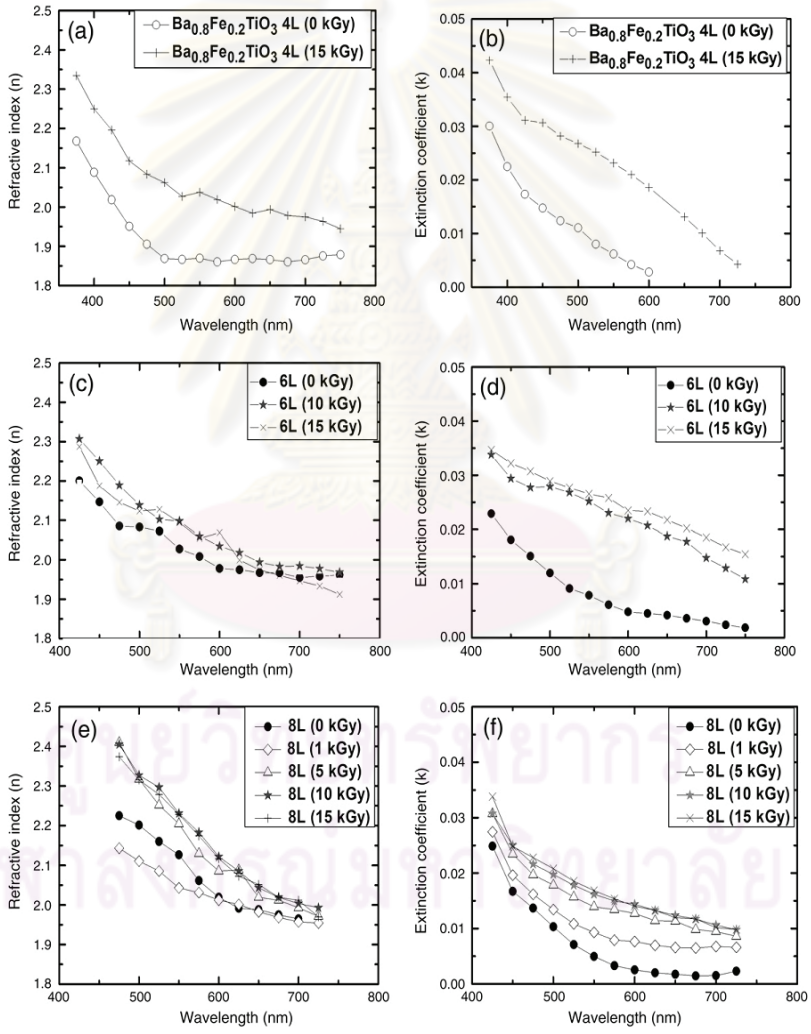


**Fig. 6.** (a,c,e) The refractive index of $Ba_{0.8}Fe_{0.2}TiO_3$ thin films with 4, 6 and 8 layers, respectively and (b,d,f) the extinction coefficient of $Ba_{0.8}Fe_{0.2}TiO_3$ thin films with 4, 6 and 8 layers, respectively.

## 4. Conclusions

Gamma irradiation effects were found to be more pronounced for the iron doped films ($Ba_{0.8}Fe_{0.2}TiO_3$) than for the undoped $BaTiO_3$. The transmittance of the films in the UV–visible range decreased after gamma irradiation with doses in the 1–15 kGy range. The refractive index and the extinction coefficient of the films were increased by exposure to higher gamma ray doses. These changes are due to the formation of color centers and the concomitant change in the complex refractive index for the irradiated the $Ba_{0.8}Fe_{0.2}TiO_3$ films.

## Acknowledgments

This work was supported by The Thailand Research Fund (TRF), the Thailand Toray Science Foundation (TTSF), National Research Council of Thailand (NRCT) and a Graduate Thesis Grant. Also, this work was supported by Research Funds from the Faculty of Science, Chulalongkorn University (A1B1), the Thai Government Stimulus Package 2 (TKK2555) under the Project for Establishment of Comprehensive Center for Innovative Food, Health Products and Agriculture, and Chulalongkorn University Centenary Academic Development Project. The authors would like to thank the Synchrotron Light Research Institute at Suranaree University of Technology.

## References

[1] I.K. Battisha, A.B.A. Hamad, R.M. Mahani, Phys. B 404 (2009) 2274.
[2] E. Brzozowski, M.S. Castro, J. Mater. Process. Technol. 168 (2005) 464.
[3] K. Daoudi, T. Tsuchiya, T. Kumagai, Appl. Surf. Sci. 253 (2007) 6527.
[4] Y. Ye, T.L. Guo, Ceram. Int. 35 (2009) 2761.
[5] S. Ke, H. Huang, H. Fan, H.I.W. Chan, L.M. Zhou, Solid State Ionics 179 (2008) 1632.
[6] F. Zimmermann, M. Voigts, W. Menesklou, E. Ivers-Tiffee, J. Eur. Ceram. Soc. 24 (2004) 1729.
[7] A. Kumar, S.G. Manavalan, Surf. Coat. Technol. 198 (2005) 406.
[8] T.K. Kundu, A. Jana, P. Barik, Bull. Mater. Sci. 31 (2008) 501.
[9] F. Lin, D. Jiang, X. Ma, W. Shi, Phys. B 403 (2008) 2525.
[10] F. Lin, D. Jiang, X. Ma, W. Shi, J. Magn. Magn. Mater. 302 (2008) 691.
[11] S.B. Herner, F.A. Selmi, V.V. Varadan, V.K. Varadan, Mater. Lett. 15 (1993) 317.
[12] J. Gao, L. Zheng, Z. Song, C. Lin, D. Zhu, Mater. Lett. 42 (2000) 345.
[13] K. Arshak, O. Korostynska, J. Harris, D. Morris, A. Arshak, E. Jafer, Thin Solid Films 516 (2008) 1493.
[14] A.Y. Fasasi, F.A. Balogun, M.K. Fasasi, P.O. Ogunleye, C.E. Mokobia, E.P. Inyang, Sens. Actuators A 135 (2007) 598.
[15] M. Caglar, Y. Caglar, S. Ilican, J. Optoelectron. Adv. Mater. 8 (2006) 1410.
[16] J. Tauc, A. Menth, J. Non-Cryst. Solids 8–10 (1972) 569.
[17] M.T. Buscaglia, V. Buscaglia, M. Viviani, P. Nanni, M. Hanuskova, J. Eur. Ceram. Soc 20 (2000) 1997.
[18] R.S. Devan, Y.R. Ma, B.K. Chougule, Mater. Chem. Phys. 115 (2009) 263.
[19] Y.C. Huang, W.H. Tuan, Mater. Chem. Phys. 105 (2007) 320.
[20] S.Y. Lee, B.S. Chiou, H.H. Lu, Mater. Chem. Phys. 108 (2008) 55.
[21] K. Shimoyama, K. Kubo, T. Maeda, K. Yamabe, Jpn. J. Appl. Phys. 40 (2001) 463.
[22] A. Stashans, H. Pinto, Radiat. Meas. 33 (2001) 553.
[23] R.S. Swanepoel, J. Phys. E Sci. Instrum. 16 (1983) 1214.
[24] A. Mansingh, C.V.R. Vasanta, J. Mater. Sci. Lett. 7 (1988) 1104.
[25] A. Onton, V. Marello, G. Lucovsky, F.L. Galeener (Eds.), AIP Conf. Proc. No., 31, AIP, New York, 1976.
[26] H.X. Zhang, C.H. Kam, Y. Zhou, X.Q. Han, Y.L. Lam, Y.C. Chan, K. Pita, Mater. Chem. Phys. 63 (2000) 174.
[27] X.M. Lu, J.S. Zhu, W.Y. Zhang, G.Q. Ma, Y.N. Wang, Thin Solid Films 274 (1996) 165.
[28] L. Burs, J. Phys. Chem. 90 (1986) 2555.
[29] T. Supasai, S. Dangtip, P. Learngarunsri, N. Boonyopakorn, A. Wisitsoraat, Satreerat K. Hodak, Appl. Surf. Sci. 256 (14) (2010) 4462.

# สมบัติทางแสงของฟิล์มบางแคลเซียมคอปเปอร์ไททาเนตเจือด้วยเหล็กภายใต้การฉายรังสีแกมมา

# OPTICAL PROPERTIES OF FE-DOPED CALCIUM COPPER TITANATE THIN FLIMS UNDER GAMMA IRRADIATION

**อรณิชา คงวุฒิ[1/] อารีรัตน์ คอนดวงแก้ว[2/] นงนุช แจ้งสว่าง[2/] และ สตรีรัตน์ โฮคัด[1/, 3/]**

Ornicha Kongwut[1/] Areerat Kornduangkeaw[2/] Nongnuch Jangsawang[2/] and S.K. Hodak[1/, 3/]

## บทคัดย่อ

ฟิล์มบางแคลเซียมคอปเปอร์ไททาเนตเจือด้วยเหล็กถูกปลูกบนแผ่นรองรับควอตซ์ที่อุณหภูมิ 800 องศาเซลเซียส โดยวิธีโซลเจล ฟิล์มบางจะถูกฉายรังสีแกมมาจากเครื่อง Gammacel 220 Excell โดยมีธาตุ $^{60}$Co เป็นแหล่งกำเนิดรังสีซึ่งมีอัตราการฉายรังสี 10 กิโลเกรย์ต่อชั่วโมงเพื่อตรวจสอบสมบัติทางแสงของฟิล์มที่เปลี่ยนแปลงปริมาณรังสีใช้อยู่ในช่วง 1-3 กิโลเกรย์ การส่องผ่านของแสงวัดที่ความยาวคลื่น 500 นาโนเมตร จะมีค่าลดลง 2.5% ภายใต้การฉายรังสีแกมมา 1 กิโลเกรย์และลดลง 4.8% หลังจากการฉายรังสีแกมมา 3 กิโลเกรย์ ช่องว่างพลังงานทางแสงของฟิล์มเท่ากับ 3.67 อิเล็กตรอนโวลต์และไม่มีการเปลี่ยนแปลงหลังจากการฉายรังสีแกมมา ค่าดัชนีหักเหของฟิล์มบางแคลเซียมคอปเปอร์ไททาเนตเจือด้วยเหล็กในช่วงความยาวคลื่น 400 - 700 นาโนเมตรเพิ่มขึ้นจาก 1.76 - 1.99 เป็น 1.91 - 2.08 หลังจากการฉายรังสีแกมมา 3 กิโลเกรย์ ค่าสัมประสิทธิ์การดูดกลืนของฟิล์มอยู่ในอันดับ $10^{-2}$ และเพิ่มขึ้นหลังจากการฉายรังสีแกมมา

คำสำคัญ: รังสีแกมมา, ฟิล์มบางแคลเซียมคอปเปอร์ไททาเนต, สมบัติทางแสง

## Abstract

The Fe-doped calcium copper titanate (Fe-doped $CaCu_3Ti_4O_{12}$) films were deposited on quartz substrates with the annealing temperature of 800°C by a sol-gel spin coating technique. The $^{60}$Co (Gammacel 220 Excell) source with the exposure rate of 10 kGy/hr was used to irradiate our film in order to investigate the changes of their optical properties. The gamma ray doses were varied in the range of 1-3 kGy. The transmittance measured at 500 nm wavelengths of films decreased to 2.5% under gamma irradiation dose of 1 kGy and decreased to 4.8% after 3 kGy irradiation respectively. The direct optical band gap energy of the films is 3.67 eV and there was no change after irradiation. The refractive index of the films measured in the 450-700 nm wavelength range increased from 1.76 – 1.99 range to 1.91 – 2.08 range for Fe-doped $CaCu_3Ti_4O_{12}$ films upon the gamma irradiation with a 3 kGy dose. The extinction coefficient of the films was on the order of $10^{-2}$ and increased after gamma irradiation.

Keywords: Gamma irradiation; Calcium copper titanate; Optical properties

[1]นิสิตบัณฑิตศึกษา สาขาวิชาฟิสิกส์ คณะวิทยาศาสตร์ จุฬาลงกรณ์มหาวิทยาลัย

[2]สถาบันเทคโนโลยีนิวเคลียร์แห่งชาติ (องค์การมหาชน)

[3]ศูนย์นวัตกรรมนาโนเทคโนโลยี จุฬาลงกรณ์มหาวิทยาลัย

## Introduction

Calcium copper titanate ($CaCu_3Ti_4O_{12}$: CCTO) is a novel ferroelectric material with high dielectric constant values and it does not show ferroelectric transition in the temperature range of 200K-600K. In the past few decades, many applications such as high dielectric constant capacitors and dynamic RAMs (Li *et al*., 2003; Fang and Shen, 2003; and Liu *et al*., 2007) have been dealt with CCTO due to the unchanged dielectric constant over a wide range of temperature and frequency. There are several methods to modify the film properties such as controlling the growth parameters, changing the growth techniques and doping with various types of dopants. It has been reported that doping Fe in the CCTO films could cause the temperature dependence of dielectric constant and the reduction in dielectric constant (Grubbs *et al*., 2005). It is worthy to investigate another way to change the electrical and optical properties of CCTO after finishing the regular film processing. Exposure materials with high energy electromagnetic radiations or high energy particles (such as X-rays, gamma rays, electrons or neutron) are considered as post-processing. For example, Arshak *et al*. observed that the energy gap of bimuth germanate film was reduced from 1.95 eV to 1.76 eV after exposure to gamma irradiation with a 0.228 mGy dose (Arshak *et al*., 2008).

In this work, the effects of gamma ray irradiation on optical properties of Fe-doped calcium copper titanate thin films were investigated. The changes in transmittance spectra induced by gamma irradiation, and the corresponding changes in refractive index and extinction coefficient of the films were measured as a function of gamma irradiation doses. Studying the effect of gamma radiation is important to design the modern dosimeters.

## Experimental Methods

Fe-doped calcium copper titanate thin film was deposited on quartz substrate by a sol-gel spin coating technique. Quartz has been suitable substrates for studying the transmission of the materials being supported due to its transparency and high temperature melting point. In the precursor processing, iron (II) sulphate ($FeSO_4$), copper acetate and calcium acetate were firstly dissolved in acetic acid, and then titanium IV isopropoxide was slowly added. Ethylene glycol and formamide were added into the solution in order to increase solution stability. In this step, the solution viscosity can be also controlled to prevent the film cracking during the baking and annealing. The precursor solution was dropped on the clean quartz substrate with the spinning speed of 1500 rpm. The film was preheated at 120□C for 20 min before annealing in the air atmosphere at 800°C annealing temperature for 60 min. We investigated the effects of the $^{60}Co$ (Gammacel 220 Excell) gamma irradiation on the changes in optical properties of CCTO and Fe-doped CCTO thin films. In this study, the activity of gamma ray was 10 kCi and the exposure rate was 10kGy/hr. The films were placed in the centre of the reactor and the doses of gamma radiation were varied up to 3 kGy. The optical transmittance spectra of the films were measured

using Perkin-Elmer Lambda 750 UV-Vis-NIR Spectrophotometer. The refractive index and the extinction coefficient of the films before and after gamma irradiation as a function of gamma dose were extracted from transmittance spectra using envelope method (Caglar *et al*., 2006). The band gap was calculated from the transmittance spectra.

## Results and discussion

Fig. 1 shows the optical transmission spectra in the 300-1200 nm wavelength range of Fe-doped $CaCu_3Ti_4O_{12}$ films before and after gamma irradiation at 1, 3 and 5 kGy dose respectively. The depth of modulation normally indicates that the films are homogeneous. We have found the reduction in transmittance decreasing to 2.5% and 4.8% after exposure with gamma irradiation dose of 1 kGy and 3 kGy, respectively. We observed that the transmittance of the films did not change after the gamma radiation dose is higher than ca. 3 kGy. In another word, there was not much change in the transmittance for the film exposed with 3 kGy and 5 kGy. This could be due to the saturation of activity of color centre phenomena. Under irradiation, a negative ion in the film could be removed and this ion vacancy can subsequently trap an electron which is so-called F-center (Fasasi *et al*., 2007) or the self-trapping of holes could occur (Stashans and Pinto, 2001). From the transmittance spectra, the energy gap for direct gap could be calculated by using the Equation (1)

$$(\alpha h\nu)^2 = B(h\nu - E_g) \qquad (1)$$

Where $\alpha$ is the absorption coefficient calculated by $\alpha = \frac{1}{d}\ln\frac{1}{T}$, $h\nu$ is photon energy, $E_g$ is energy gap and B is a constant. Fig. 2 shows plot between $(\alpha h\nu)^2$ versus $h\nu$ (eV) of Fe-doped $CaCu_3Ti_4O_{12}$ thin films. The resulting energy band gaps were 3.67 eV. For comparison, the energy band gap value of $CaCu_3Ti_4O_{12}$ thin films is 2.88 eV (Tingyin *et al*., 2009). The discrepancy will be further investigated. The refractive index can be obtained using envelope method;

$$n(\lambda) = [N + (N^2 - n_s^2)^{1/2}]^{1/2} \qquad (2)$$

Where $N = (\frac{n_s^2+1}{2}) + 2n_s(\frac{T_{max} - T_{min}}{T_{max}T_{min}})$, $n_s$ is the refractive index of the substrate, $T_{max}$ and $T_{min}$ are the maximum and minimum transmittance. The extinction coefficient can be obtained from

$$k = \frac{2\alpha}{4\pi} \qquad (3)$$

where $\alpha$ is the absorption coefficient ($\alpha = \frac{1}{d}\ln\frac{(n-1)(n_s-n)}{(n+1)(n_s+n)}\frac{[1+(T_{max}/T_{min})^{1/2}]}{[1-(T_{max}/T_{min})^{1/2}]}$) and *d* is the film thickness. The film thickness was simply determined through the equation;

$$d = \frac{\lambda_1\lambda_2}{2(n(\lambda_1)\lambda_2 - n(\lambda_2)\lambda_1)}. \quad (4)$$

Where $n(\lambda_1)$ and $n(\lambda_2)$ are refractive indices of two adjacent maximum at wavelength $\lambda_1$ and $\lambda_2$, respectively. The calculated thickness was 360 nm.

Fig. 3 shows the refractive index and the extinction coefficient of the Fe-doped $CaCu_3Ti_4O_{12}$ film measured in the 350-750 nm wavelength range. The refractive index of the films measured in the 450-700 nm wavelength range increased from 1.76 - 1.99 range to 1.91 - 2.08 range for Fe-doped $CaCu_3Ti_4O_{12}$ film upon the gamma irradiation with a 3 kGy dose with a corresponding increase in the extinction coefficient as shown in Fig. 4. There was not much change in the refractive index of the films until the dose increased to 3 kGy. The increase in the extinction coefficient with the irradiation dose indicates that high optical losses causing by the irradiation. The increase in the extinction coefficient with the irradiation dose indicates that high optical losses causing by the irradiation. The value of the extinction coefficient of the films before and after gamma irradiation was still on the order of $10^{-2}$. The shape of refractive index was similar to the result of Raffaella *et al* group (Raffaella *et al*., 2006).

## Conclusions

The transmittance of Fe-doped $CaCu_3Ti_4O_{12}$ films was reduced after gamma irradiation in the dose range of 1-5 kGy. The refractive index of as a function of wavelength the Fe-doped $CaCu_3Ti_4O_{12}$ films can be change by exposure to gamma rays doses higher than 3 kGy where as the change in extinction coefficient could be observed with exposure only 1 kGy.

## Acknowledgement

This work was supported by The Thailand Research Fund (TRF), the Thailand Toray Foundation (TTF), National Research Council of Thailand (NRCT) and Graduate Thesis Grant. The authors would like to thank Thailand Institute of Nuclear Technology (TINT) for the help in gamma irradiation experiment.

## References

Li, Y.W., Hu, Z.G., Sun, J.L., Meng, X.J. and Chu, J.H., 2008. Preparation and properties of $CaCu_3Ti_4O_{12}$ thin film grown on $LaNiO_3$-coated silicon by sol–gel process. Journal of Crystal Growth 310: 378.

Fang, L. and Shen, M., 2003. Deposition and dielectric properties of $CaCu_3Ti_4O_{12}$ thin films on Pt/Ti/$SiO_2$/Si substrates using pulsed-laser deposition. Thin Solid Films 440: 60.

Liu, L., Fan, H., Fang, P. and Jin, L., 2007. Electrical heterogeneity in $CaCu_3Ti_4O_{12}$ ceramics fabricated by sol–gel method. Solid State Communications 142: 573.

Grubbs, R.K., Venturini, E.L., Clem, P., Richardson, J.J., Tuttle, B.A. and Samara, G.A., 2005. Dielectric and magnehic properties of Fe-and Nb-doped $CaCu_3Ti_4O_{12}$. Physical Review B 72:104.

Arshak, K., Korostynska, O., Harris, J., Morris, D., Arshak, A. and Jafer, E., 2008. Properties of BGO thin films under the influence of gamma radiation. Thin Solid Films 516:1493.

Caglar, M., Caglar, Y. and Ilican, S., 2006. Preparation and characterization of ZnO thin films deposited by sol-gel spin coating method. *Journal of Optoelectronics and Advanced Materials* 8:1410.

Fasasi, A.Y., Balogun, F.A., Fasasi, M.K., Ogunleye, P.O., Mokobia, C.E. and Inyang, E.P., 2007. Thermoluminescence properties of barium titanate prepared by solid-state reaction. Sensors and Actuators A 135: 598.

Stashans, A. and Pinto, H., 2001. Analysis of radiation-induced hole localisation in titanates. Radiation Measurements 33:553.

Tingyin, N., Cong, C., Yueliang, Z., Heng, L., Dongxiang, Z., Hai, M. and Guozhen, Y., 2009. Large optical nonlinearity in $CaCu_3Ti_4O_{12}$ thin films. *Applied Physics A* 94:567.

Raffaella, L.N., Roberta, G.T., Graziella, M., Ignazio, L.F., Maria, L., Michelaria, M.G., Giovanni, B., Vito, R. and Patrick, F., 2006. Calcium Copper Titanate Thin Film Growth: Tailoring of the Operational Conditions through Nanocharacterization and Substrate Nature Effects. *Journal of Physical Chemistry B* 110:17460.

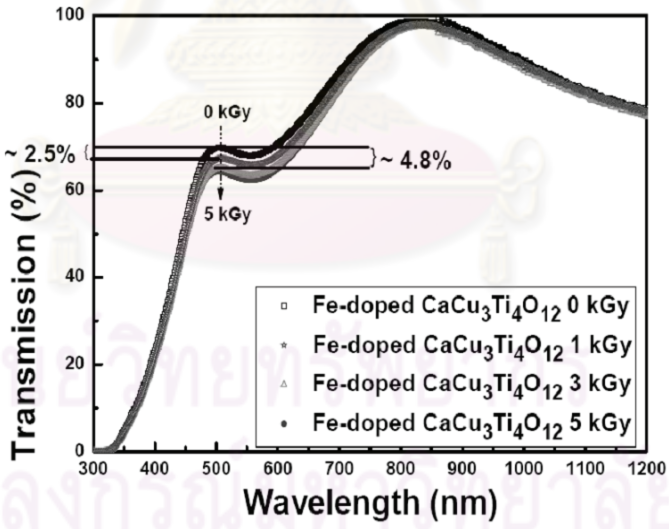


Figure 1. The transmission spectra of Fe-doped $CaCu_3Ti_4O_{12}$ thin films for different gamma radiation dose.

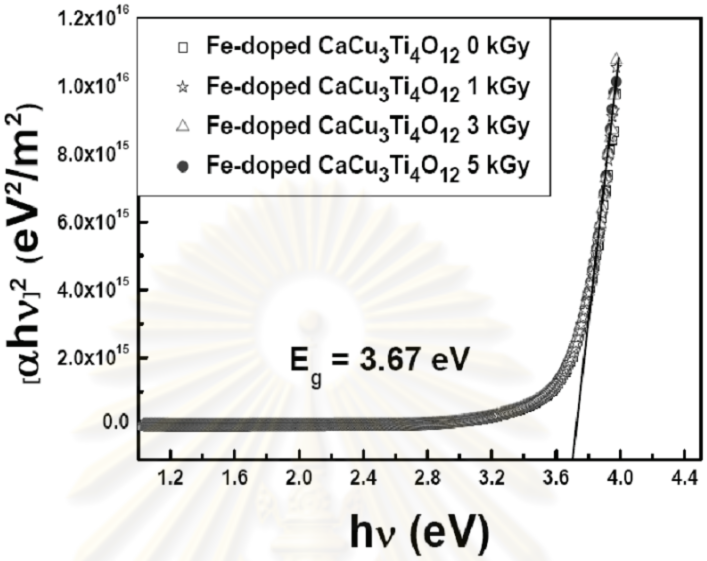


Figure 2. Plot between $(\alpha h\nu)^2$ versus $h\nu$ of Fe-doped $CaCu_3Ti_4O_{12}$ thin films

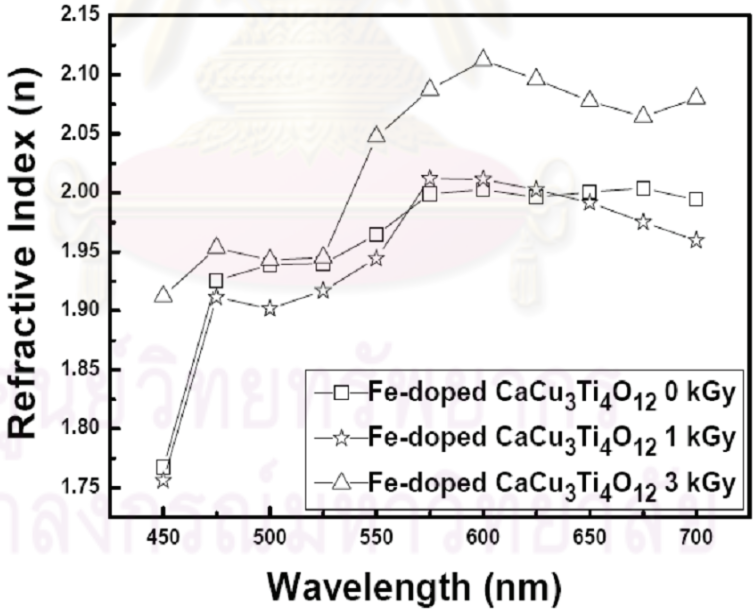


Figure 3. The refractive index of Fe-doped $CaCu_3Ti_4O_{12}$ thin films for different gamma radiation dose.

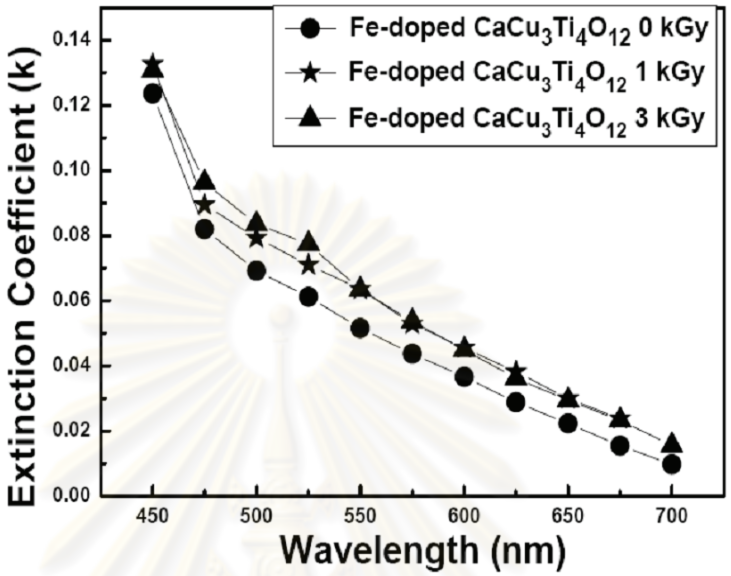


Figure 4. The extinction coefficient of Fe-doped $CaCu_3Ti_4O_{12}$ thin films for different gamma radiation dose.

# Vitae

Miss. Ornnich Kongwut was born on December 18, 1984 in Kanchanaburi, Thailand. She finished high school from Kanchananukroh, Kanchanaburi in 2002, then received her Bachelor degree of Science in Physics from Mahidol University in 2006, and continued her Masters study in Physics at Chulalongkorn University.